University of Strathclyde

Department of Chemical and Process Engineering

Investigating Mechanisms of Laser Induced Nucleation

Thomas Kendall

A thesis submitted to the Department of Chemical and Process Engineering in fulfilment of the requirements for the degree of Doctor of Philosophy.

2017

Declarations

This thesis is the result of the author's original research. It has been composed by the author and has not been previously submitted for examination which has led to the award of a degree.

Signed: 

Date: 31/7/17

Acknowledgements

Firstly, I would like to thank my supervisor Professor Jan Sefcik for all of his help and advice over the last four years and for giving me the opportunity to work on this project in the first place. His knowledge and enthusiasm for research has been a constant driving force and source of new experiment ideas when presented with surprising results. I would also like to thank Dr Iain Burns for his help setting up and using the laser and in designing the biexponential function for analysing data, Dr Martin Ward and Dr Nadeem Javid for help setting up experiments and discussing laser induced nucleation, CMAC and EPSRC for funding the project, and finally, I would like to thank my family whose continuous support and encouragement for the past 4 years has been invaluable, and without their help completion of this thesis would not be possible.

Abstract

This thesis describes work investigating the mechanism of non-photochemical laser induced nucleation in aqueous glycine and urea solutions. Nucleation is the first step of the crystallisation process, the second being crystal growth. Crystallisation is an important process used by many industries including chemicals, food and pharmaceuticals. It can also be used as a way of installing a set of particulate solid properties onto the compound which can be beneficial for production and use. Uncontrolled nucleation can lead to unwanted crystal forms or uncontrolled particles size distributions which can cause wasted time and money in production. Non-photochemical laser induced nucleation offers the possibility of controlling when and where the nucleation occurs. However, the mechanism is not understood which would need to be addressed before it could be considered a viable tool.

An experimental set up was used for irradiation and monitoring to measure induction time. With this set up it was demonstrated that by increasing supersaturation and laser power you could increase the probability of laser induced nucleation. With the monitoring set up it was shown that two simultaneous nucleation mechanisms are present: the first fast laser induced nucleation and the second slower spontaneous nucleation. Through the use of a biexponential function it was possible to identify the proportion of laser induced samples undergoing laser induced nucleation and a characteristic time which could be used to calculate the respective nucleation rate.

Nano-filtration was shown to suppress laser induced nucleation. Through a series of dynamic light scattering and irradiation experiments it was shown that even when solute clusters were present in solution after nano-filtration with larger pore size, laser induced nucleation was suppressed. Thus, it is possible to exclude any mechanistic theory that solely involves the presence of solute clusters. Subsequent experiments found that the source of a necessary initiator was in the solvent (deionised water). Treatment of the deionised water by rotary-evaporation, distillation, and reflux increased the proportion of samples undergoing laser induced nucleation, which will considered the nucleation efficiency. It was found that this increase was also achieved by degassing the deionised water, which suggests that the processing of the deionised water was improving the distribution of initiators particles as nothing is being

added and only gas is being removed. It was found that different sources of water have different effects on laser induced nucleation and the greater treatment resulted in greater proportion of samples undergoing laser induced nucleation.

Polymorphism is an important aspect of crystallisation, and laser induced nucleation has shown an influence on glycine polymorphism. It was demonstrated that a consistent 60:40 alpha:gamma polymorphism split is achieved when using linear polarized laser light. This was shown in deionised water, HPLC grade water, and the residue and distillate of distilled deionised water, which all had different proportion of samples undergoing laser induced nucleation. This suggests that the polymorphic influence is an independent aspect of the mechanism from the amount of initiators present.

Conferences and Publications

Conferences

Manufacturing for the future, Glasgow
23rd – 24th September 2014

European Conference on Crystal Growth, Bologna
Filtration suppression of laser induced nucleation
9th-11th September 2015

International School of Crystallization 2016, Granada
Filtration suppresses laser induced nucleation of glycine in aqueous solutions
29th May-3rd June 2016

British Association for Crystal Growth 2016, Leeds
Filtration suppresses laser induced nucleation of glycine in aqueous solutions
26th-30th June 2016

British Association for Crystal Growth 2017, Manchester
Investigating laser induced nucleation mechanisms
27th-30th June 2017

Papers

- Javid N., Kendall T., Burns I., Sefcik J.; Filtration suppresses laser-induced nucleation of glycine in aqueous solutions, Crystal Growth and Design Vol 16, pp. 4196−4202, (2016)

- Lau A., Castelletto V., Kendall T., Sefcik J., Hamley I., Reza M., Ruokolainen J.: Self-assembly of ultra-small micelles from amphiphilic lipopeptoids, Chemical Communications, Vol. 53, No. 13, 09.02.2017, p. 2178-2181.

- Kendall T., Javid N. Hobbs D., Burns I., Sefcik J.; Investigation of the role of pre-nucleating cluster and initiators in the laser induced nucleation mechanism of aqueous glycine solution. (pending)

- Kendall T., Javid N. McGill R., Burns I., Sefcik J.; Discussion of non-photochemical laser induced nucleation mechanisms. (pending)

Thesis Layout

1. Introduction

This chapter summarises relevant background information on crystallisation and specifically nucleation and laser induced nucleation. This will cover classical nucleation theory and two step (non-classical) theory, solute clusters in solution and issues with systems showing poor crystallisation propensity.

The chapter will also cover induced nucleation by external fields including a brief discussion on the different types of laser induced nucleation (femto and nano second pulsed, continuous wave, and photo chemical Laser Induced Nucleation), examples of non-photochemical laser induced nucleation, and information learned from them and a summary of the proposed mechanism theories including evidence for each case.

2. *Methodology*

In this chapter the experimental methods are outlined, describing how each technique was applied and used in this thesis. Experimental sections in each chapter will refer back to the relevant sections in this chapter.

3 Effect of laser intensity and duration, and bimodal model estimation of nucleation rates.

In this chapter the building of the laser induced nucleation set up used in experiments will be discussed and tested by demonstrating the effect supersaturation, laser intensities and irradiation duration have on nucleation efficiency in aqueous glycine and urea solutions. This is then expanded on further through a model based on bimodal distribution of induction times to estimate associated nucleation rates and proportion of samples undergoing laser induced nucleation.

4. Suppression of laser induced nucleation with nano-filtration and solute cluster analysis

Of the previously proposed mechanistic theories in NPLIN, two solely involve the presence of solute clusters and previously it had been demonstrated that through nano-filtration it was possible to remove mesoscale clusters from glycine solutions.

Thus, in this chapter the role mesoscale clusters have in NPLIN will be investigated by dynamic light scattering with laser induced nucleation experiments on supersaturated aqueous glycine solutions after nanofiltration using various filter pore sizes.

Based on observations in this chapter, a series of experiments were designed to investigate the presence of initiators in solution, mixing equal parts filtered and non-filtered supersaturated aqueous glycine solutions, and their effect on laser induced nucleation efficiency. Further experiments were conducted investigating the source of these initiators where each component, solute (glycine) and solvent (deionised water), were respectively subjected to a nano-filtration stage before use in laser induced nucleation experiments.

5. Water treatments and sources

Advancing the work described in chapter 4, chapter 5 will describe the series of experiments investigating the nature of these initiators. Through treatment of deionised water with distillation, it was attempted to separate and concentrate the initiators to increase laser induced nucleation efficiency. Subsequent experiments were conducted to reproduce the observations made in these experiments through degassing deionised water prior to laser induced nucleation experiments. This chapter will also discuss the effect different water supplies have on laser induced nucleation efficiency.

6. Observations on polymorphism

Chapter 6 will cover all the polymorphic results for glycine that were obtained during investigations reported in the previous chapters, including different supersaturation, various treatments and sources of water, and laser polarization.

7. Conclusions, future work and suggestions

The findings and conclusions from the previous chapters will be summarised in this chapter and, based on these, I will make suggestions on what future work should be undertaken in order to follow on from the findings in this thesis.

Main Conclusions

- Laser induced nucleation appears to be related to the peak laser intensity rather than the total energy input.

- Laser induced nucleation is dramatically suppressed by nanofiltration with polyerthersulfone filters of any pore size.

- Solute rich mesoscale clusters, whilst they could play a role in the mechanism, they are not the sole cause of laser induced nucleation. This allows for the exclusion of mechanisms where solute precursor clusters are solely responsible, such as optical Kerr's and isotropic polarizability of solute clusters. Therefore, an initiator is required for laser induced nucleation

- By mixing equal parts of filtered and non-filtered solution it was demonstrated that the nucleation efficiency is related to the concentration of initiators.

- Through distillation it is possible to increase nucleation efficiency in both distillate and residue waters. Distillation appears to be degassing the solvent, so either creating more or changing the distribution of initiators. This effect was also achieved first through reflux and then through degassing.

- Results from the different processing of water suggest that degassing, distillation, and reflux is improving the distribution of initiators in the solvent as no material was added and only gas was removed.

- HPLC grade water has higher nucleation efficiency and tap water has lower nucleation efficiency compared to deionised water.

- Spread of induction times present in glycine solutions is also observed in urea but nucleation is occurring during the irradiation period, suggesting that it is related to the probability of the laser interacting with the initiator.

- In all treatments water, when irradiated with linear polarised light results in 60:40 alpha:gamma split in polymorphism indicating that the influence is intrinsic to the laser pulses and is independent of the initiator.

Contents

1. Literature

1.1 Crystallisation

Crystallisation is a commonly used process in a wide range of manufacturing industries including food, chemical, and pharmaceuticals. Primarily in the pharmaceutical industry it is used as a way of separating, purifying, and isolating a desired compound. However, it has another effect of installing properties, such as size, morphology, and polymorphism, into the crystal which can improve its performance economically, such as how well it performs in downstream process, and biologically, how well it does its job in the body.

Crystallisation is a two-stage process; first nucleation, the arrangement of molecules into a 3D ordered array, and crystal growth. A reason why uncontrolled crystallisation is an issue is that nucleation is not very well understood. Better understanding of nucleation from solution would allow for the design and control of particle properties such as morphology, size distribution, and polymorphism in a consistent and reproducible way. In pharmaceuticals controlling polymorphism is paramount. Most pharmaceutical compounds are polymorphic, having more than one stable or metastable internal structure, and differences in properties of polymorphs can be significant.

Classical nucleation theory (CNT) (chapter 1.4.1) is used to describe how nucleation occurs in solution. However, there are many shortfalls of this theory to describe crystallisation. As an alternative, a two-step nucleation mechanism has been proposed, but there is a lack of evidence supporting this due to the difficulty of monitoring the process.

A growing problem in the pharmaceutical industry is that more and more new compounds are becoming harder to crystallise. Traditional methods such as anti-solvent, cooling and evaporation can result in oiling out, amorphous formation or no

solid form being obtained. Thus new methods for inducing nucleation are being investigated, including ultrasound, additives, and laser induced nucleation.

A much longer standing issue for the pharmaceutical industry has been polymorphism. New crystallisation techniques that can influence polymorphism can be of interest due to the different particle properties polymorphic systems can show.

Through laser induced nucleation it is believed it is more possible to study and control nucleation due to its high spatiotemporal control of the nucleation event confining the event to the beam path, and duration of the laser pulse. However, the mechanism of laser induced nucleation is also unknown. It is hoped that through better understanding the mechanism laser induced nucleation could be used as a new crystallisation technique addressing both the difficulties in achieving a crystalline form and in controlling polymorphism.

1.2 Polymorphism

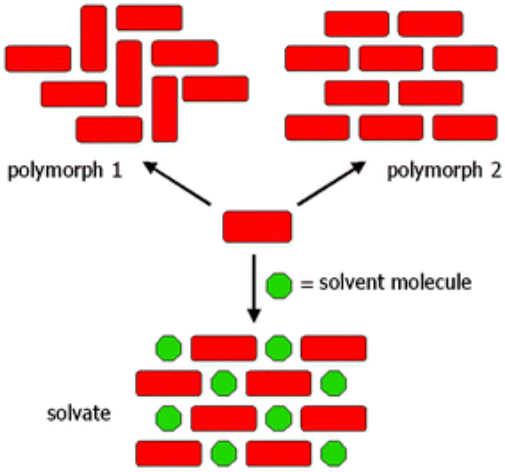

Figure 1.1: visual representation of polymorphism[1]

Polymorphism is defined as the ability of a molecule to have more than one stable solid form that is the result of having multiple 3D packing arrangements which can be expanded to include the incorporation of solvent molecules or other molecules, co-crystals, or salts, to bridge gaps between compound molecules which would not be viable. Polymorphism can arise from multiple molecular factors such as conformational flexibility, isomerism or hydrogen bond sites. Molecules with a high

degree of conformation flexibility can show polymorphism based on one or more stable confirmations [2] cases such as Effexor [3] and Zyprexa [4]. Polymorphism can also arise from the incorporation of solvents into the lattice. This is done by bonding with a solvent molecule bridging a gap, creating a site for further molecules to bond and stabilizing a lattice. These are known as solvates. A common solvent which can fulfil this role is water due to its hydrogen bonding donor and acceptor character, and because of its small size it can be incorporated easily. These are known as hydrates examples of which include olanzapine [5] and nitrofurantoin [6]. Polymorphism is a prominent occurrence in organic molecules. Studies have shown that a third of organic molecules exhibited more than one stable solid form and 80% of pharmaceutical compounds exhibit polymorphism[7].

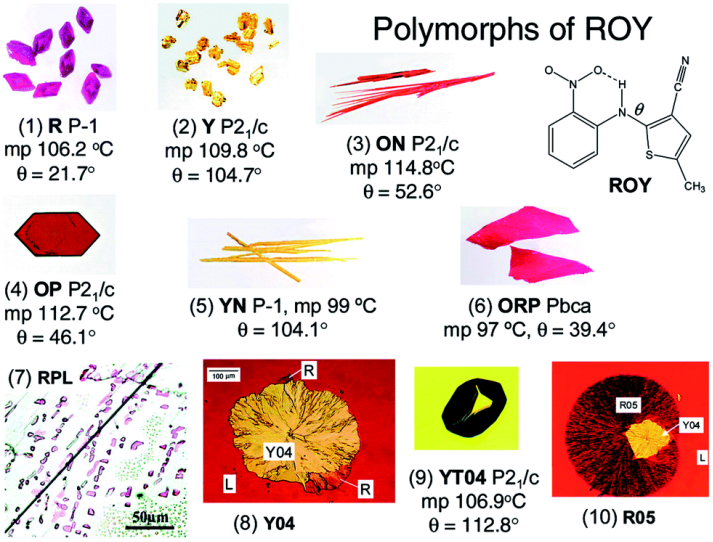

Figure 1.2: The different crystal polymorphs of 5-Methyl-2-[(2-nitrophenyl)amino]-3-thiophenecarbonitrile[8]

Polymorphism in industry is seen in multiple sectors including agricultural, explosives and fine chemicals, and polymorphism can be both an advantage and a disadvantage, due to their different physical properties and morphology. Having polymorphs of molecules can allow you to choose the solid form with the desired properties that best suit the molecules use. However, the presence of another more stable form can result in disappearing polymorphs.

Different polymorphic forms of the same molecules can have drastically different physical and chemical properties[9], which can be beneficial for companies, as one form might have a higher absorption rate in the body,[10] which would mean less API would

need to be included in any formulation and reducing costs for that compound. Furthermore, some polymorphs have a better morphology for secondary processing[11], such as cubic instead of needles, for filtering and drying, which would reduce the manufacturing time and increase profits.

Pharmaceutical products tend to aim for the most stable form which typically is the solid form. However, with multiple stable solid forms and the heavily regulated and controlled industry[12], it can be very costly to develop molecules. In pharma there is a need for a process to reliably produce with high purity, single solid form that will not spontaneously transform into another one. There have been multiple cases of polymorphism being both devastating for both patient and company.[13]

1.2.1Polymorphism in glycine

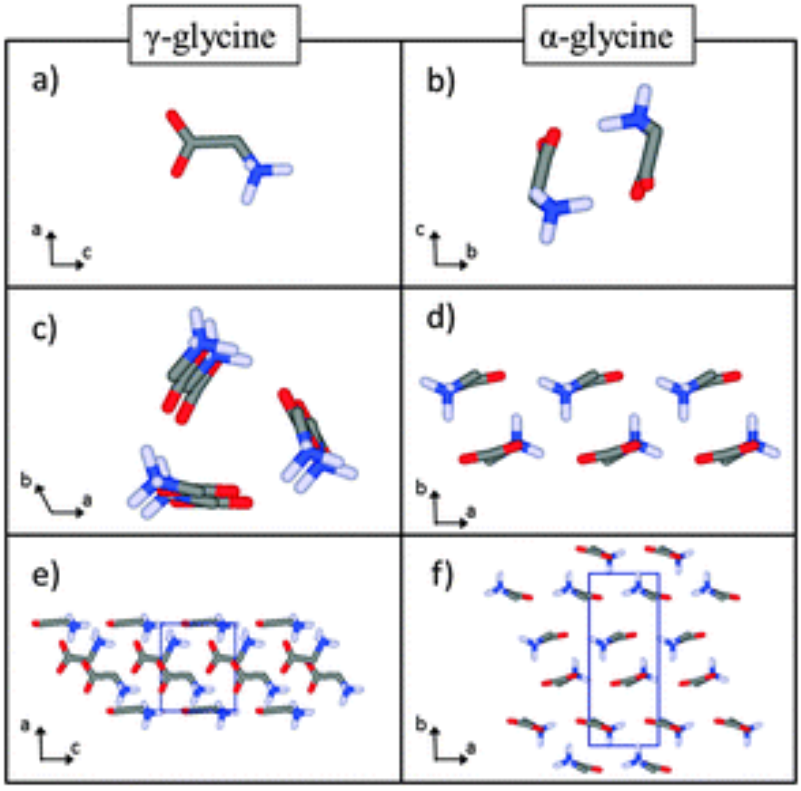

Figure 1.3: Crystalline structures of a) γ-glycine and b) α-glycine[14]

Glycine can form in three polymorphic forms; α, γ, and β under ambient laboratory conditions. The α-polymorph is formed at neutral pH and under rapid cooling conditions, the γ-form, the thermodynamically stable polymorph[15], is crystallised under acid or alkaline conditions, from a slow cooling rate, or with the addition of

additives (inorganic salts)[16]. All 3 glycine polymorphs are enantiotropic, the β-polymorph will readily convert to either the α or γ form, and the α and γ polymorph will interconvert to the other if left in saturated solution but both are stable when dry.[17, 18]

Previous work by Garetz *et al*,[19] showed that it is possible at 1.5 supersaturation to selectively crystallise the α or γ form dependent on the polarization of the laser light related to the anisotropic polarizability of glycine molecules. Using circular polarized light, it is possible to form 100% α polymorph and with linear polarized light it is possible to form 100% γ-polymorph. It was believed that the electric field is strong enough to force alignment of the induced dipole in glycine molecules within pre-existing clusters to induce crystallisation of a specific polymorph. The observation is considered the strongest evidence for the optical Kerr's effect to describe laser induced nucleation[20] which will be discussed later (Chapter 1.9.1).

1.3 Supersaturation and metastability

1.3.1 Supersaturation

The driving force for crystallisation is the saturation level of the solution. Solutions can exist in three states; undersaturated, saturated, and supersaturated, which is dependent on the amount of solid in solution relative to the solubility at a given temperature. Solubility is defined as the amount of solid that can be dissolved at a given temperature. If there is less solid dissolved than the solubility, then a solution is undersaturated. When a solution has more solid dissolved in it than the solubility, then the solution is considered supersaturated. When it is in the supersaturated state it is thermodynamically unstable, and in a crystallisation process this instability is will result in crystallisation.

Supersaturation can be expressed using[21]:

$$\Delta c = c - c_{sat} \qquad \textbf{Eq.1}$$

$$S = \frac{c}{c_{sat}} \qquad \textbf{Eq.2}$$

$$\sigma = \frac{\Delta c}{c_{sat}} = S - 1 \qquad \textbf{Eq.3}$$

Where Δc is the concentration driving force, c is the concentration, c_{sat} is the saturation concentration, S is the supersaturation ratio and σ is the relative supersaturation. When $S<1$ solution is undersaturated, when $S=1$ sample is saturated and when $S>1$ then sample is supersaturated.

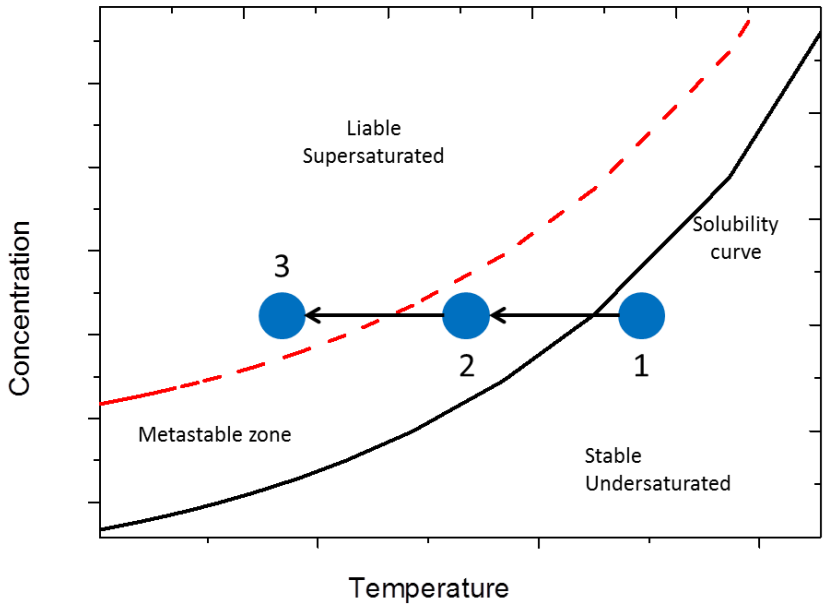

Figure 1.4: Phase diagram for a two-phase system demonstrating the link between solubility, metastability, temperature and concentration. 1) Undersaturated, 2) supersaturated metastable, 3) supersaturated labile.

Solutions that are at or below the solubility line are stable and will not crystallise spontaneously at any time, an induction time of ∞ (figure 1.4 point 1). Once the solution moves past the solubility curve it becomes supersaturated, labile and will crystallise spontaneously (figure 1.4 point 3). However, there is a state where a supersaturated solution, despite being unstable, can remain un-crystallised for several days if not agitated. This solution is considered metastable (figure 1.4 point 2)

1.3.2 Supersaturation generation

For nucleation to happen the solution must be in the thermodynamically unstable supersaturated state. This can be traditionally achieved in three ways, and corresponds to crystallisation techniques.

The most common way of generating supersaturation is by lowering the temperature of the system used in cooling crystallisation. By decreasing the temperature, you lower the solubility of the solvent, generating supersaturation. Cooling crystallisation can be the preferred method as temperature profiles can be easily controlled and thus the supersaturation profile also. It is possible to calculate the potential yield of the crystallisation based on the solubility at the final temperature, and by temperature cycling you can further improve the crystallisation through ripening; dissolving small crystals to grow larger ones. However, an issue associated with this technique is it depends on the change in solubility between starting and final temperatures to be large, if this is not the case it could be impractical to use.

Evaporation of solvent achieves supersaturation by increasing the concentration of the solute by driving off the solvent. The solubility does not change but as the solvent is removed the solute remains and the concentration increases. This method is an alternative when there is a weak dependence on solubility with temperature. There is an issue with crust formation on the walls as the solvent evaporates. However using temperature controlled jackets this can be minimised.

By introducing a solvent in which the target compound is poorly soluble (anti-solvent) the solubility can be altered by changing the solvent composition. For this to be viable the solvent and anti-solvent need to be miscible and the anti-solvents introduction controlled. The effectiveness of the supersaturation generation is dependent on the control of anti-solvent addition and rate of dispersion. A high rate of addition forms localised high supersaturation with a high nucleation rate forming a lot of small crystals. An issue can be that crystallisation occurs at the outlet of the anti-solvent addition, potentially causing blockages in any tubing.

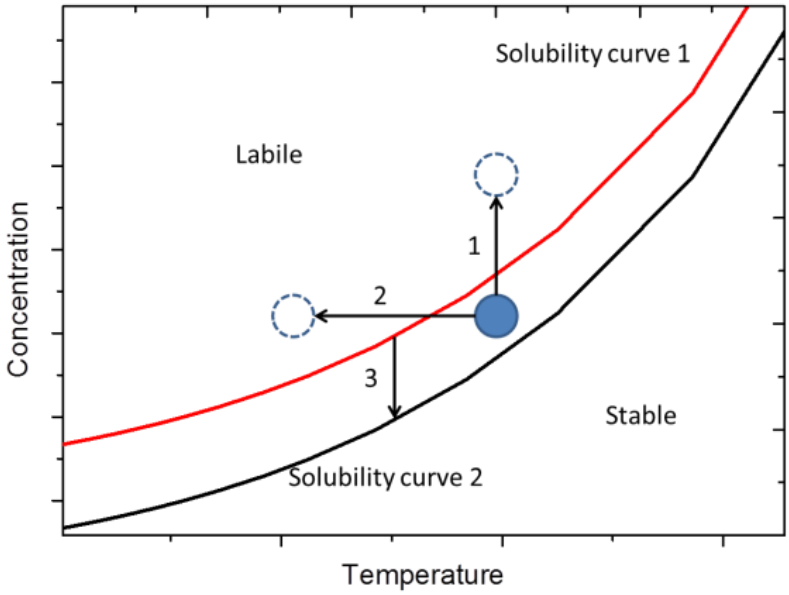

Figure 1.5: Graph demonstrating how supersaturation can be generated. Sample starts undersaturated with respect to the red solubility curve, 1) supersaturation generated by evaporation, 2) supersaturation generated by cooling, 3) supersaturation generated by anti-solvent addition. Expressed with respect to the black solubility curve in the new solvent composition.

1.4 Crystal Nucleation from Solution

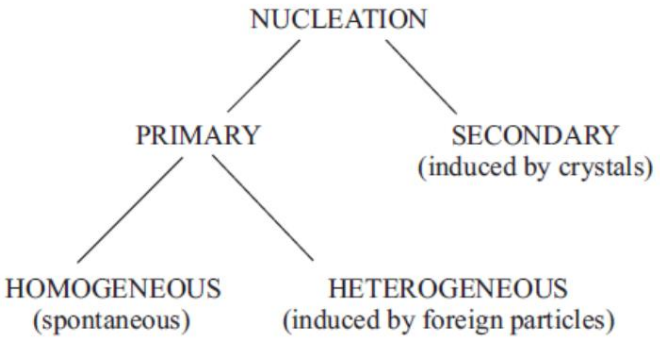

Figure 1.6: Diagram of the classification of different nucleation types[21] (reproduced from reference)

Nucleation is the primary step in crystallisation. It is the aggregation of molecules in solution into a dense nucleus, moving from the solution phase to the solid phase. Nucleation can be classified into different types; secondary, which is the nucleation by pre-existing crystalline material; primary which can be heterogeneous, induced by a foreign entity such as solid impurity or hetero seed (crystalline material added as a surface for nucleation and growth of the API typically by epitaxy); and homogeneous, which is considered completely spontaneous. Homogenous nucleation can be induced by mechanical external shock,[22] electric field,[23] ultrasound [24] or waiting after the supersaturation has been produced via cooling, evaporation or anti-solvent addition.

1.4.1 Classical Nucleation Theory

Classical nucleation theory was originally used to describe formation of liquid droplets by condensation from the vapour phase. Described as the molecular aggregation by a sequence of bimolecular additions, subsequent additions grow the cluster to a critical size. The nucleus then undergoes a molecular reorientation into a crystal lattice. Once a nucleus grows to a critical size, $r \geq r_{crit}$ it will continue to grow until a liquid droplet is formed. Nuclei smaller than the critical size, $r < r_{crit}$ will dissolve.[21] (Fig. 1.7)

$$A + A \rightleftharpoons A_2 \quad \textbf{Eq.4}$$

$$A_2 + A \rightleftharpoons A_3 \quad \textbf{Eq.5}$$

$$A_{n-1} + A \rightleftharpoons A_n \quad \textbf{Eq.6}$$

The adoption of this theory to the phase transition of liquid to crystal comes from the work of Volmer[25], Becker and Döring[26]. With respect to spontaneous homogenous nucleation, it can be described in terms of changes in Gibbs free energy. Where ΔG is the overall Gibbs free energy, ΔG_s the excess free energy between the surface of the particle and the bulk of the particle (positive value), and ΔG_v excess free energy between large particles and the solute in solution (negative value). The change in the

free energy passes through a maximum which corresponds to the critical radius, r_{crit}, of nuclei needed to grow into a crystal.

$$\Delta G = \Delta G_s + \Delta G_V \quad \textbf{Eq.7}$$

$$= 4\pi r^2\gamma - \frac{4}{3}\pi r^3 AlnS \quad \textbf{Eq.8}$$

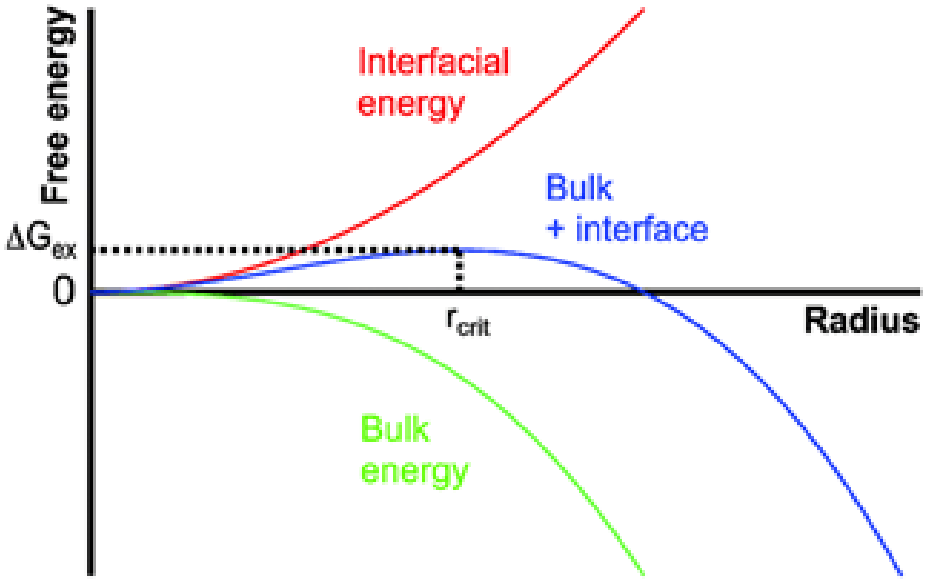

Figure 1.7: Diagram of Gibbs free energy showing the effect of radius generated using the classical nucleation theory[27]

Where r is the cluster radius, γ is the interfacial tension, S is the supersaturation, A = ρRT/M, R is molar gas constant, T is the absolute temperature, M is molar mass, ρ is the mass density.

There are however some assumptions that must be made for CNT to be considered valid.

- The nuclei are smooth spherical droplets that have a consistent density at both the surface and bulk
- The surface tension from the curvature of the nuclei is ignored.

- The growth of the nuclei is the resultant of single molecular additions; the nuclei are static so collisions between clusters are ignored.
- The nuclei form instantaneously after supersaturation is generated
- The nuclei do not change the vapour state surrounding them.

  It is with these assumptions that the problems and shortcomings of classical nucleation theory are found.

1.4.2 Problems with Classical Nucleation Theory

Whilst CNT is a commonly used and accepted model for describing and calculating nucleation rates, there are several problems that have been identified that can lead to large difference between calculated and experimental values. This can be seen in condensation experiments in alcohols, [28] where the values used in the calculation for nucleation of liquid from vapour are well known with good degree of accuracy. However, the difference between calculated and experimental rates was several orders of difference. For crystallisation of binary systems, these values used to calculate nucleation rates are not known with the same degree of accuracy, thus it can be expected these differences to be potentially even greater.[29] Furthermore, the assumptions made for the CNT model to be applicable to the liquid solid phase transition appear to be an oversimplification of crystal nuclei. The model assumes that the droplets that become nuclei have a constant density at both the surface and in the bulk. However, it has been shown that the density at the surface is greater than in the bulk.[30] Furthermore, the assumption is that clusters are just present in solution the moment supersaturation is generated and their size distribution is unchanged and only the number in solution changes. However, there requires a time period in order for the steady state to materialize.[31, 32] The assumption that collisions between clusters are ignored because they only form for monomer addition also means that the clusters are stationary, which is an issue with calculating the nucleation rate as the pre-exponential factor is related to mobility. Additionally, it has been found that cluster-cluster interactions do play a role in nucleation[33].

The oversimplification of the model can also be seen in how it was adapted from a liquid-vapour description, where the orientation of molecules is not taken into consideration. However, the orientation and organisation of molecules into a crystal

lattice is a necessary step, so a two-step nucleation model was proposed to address this.

1.4.3 Two-step nucleation

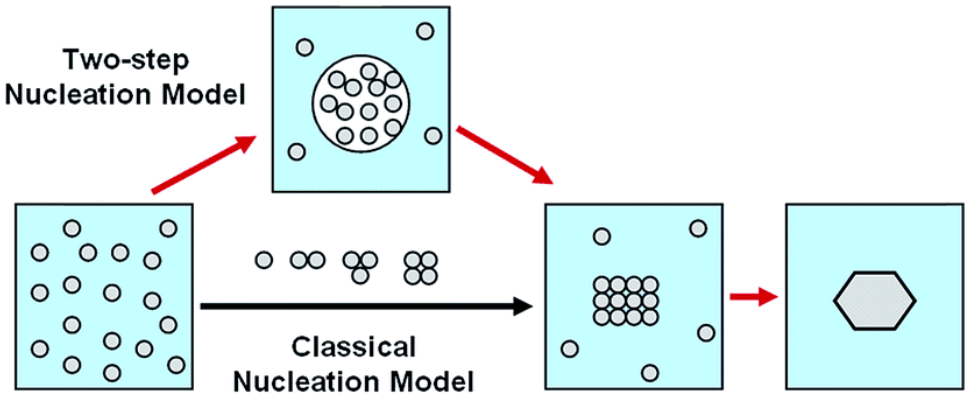

Figure 1.8: Visualisation showing differences between Classical Nucleation Theory and two-step nucleation theory. [34]

An alternative to classical nucleation theory is the two step nucleation, which differs in that it takes into account the formation of mesoscale solute clusters in solution before a crystal nuclei.[35]

The computational work done by ten Wolde and Fenkel[36] observed the formation of highly dense clusters in globular proteins. The mechanism passed through a self-assembly of monomers in solution to a liquid-like mesoscale metastable dense solute cluster. The monomers within the cluster will undergo a reorganisation and a crystal nucleus will form. Classical nucleation theory has only one free energy barrier; monomer addition to form the crystal nuclei. The two-step mechanism has two energy barriers; the first, the assembly of monomers into the dense cluster, the second, the energy required to re-organise the molecules into the crystal nuclei (figure 1.8).

Evidence that supports the two-step nucleation theory is seen in crystallisation of proteins. Light scattering techniques have demonstrated the presence of the pre-nucleating clusters in lysozymes, [37] amyloid beta peptides[38], and haemoglobin polymers.[39]

1.5 Probability distribution of induction times

A way of determining nucleation rates from a series of identical small-scale experiments has been devised using the cumulative probability distribution of induction times based on Poisson distribution.

Poisson distribution is the probability of a number of events occurring in a population of number of samples, in this case the number of vials crystallising out of the total number tested, in a fixed time interval where the probability of the event occurring is independent of preceding events. From this understanding the nucleation rate of a system can be determined from a series of small scale experiments through measurements of their induction time as a cumulative probability distribution.[40] For constant supersaturation, appearance of a nucleus can be regarded as a random process and appearance of the nuclei is independent of the probability of forming at a given time. An example of how this data of these samples is processed is shown in figure 1.9.

$$P_0 = \exp(-N) \quad \textbf{Eq.9}$$

P_0 probability that no nuclei are formed
N average number of nuclei formed

$$P_{\geq 1} = 1 - P_0 = 1 - \exp(-N) \quad \textbf{Eq.10}$$

$$N = JVt_J \quad \textbf{Eq.11}$$

$$P^*(t_J) = 1 - \exp\left(JVt_J\right) \quad \textbf{Eq.12}$$

$$P(t) = 1 - \exp(-JV\left(t - t_g\right)) \quad \textbf{Eq.13}$$

$$P(t) = \frac{M^+(t)}{M} \quad \textbf{Eq.14}$$

P* probability at least 1 nuclei being detected,

V volume,

J nucleation rate,

t detection time,

P(t) probability of detection ≤t, (cumulative probability distribution of induction times)

t_g growth time,

M^+ number of samples that yielded crystals,

M is the total number of samples.

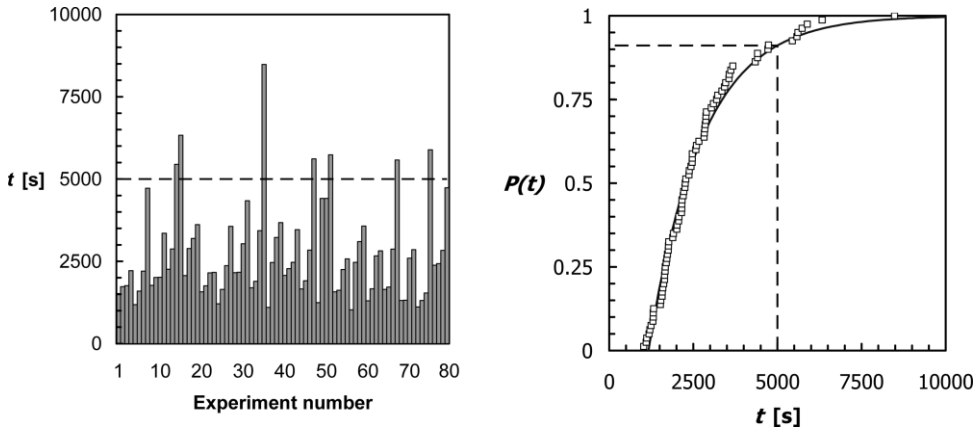

Figure 1.9: Example of probability distribution of induction times[40]

In a recent paper the cumulative probability and nucleation rates in competing polymorphs was disscussed.[41] They concluded through a series of equations and theoretical experiments that both the sum of the cumulative probabilities for the respective polymorphs (Eq 16) and the respective nucleation rates for each polymorph (Eq 15) must equal the total values. Furthermore, the ratio of the nucleation rates is equal to the ratio of the nuclei of each polymorph formed (Eq 17). This can be seen in figure 1.10, where a) shows that non-competing polymorphism have independent nucleation rates and cumulative probabilities (P(t) =1), b) shows competing polymorphism where the nucleation rates and cumulative probabilities are linked (Eq 15-17). Polymorphism results will be discussed in chapter 6.

$$J_T = J_\alpha + J_\beta \quad \textbf{Eq.15}$$

$$P_t = P_\alpha + P_\beta \quad \textbf{Eq.16}$$

$$\frac{J_\alpha}{J_\beta} = \frac{N_\alpha}{N_\beta} \qquad \textbf{Eq.17}$$

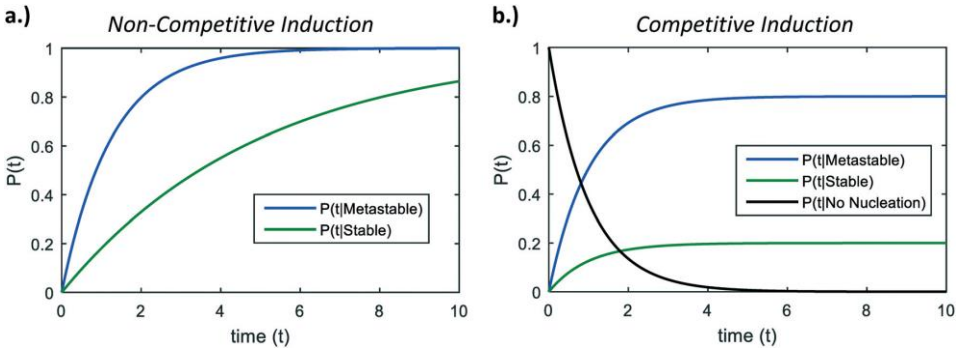

Figure 1.10: a) Induction times of two non-competing polymorphs, b) induction probabilities in a system with competitive polymorphism.

When there are two nucleation regimes in a probability distribution (bimodal distribution) it is possible to estimate nucleation kinetics of both regimes through an adaptation of ter Horst method. To describe the bimodal nucleation kinetics quantitatively, a function based on a weighted sum of two exponential distributions with different time constants was used, as shown below. This model assumes that there are two independent nucleation regimes, each with a constant nucleation rate,

$$P(t) = A(1 - \exp^{\left(-\frac{t-t_d}{\tau_1}\right)}) + (1 - A)(1 - \exp^{\left(-\frac{t-t_d}{\tau_2}\right)}) \qquad \textbf{Eq.18}$$

Here *A* is the fraction of samples that underwent laser induced nucleation, τ_1 is the characteristic time for the laser induced nucleation regime, τ_2 is the characteristic time for the spontaneous nucleation regime, t_d is the delay time between laser irradiation and appearance of the first crystals, which can be considered growth time and can be confirmed by using published growth kinetics, and *t* is time after laser irradiation. Note that the nucleation rate *J* is related to the characteristic time of nucleation τ as $JV=1/\tau$, where *V* is the sample volume. It is possible to get the nucleation rates from τ. However, the value that should be used as V is not clear between the volume of the sample and volume which is irradiated.

1.6 Problems in crystallisation

Many drug compounds have difficulties in forming a stable crystal form. [42] This has led many pharmaceutical companies to pursue polymorphic screening to identify what stable crystal forms are available. However, this can be a time consuming and costly process, and can still not yield any stable crystalline form. As molecules are becoming more difficult to crystallise using traditional techniques such as cooling, evaporative, and anti-solvent, there is now an effort to investigate the use of new crystallisation methods, such as laser induced, ultrasound induced, and the use of co-crystals; as well as ways of predicting if a molecule will be difficult to crystallise by analysing molecular markers and attributes such as flexibility, solvent interactions, and number of conformers. Predicting crystallising tendency could be a useful way of screening initial drug candidates that could be prescribed as a solid formulation. There is currently a lack of published literature on markers such as size, polarity, and experimental conditions,[43] that would help predict if molecules will have difficulties crystallising.

One marker that can signal if a molecule will have difficulty crystallising is having multiple stable conformers or slow interchanging conformers in solution. Conformers can be stabilised in solution via steric blockages and intermolecular hydrogen bonding restricting bond rotation[44] resulting in a high energy barrier, and slow inter-conversion. The presence of multiple conformers in solution inhibits nucleation by diluting the effective concentration of the crystallisable conformer in solution relative to the total concentration[2] so a supersaturated solution will be undersaturated in the crystallisation conformer. Furthermore if the crystallisation conformer has a higher energy level with respect to the other conformers in solution, there will be less in solution due to its thermodynamically favourability.[45, 46] Evidence for this can be seen in alditols where galactitol, and mannitol crystallise easily, sorbitol and idlitol are more difficult to crystallise, and xylitol, which has a disappearing polymorph, which crystallises with even greater difficulty. This can be explained by increased number of stable geometries, due to the increased flexibility from extra carbons.[2] This effect is also exemplified in L-glutamic acid whose nucleation is dependent on the amount of the correct conformer in solution which varies with temperature.[47] Further evidence indicating that the number of conformers can inhibit the nucleation rate can be seen

in the study, Baird *et al*[48] where, 51 small organic molecules were tested for crystallisation from undercooled melts and by rapid evaporation.[48] It was observed that similar results occurred in both crystallisation methods suggesting that the method of crystallisation is less important and that molecules have physiochemical properties that determine if a compound will crystallise. Subsequent work made conclusions that the molecular mobility, and configurationally diversity, which is related to the molecular weight, are important indicators of ease of crystallisation.[49-51]

The idea that molecular mobility can act as an inhibitor of nucleation can be seen in aqueous citric acid solution, when the supersaturation increases there is a steep increase in viscosity and this increase in viscosity corresponds to a decrease in nucleation rate.[52] This observation was then followed up by demonstrating the suppression of ice crystallisation in high viscous citric acid solution droplets.[53] The reduced molecular mobility in citric acid solutions was attributed to a large number of hydrogen bonding networks the molecule can form.

Analysis of databases using statistical models is another way of investigating molecular crystallisation propensity. Analysis of both the Cambridge crystallography and ZINC databases, excluding salts and organometallic complexes, for single crystals of drug-like compounds revealed that it only required two descriptors, these were the molecular volume and the number of rotational bonds, to identify if a molecule would crystallise with 80% success rate. Similar trends have been observed in an analysis of published data of acrylamide compounds. It was identified that the most important descriptor was the number of rotational bonds.

1.7 Laser-induced nucleation

There are several ways in which crystallisation can be induced, cooling, anti-solvent, evaporation etc. However, in industries where compounds are becoming increasingly more difficult to crystallise, new methods are being explored such as ultrasound induced crystallisation or co-crystallisation. One of the latest techniques being investigated for its utility in addressing this issue of crystallisation tendency is laser induced nucleation. Laser induced nucleation is being investigated due to its non-invasive spatiotemporal control of nucleation with influence of polymorphism and

morphology. Whilst in this thesis, it will solely discuss non-photochemical laser induced nucleation (NPLIN) using nanosecond pulses, the other forms for laser induced nucleation, continuous wave, photochemical, and femtosecond non-photochemical, will be discussed briefly.

1.7.1 Photochemical

The use of photochemical laser-induced nucleation has been demonstrated to be highly effective in forming single crystals of proteins but has also been shown to nucleate larger organic molecules. The mechanism by which photochemical laser induced nucleation happens is known. There is an absorption of the irradiation wavelength by the molecule of interest, the absorption breaks bonds in the molecule which form radicals, the radicals then react causing a chemical reaction via intermediates, forming the desired product which has a lower solubility than the starting material[54] and has shown an ability to control some particles properties such as morphology. However, an issue with this form of laser induced nucleation is that is destructive and the formation of radicals, which can be difficult to control, make this a less favoured nucleation technique.

1.7.2 Continuous wave (CW)

Continuous wave laser induced nucleation has been shown to achieve polymorphic control based on the laser intensity and polarization. Experiments that irradiated supersaturated and under saturated D_2O Glycine solutions with near Infrared-CW with the focal point at the air-solution interface,[55] after a few seconds of irradiation single crystals would form at the focal point. Rungsimanon *et al* were successful in demonstrating control of the resultant polymorphic form by irradiating with either circular or linear polarised light. They attribute this control in polymorphic outcome to a mechanism that is a combination of alignment of molecules with the electric field, aggregation of trapped molecules, temperature changes, and photon pressure.[56]

1.7.3 Femtosecond pulsed (FS)

There are several similarities between nanosecond and femtosecond laser induced nucleation. Both are non-photochemical and demonstrate high spatiotemporal control, however, due to the differences in pulse lengths these mechanisms could be different as a mechanism happening in the nanosecond timescale is highly unlikely to happen in the femtosecond scale. FS mechanism is believed to induce by multiphoton absorption leading to heating and vaporisation, with shockwaves and cavitation bubbles as a result, this agitation is sufficient to induce nucleation.[57] It has been demonstrated the repetition rate is an influence on several properties including nucleation efficiency, morphology, and number of crystals formed. By using a single pulse it is possible to nucleate a single crystal, increasing repetition rate allows for the formation of more crystals.[58]

1.8 Non-photochemical laser induced nucleation

NPLIN offers a possible way of achieving surgical homogeneous nucleation, where there is high spatiotemporal control of nucleation events. This method of crystallisation allows for the control or influence of polymorphism without the need for additives, and it has been shown to work across a wide range of compounds, small and large salts, proteins, and small and large organics. Much like other crystallisation techniques NPLIN provides parameters that can be altered to achieve the desired crystal properties.

1.8.1 Discovery, urea, glycine and L-histamine

Non-photochemical laser induced nucleation was observed by Garetz *et al* [59] in experiments attempting to observe second harmonic generation in aqueous urea solutions using a nanosecond pulsed Q-switched Nd:YAG laser. They deduced because the light used was near infrared, 1064 nm, that a photochemical reaction was unlikely. Furthermore, they observed the orientation of crystals formed in solution was dependent on the polarization used. However this has been shown to happen not to a significant degree.[60] Using the 20 ns pulses with a beam diameter of 2 mm, frequency of 10 Hz and a power density between 50 and 250 MW cm^{-2}, they tested

aqueous urea solutions supersaturation in the range of 1.10-1.29. Samples used were aged a week as a period for steady state to be established in accordance with the two-step nucleation theory. They observed that the 1.10 supersaturated samples did not undergo laser induced nucleation which indicates a concentration threshold. It was from this work that the optical Kerr's effect was suggested as a possible mechanism (see section 1.9), that the orientation of the urea crystals formed was a result of alignment of molecules within cluster with the polarization of the laser light. Further work investigating laser induced nucleation of urea was done by Matic *et al* [61], who investigated intensity and wavelength dependence on nucleation efficiency. This was done by irradiating 30 identical 1.23 supersaturated aqueous urea solutions after ageing 2-4 days, for 1 minute, (1.85 mm beam diameter, 7ns pulse duration at 10 Hz pulses), changing the intensity, wavelength and polarization. Their results discovered the presence of an intensity threshold, 0.02-0.06 GW cm^{-2}. A sample would not crystallise when irradiated with intensity below this value. They demonstrated that the 532 nm threshold was lower than the 1064nm, and as intensity was increased, the nucleation efficiency would increase.

After NPLIN discovery in 1996, the next system investigated by NPLIN was aqueous glycine solutions.[20] Irradiating 1.5 supersaturated solution for 1minute with 0.7 Gw cm^{-2} intensity (2 mm beam diameter, 7ns pulse duration, at 10Hz repetition rate). 30 minutes after irradiation small crystals were noted at the base of the samples. Similar to urea, glycine has an axis where a dipole could be induced and then be aligned. It was observed that with a linear polarization of light that only the less common γ-polymorph was formed. This research was continued by Garetz *et al*[62], who investigated the effect that changing supersaturation and laser polarization have on the nucleation efficiency and polymorph of the resultant crystals. Samples ranging 1.3-1.7 supersaturation were tested with both linear and circular polarised light. A key discovery was polarized switching which will be discussed in greater detail in the mechanism theories. A similar effect could be seen in L-histamine irradiated with green 532 nm, 0.27GW cm^{-2} (7 ns pulse duration, frequency 10 Hz) which influenced the resultant polymorph. Samples with a supersaturation between 1.4-1.6 showed the behaviour of circular light favoured A-polymorph whilst linear gave a mix of both A and B polymorph.

1.8.2 Ionic solids, KCl, KBr and Ammonium chloride

Ionic molecules have been shown to undergo laser induced nucleation by Alexander *et al* [63] using single pulses to produce multiple crystals in aqueous potassium chloride solutions. Irradiation of 1.053-1.102 supersaturated solution was with a single pulse of 20 mm diameter, 1064 nm and an intensity of 6.4 MW cm^{-2}. Much like organic molecules they observed a threshold intensity and supersaturation below which laser induced nucleation would not be possible. Further work by Ward *et al* [64] found that there was no dependence on nucleation efficiency with pulse duration but with peak pulse intensity. Subsequent work investigating laser induced nucleation in potassium halides[65] investigated the effect that changes in temperature and wavelength can have on nucleation efficiency. It was discovered that KBr had higher nucleation probability than KCl at both 532 nm and 1064 nm after a single pulse at several energies. Furthermore, it was demonstrated that nucleation efficiency was greater in samples irradiated with 532 nm than 1064 nm. For KCl samples two temperatures were tested, 23 °C and 33 °C, and it was found that samples at 33 °C had a higher nucleation rate than those irradiated at 23 °C. Observations made in these experiments would go on to form part of the isotropic polarizability theory (see section 1.9.3).

1.8.3 Drug-like compounds in organic solvents

Non-photochemical laser induced nucleation has potential to be a useful technique in industrial crystallisation, and in order for this it must be demonstrated on industrial systems such as small organic molecules in organic solvents. As more research is being done this is one area that is attracting more interest. The first demonstration of non-photochemical laser induced nucleation in drug-like molecules was by Biré *et al* [66] on carbamazepine in acetonitrile and methanol. Irradiations of supersaturated solution ranging from 1.4-1.6 were tested with powers 0.05-0.5 GW cm^{-2} for 1 minute with using 532 nm wavelength, linear and circular polarized light. Carbamazepine was chosen for investigation due to it exhibiting multiple polymorphs[66], and it was observed that non-photochemical laser induced nucleation could be used to influence the polymorphic outcome of the crystals by changing the polarization, solvent, and supersaturation. In methanol all solution supersaturations tested, both linear and circular polarised light yielded form III. However, for acetonitrile with circular polarised

light, the majority polymorph was form III. Linear polarised light at 1.1-1.2 supersaturation equal amounts of form I and III were formed, but at 1.3 supersaturation the majority was still form I but an increased number of form III present, with some crystals showing both form I and III. The second system selected for investigation was sulfathiazole [67] in a water/ethanol solvent mixture. This molecule was selected for the same reason carbamazepine as it showed several polymorphs. Supersaturated solutions ranging 1.1-1.7 supersaturation were irradiated for 1s (10 pulses) or 60s (600 pulses) of intensities 0.15-0.3 GW cm^{-2} of linear and circular polarized light. It was observed that as supersaturation increases, the number of crystals formed increases, and as irradiation time increases, the number of crystals formed increases. As the number of crystals formed increases, the size decreases. The influence on the polymorphic form was that linear polarized light yielded more form IV, and circular polarization gave majority form III.

1.9 Mechanism Theories

Laser induced nucleation, relative to other forms of nucleation, is fairly infant in its development and implementation. Since its discovery in 1996, like most crystallisation processes the mechanism is still largely unknown. There are four competing theories on how non-photochemical laser induced nucleation (NPLIN) mechanism can produce crystals. The first, optical Kerr's mechanism was first proposed by Garetz *et al*[68] in their 1996 paper discovering NPLIN, since which several experiments have been carried out which support this mechanism. The second, cavitation theory, demonstrated by Soare *et al*[69] in 2007. The third, a theory developed by Ward *et al*[64] in relation to the structural arrangement of molecules reducing entropic energy requirement, called isotropic polarizability. The final proposed theory is the presence of photoactive impurities that creates an environment favouring crystallisation.

1.9.1 Optical Kerr's Effect

The optical Kerr's mechanism was first suggested and formulated from the initial observations in the discovery of NPLIN, the dramatic reduction in nucleation time of urea estimated to be 10 times faster [59]. Attempting to observe second harmonic generation in aqueous urea solution, they noticed that pulses from a Q-switched Nd:YAG laser would induce nucleation in their samples. They initially ruled out a

photochemical reaction as the light is near infra-red, and ruled out presence of foreign bodies as the vial was heat sealed. They also noticed that the needle like crystals formed in line with the polarization of the light, horizontally polarized light crystals appeared approximately horizontally aligned and vertically polarized light yielded vertically aligned crystals. This lead to the conclusion of an alignment of the molecules with the light. Urea has a permanent dipole along the C_2 axis[70] which is also the most polarizable[71] and is parallel to the growth of needles in solution.[72] However, they noted that the frequency of the electric field of the light (E) was too fast to influence the permanent dipole but could influence the induced dipole $\mu_{ind(t)}$, generating an alignment torque (figure 5). The collection of this alignment torque for the molecules in a pre-nucleating cluster results in a reduction of the entropic contribution of the free energy of activation for the induction of nucleation.

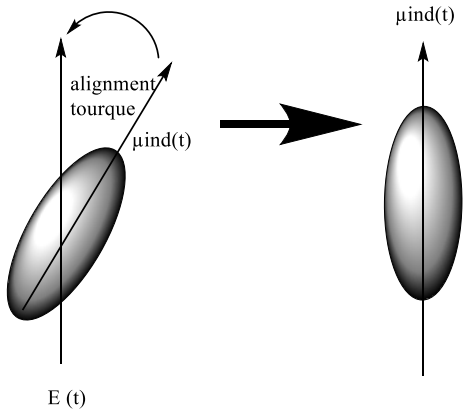

Figure 1.11: visualisation of the optical Kerr's effect

The next evidence for the optical Kerr's effect in NPLIN was in 2001 when Garetz *et al*[20] were able to nucleate the unexpected γ-polymorph glycine from water. Glycine has three known polymorphs; α, β, and γ,[73-76] with the α polymorph being the most thermodynamically stable form, which both β and γ will convert to. Previously γ was formed by the addition of additives.[77, 78] This is because the glycine is zwitterionic, forming hydrogen bond which directs the formation of the α-polymorph. The electric field associated with the laser pulses $6X10^7$ V m^{-1} which would be sufficient to cause a partial small alignment causes the molecules to experience a torque aligning with the most polarizable axis.[79] The most polarizable axis in glycine molecules is the C^{α}-$C'O_2$[80], and the influence of aligning molecules alters which directional axis the

bonding interactions will form along, (*z*) γ-glycine, (*x*) α-glycine. They concluded that the optical Kerr's effect must be strong enough to overcome the hydrogen bonds to orientate in a different crystal structure. They calculated that the effect of one single molecules torque would not be strong enough to account for overcoming the hydrogen bonds. However, the collective effect of aligning of the molecules might be great enough to form the γ polymorph. Further investigation on the glycine in water system by Myerson *et al*[62] found that you could control the polymorph formed by using differently polarised light, and could be more likely to induce nucleation if the pulse of laser light was of greater intensity.

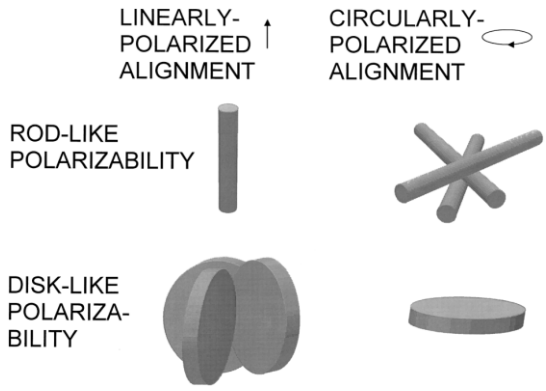

Figure 1.12: Alignment of molecules with different polarizations of light[62] demonstrating that rod like polarizability is more effectively aligned by linear polarised and disk like polarizability more effectively aligned to circular polarisation light.

They found that linearly polarised light will produce γ-polymorph and circularly polarised light will always form α polymorph further enforcing the idea of an aligning effect influenced by the electric field of the light. This observation of polarized switching of the polymorphs allows for absorption to be ruled out as a photon of energy being absorbed would have the same effect regardless of the polarisation. Their later work on urea[61] would develop the threshold intensity aspects of the optical Kerr's mechanism as well as investigate the influences of wavelength. Furthermore, the optical Kerr's mechanism predicts that threshold intensity is independent of wavelength. However, their experiments investigating the effect of different wavelengths and polarisation showed that this was not the case (figure 1.13). The difference in threshold between 1064 nm and 532 nm can be attributed to the

differences in the absorption coefficient of de-ionised water. The difference in the greater absorption coefficient of 1064 nm and 532 nm is 0.1 cm^{-1} and 5x10-4 cm^{-1} respectively. This would lead to greater heating of the sample and reduce the supersaturation increasing the intensity threshold. The difference in the threshold intensity for polarisation can be attributed to the different directional alignment of the polarizable axis. The alignment of molecules with the linear polarized light is along the axis that creates stronger interactions, while the alignment by the circular light is weaker (figure 1.13). They found that NPLIN in urea had a lower intensity in linear polarised light adding to the alignment theory of pre-nucleated clusters. However, they also found that near infrared (1064 nm) had lower efficiency and higher threshold than green laser light (532 nm). They attributed this to greater absorption by the solvent (water) at the near infrared laser light resulting in localised heating stabilising the system, but still asserted that this was in line with the optical Kerr's mechanism. The greatest evidence of the optical Kerr's effect, the polarised switching of the laser light resulting in formation of different polymorphs, would be further investigated and demonstrated by Xiaoying Sun *et al*[81, 82] in greater detail in glycine and for the first time in l-histidine.

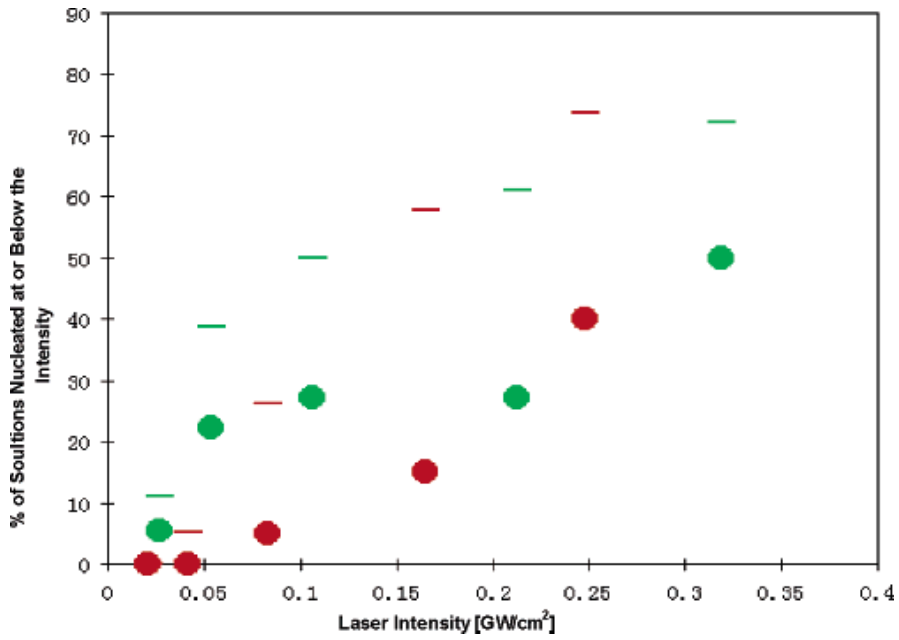

Figure 1.13: Nucleation efficiency of urea irradiated laser light. Circles are circular polarised light, lines are linear polarized light. Red is 1064nm, green is 532nm

Polymorphic control of glycine had been demonstrated with a dependence on the polarisation of the light. This was expanded upon through the dependence on supersaturation level. They were able to show there was great dependence on the supersaturation of solution and of the polymorphic outcome NPLIN where lower levels of supersaturation would selectively form α-polymorph independent of the polarisation of the laser light, and higher supersaturation would selectively form γ-polymorph. They were also able to demonstrate a polarised switching window in glycine, a supersaturation range where it is possible to obtain different polymorphs depending on the polarisation of light, linear polarised light forming γ and circular polarized light giving α-form (figure 1.14).

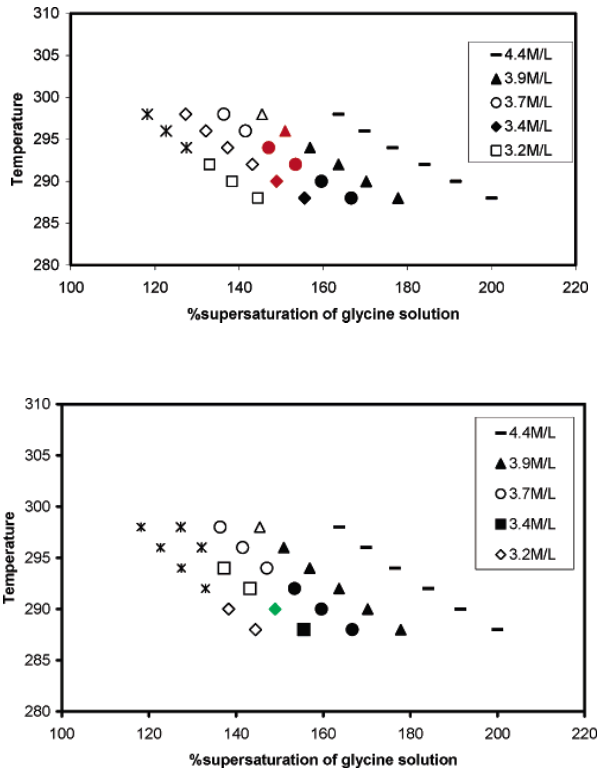

Figure 1.14: Polymorphism formation in NPLIN with near infra-red light at 1064nm wavelength and 0.46GW/cm^2 (top), green light at 532nm wavelength and 0.24GW/cm^2 intensity (bottom). Filled in black symbols indicate that both linear polarisation (LP) and circular polarized light (CP) form $_\gamma$-glycine. Open symbols indicate that both LP and CP form α-glycine. Red symbols indicate polarized switching. Asterisk symbols indicate that no NPLIN was observed. [19]

The NPLIN investigations on l-histidine revealed similar trends to those found in glycine. Their findings in l-histidine were similarly supportive of the optical Kerr's effect through the polarized switching window, in this case circularly polarized laser pulses tended to nucleate the orthorhombic A polymorph, whereas linearly polarized pulses tended to nucleate a mixture of the orthorhombic A, and monoclinic B polymorphs. These observations supported the optical Kerr's hypothesis by suggesting that the alignment of the molecules' hydrogen bonds promoted the growth of one the crystal structures.

However, several calculations [83] have since suggested that the optical Kerr's effect is insufficient to explain the dramatic reduction in crystallisation time. The alignment of formed urea crystals with the polarization of light was shown not to be statistically significant [60]. Furthermore non-photochemical laser induced nucleation is observed in ionic compounds where no dipole could be induced so the mechanism could not be the cause, since then alternatives explanation have been proposed.

1.9.2 Cavitation

The cavitation theory is one alternative that has arisen from the short-comings of the optical Kerr's effect. Ten years after the discovery of NPLIN, it was observed that bubbles formed near the site of the laser pulse and the subsequent crystals formed at or near the site of the bubbles.[84] Work done by Nakamura *et al*[84], investigated the effect on femtosecond laser pulses on supersaturated solutions of anthracene. They noted that solutions crystallized immediately after irradiation in the vicinity of the focal point. They also note that the energy of crystallisation is in agreement with the energy required to induce bubble formation. Firstly, the growth and collapse of the bubble results in fluctuation in pressure and concentration, secondly, the collapse of the bubble results in a shockwave which similarly generates pressure and concentration fluctuations and thirdly, the surface of the bubble provides a surface for hetro-nucleation to occur. (figure 1.15)

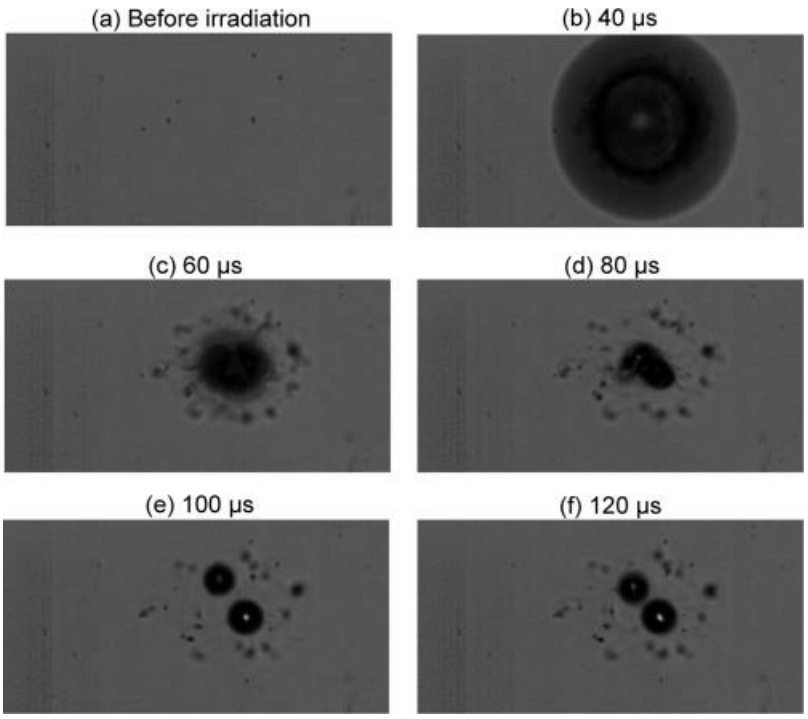

Figure 1.15: microscopic images of effects of femtosecond pulse of laser radiation[69].

Similar observations were made by Soare *et al*[69] using nanosecond laser pulses on supersaturated samples of aqueous $(NH4)_2SO_4$ and $KMnO_4$ in methanol and ethanol solutions pressed between two glass slides and observed using a high speed camera. They were able to expand on the cavitation theory by identifying the bubbles as having the same dynamics of growth or collapse as vapour cavities formed in microtubes under similar conditions (figure 1.16). Further images have been captured by Knott *et al*[85]. They observed that CO_2 nucleation was induced by laser pulses[86], suggesting that it could not be any form of molecular alignment. They also noted that nucleation of glycine occurred at the sites of the bubble nucleation, however, they were unable to elaborate on why this increased the nucleation rate. Han Liu *et al*[58] were able to demonstrate that nucleation occurred more readily if the pulse was fired at the air-solution interface. This suggests that the forces involved in the crystallisation process are a result of interactions at the vapour-solution interface which are greatest when interacting with the air-solution interface. However, in this experiment there was a use of a dye that absorbs the 1064nm wavelength in an attempt to induce cavitation so it cannot be certain how representative this observation is of what is observed in other NPLIN experiments and observation about the influence on polymorphic form of crystals was not taken into account.

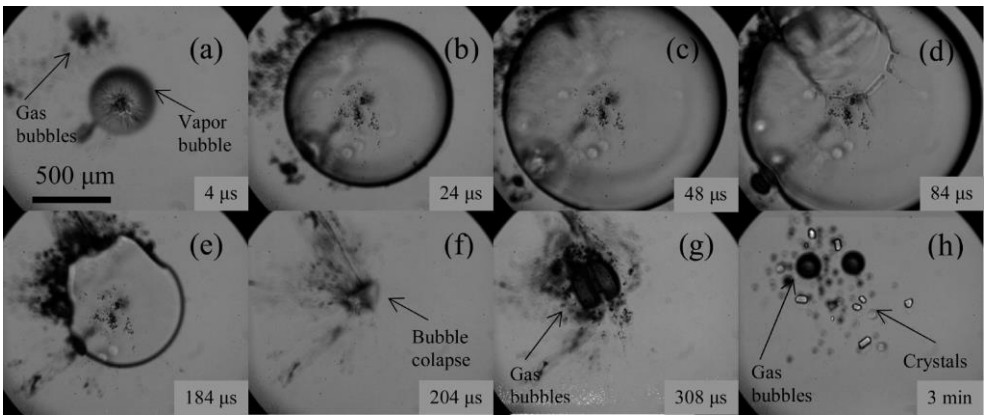

Figure 1.16: Evolution of cavitation bubble with time, $(NH_4)_2SO_4$ solution, 0.4% supersaturation, 100 µm gap size. After the laser pulse, the bubble forms rapidly by vaporisation, grows, and collapses, over a time scale of 200 µs, leaving behind crystals which in time grow to sizes of tens of micrometres [69].

1.9.3 Isotropic polarizability

The third possible mechanism is the theory and model developed by Ward *et al,* from their work with KCl and KBr where observations in the rate of nucleation were not compatible with the optical Kerr's mechanism as no dipole can be induced in ionic molecules. The model they developed is that in the presence of an electric field, the ions will rearrange within a sub-critical liquid like cluster to transform to a solid. (Figure 1.17) Using this model, they were later able to run calculations and predict the presence of a non-zero threshold and a linearly dependence on the probability of nucleation and increasing electric field strength.[63] They were then able to show for KCl that the model fitted very well. However, this cannot account for the observations in polymorphic influence seen in glycine.

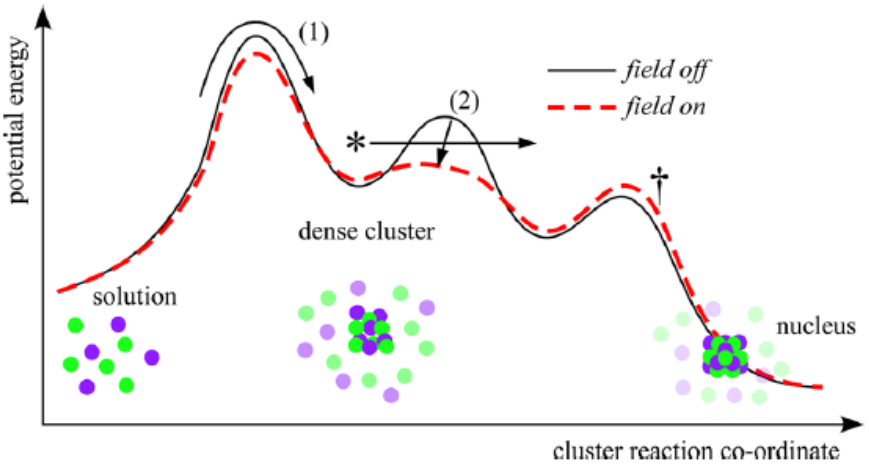

Figure1.17: Diagram illustrating isotropic polarisation mechanism (1) formation of solute cluster, (*) dense cluster becomes crystal nucleus on application of the electric field from the laser pulse (2). [65]

1.9.4 Photoactive impurities

The idea of photoactive impurities has been considered since issues with the optical Kerr's effect were raised, however, there was little evidence for it. Ward *et al*[86], after demonstrating laser induced nucleation of carbon dioxide gas, followed this up by investigating the role impurities have in solution[87]. This was done by filtering solutions of ammonium chloride with 0.2µm polyethersulfone membrane syringe filter which can suppress laser induced nucleation, then doping the sample with iron oxide nano particles. Iron oxide nanoparticles were used after analysis of the filter membrane by inductively coupled plasma mass spectrometry (ICP-MS) showed the largest concentration of ions were Fe 0.44 mg kg^{-1} and phosphate 0.17 mg kg^{-1}. By doping their samples in which laser induced nucleation had been suppressed, they were able to reinstate the laser induced nucleation activity. The stages of the mechanism is described in figure 1.18. Despite being able to bring laser induced nucleation into a sample after being filtered. The theory cannot explain polymorphic observations.

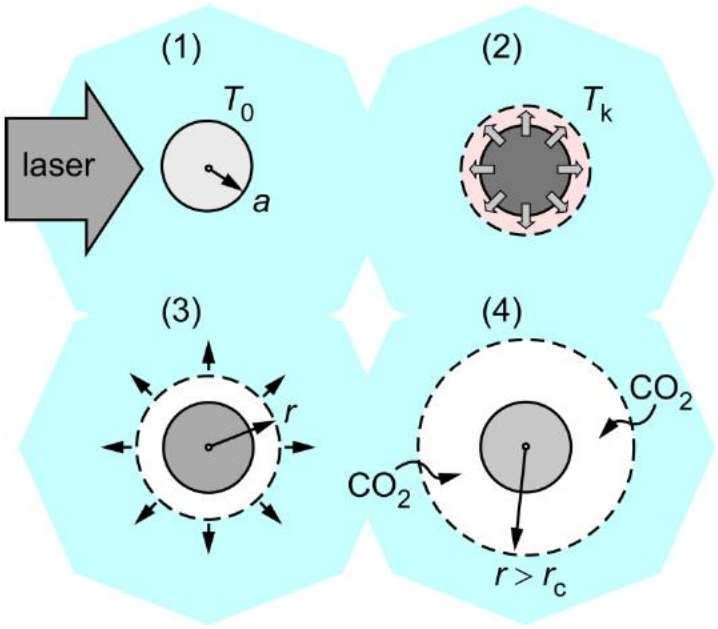

Figure 1.18 Illustration of photoactive impurities theory, (1) laser light is absorbed by nanoparticle of radius a, (2) heat transfer to the surrounding liquid causing vaporisation (3) vapour causes a bubble which expands (4) bubble grows until reaching a critical size bubbles form[86].

1.10 Parameter Identification

1. Supersaturation

   The level of supersaturation has been shown to be an important factor that needs controlling.It has been shown numerous times to influence the likelihood of nucleation occurring, the rate at which the nucleation will occur, at and the polymorphic form that will result. Work by Zaccaro *et al*[20] found that supersaturation determined whether a solution would nucleate when exposed to laser pulses. Too low a level of supersaturation would result in no nucleation, and increased level of supersaturation reduced the nucleation time. And in the case of ionic compounds, Ward *et al*[64] have demonstrated that solutions of KCl exposed to single pulse resulted in single crystals at low supersaturation, but at high supersaturation they have experienced in some cases four crystals formed from single pulses. Supersaturation can influence the polymorphic outcome, which has been shown by the polarized switching window where there is a supersaturation in which polymorphic form can be selected based on the polarisation of the irradiation. Supersaturation would need to be controlled in

experiments which can investigation of the solubility and metastable limit of each system to correctly establish the supersaturation level.

2. Solvent

   Currently there is only one requirement for a solvent to fulfil in order to be used for NPLIN, and that it must not absorb at the irradiation wavelength. This results in absorption and localised heating stabilising the system and changing supersaturation levels, however the work of Ikni *et al*[66] on carbamazepine have shown a rate dependence in the solvent used, They showed faster nucleation in methanol than in acetonitrile.

3. Wavelength (1064, 532, 355nm)

   The different wavelengths influence the effectiveness of NPLIN. This has been shown by Ward *et al*[65] by firing different wavelengths at vials of the same level of supersaturation. They observed that the threshold, the minimum energy level at which NPLIN occurs, is lower at shorter wavelengths.

4. Pulse energy

   The energy that each pulse has must be sufficient to overcome the threshold to induce nucleation; this is controlled from the laser. Higher pulse energy results in a higher probability of crystallisation in glycine[19], urea[61], and carbamazepine[66], and forms more crystals in KBr and KCl[65].

5. Position of radiation (e.g. bulk or interface)

   Work done by Tsung-Han Liu *et al*[58] reveals that the focal point of the laser radiation influences the probability of nucleation. They found nucleation could be increased when the focal point is at the solution-air interface. It has also shown to have an effect on the morphology.

6. Temperature

   Higher temperature has shown a greater nucleation efficiency of laser induced nucleation in KCl and KBr at the same supersaturation.[65]

7. Pulse rate (pulses per minute)

In KCl, single pulses result in the nucleation of a single crystal, while multiple pulses resulted in multiple crystals being formed. However, in other compounds (non-ionic) it can take several pulses to observe NPLIN.

8. Polarisation (Linear and circular Polarization)

Different polarization results in a degree of controlling polymorphic outcome of NPLIN. It was previously reported that NPLIN offered a way of selectively forming a glycine polymorph at a given supersaturation and temperature based on the polarisation of laser light, referred to as polarised switching. At a glycine supersaturation 1.5 you can form 100% of the γ-polymorph using linear polarised laser pulses; the same solutions would form 100% α-polymorph when irradiated with circular polarised laser light.[19] This result however has not been reproduced. Experiments using similar conditions found that it was possible to influence the resultant polymorph, increasing it compared to non-irradiated samples, but they were unable to demonstrate the 100% control. This influencing of the polymorph was also demonstrated in both Carbamazepine[66] and Sulfathiazole.[67]

From these highlighted parameters, a design of experiments will be undertaken to best address how each parameter could influence outcome, could be controlled and be tested in a series of experiments.

1.11 Table summarising available data

Compound	Solvent	Supersaturation (M)	Temp (°C)	Wavelength (nm)	Result	Year	REF
Urea	Water	1.10-1.29	25	1064	Nucleation of urea	1996	[59]
Glycine	Water	1.38-1.45	21	1064	Nucleation of glycine	2000	[20]
Glycine	Water	1.38-1.45	21	1064	γ– polymorph polarized switching	2002	[62]
Urea	Water	1.22	21	1064, 532	Effect different wavelengths, intensity and polarisation have	2005	[61]

Glycine	Water	1.45-1.55	15-25	1064, 532	Supersaturation window polarization switching	2005	[19]
Glycine	Water	1.45-1.55	21	1064, 532	Polarised supersaturation window	2006	[81]
l-histidine	Water	1.40-1.60	21	532	Switching window L-histidine	2008	[82]
NaOCl3	molten	N/A	280	1064	Nucleation of melts	2011	[88]
Glacial acetic acid	N/A	N/A	-9	1064	NPLIN observed for supercooled system	2011	[89]
Glycine with argon	Water	1.253	23	1064, 532, 355	Crystal nucleation after bubble nucleation	2011	[85]
$(NH_4)_2SO_4$ and $KMnO_4$	Ethanol, methanol	1.02-1.06	22.5	532	Cavitation observed	2011	[69]
Carbamazepine	Acetonitrile, ethanol	1.1-1.5	22	532	First reported drug Polarisation effect on polymorph	2014	[66]
Sulfathiazole	Water: ethanol 50%	1.1-1.7	15, 25, 40	532	Demonstrated influence of polarisation of polymorphic outcome	2015	[67]
Glycine	water	1.4-1.6	25	1064	By filtering samples, laser induced nucleation was suppressed	2016	[90]
Ammonium Chloride	water	1.20	22	1064	Was able to make samples undergo laser induced nucleation by introducing iron nanoparticles	2016	[87]
Urea	water	1.5		532	Alignment of urea with polarization of	2017	[60]

					laser pulse is not statistically significant		
Glycine	Water	1.3-1.6	20 and 25	1064	Increased probability of gamma polymorph formed above 1.4 supersaturation	2017	[22]
KCl	Water	1.053-1.102	23	1064 and 532	Laser included nucleation in inorganic salts	2011	[63]
KCl and KBr	water	1.06	23	1064 and 532	Effect of wavelength and temperature	2012	[65]
Urea	water	1.5	23	1064 and 532	Urea crystals do not align with the polarisation of laser light to a significant degree	2017	[60]
Glycine	water	1.5	23	1064 and 532	Laser induced nucleation effect like ultrasound and shock induced nucleation	2017	[91]

Table 1: Summary of publications on laser induced nucleation

2. Methodology

2.1. Sample Preparation

Glycine (Sigma Aldrich, electrophoresis grade ≥99%) and urea (Sigma Aldrich) was used without further purification and deionised water, with conductivity lower than 15µS/m, was obtained from an in-house dispenser (Millipore 1.18 MΩ cm).

Solutions were prepared in an incubator at 333 K using a magnetic stirrer. Supersaturated solutions were made using solubilities of glycine and urea at 298K, 250g/Kg[92] and 1200g/Kg[93] respectively. Supersaturations 1.4, 1.5 and 1.6 correspond to concentrations for 350 g, 375 g and 400 g of glycine/kg of water, respectively. Urea supersaturations 1.4 correspond to 168g/kg urea/kg of water.

Small 2ml HPLC vials (Scientific Glass Laboratories, part number T101/V1, diameter 11mm, volume 2ml) with screw caps were cleaned with deionised water and kept in the incubator at 333 K. The solutions were hot-filled into the HPLC vials at 333 K and then gradually cooled to 298 K over 3-4 hours, followed by holding for 20 hours at 298 K. Samples which crystallised within this time were removed before proceeding further. It has been suggested previously that length of holding time appeared not to influence the outcome of laser-induced nucleation, but this time was used for practical reasons to keep holding time before irradiation consistent for all samples.

2.2. Laser irradiation

The vials were transferred to a temperature controlled water bath kept at 298 K and from there they were moved to a Peltier temperature controlled sample holder and exposed to irradiation by a pulsed Nd:YAG laser (Continuum Surelite II-10) with a wavelength of 1064 nm (pulse duration: 6 ns; repetition rate: 10 Hz). The standard polarization of the laser pulses is linear polarized, and is used in all experiments unless stated otherwise. Circular polarized light was produced using a ¼ wave plate and polarizer purchased from Thorlabs. A 1 mm circular pin-hole was used to select the central portion of the Gaussian beam, resulting in spatial profile that was near to top-hat (figure 2.1). It should be noted that the laser spatial profile will change

considerably as it passes through the circular sample vial, which acts as a powerful cylindrical lens, just as it does in previous studies of laser induced nucleation. The higher optical power density (HP) was generated by passing the laser light through a home-built telescope to increase the intensity 4X before it reached the 1 mm pinhole. The lower optical power density (LP) was achieved by not using the telescope. HP intensity was calculated to be ~0.47 GW/cm^2 and LP was calculated ~0.11 GW/cm^2 (calculated based on a circular, top-hat spatial profile and a top-hat temporal profile).

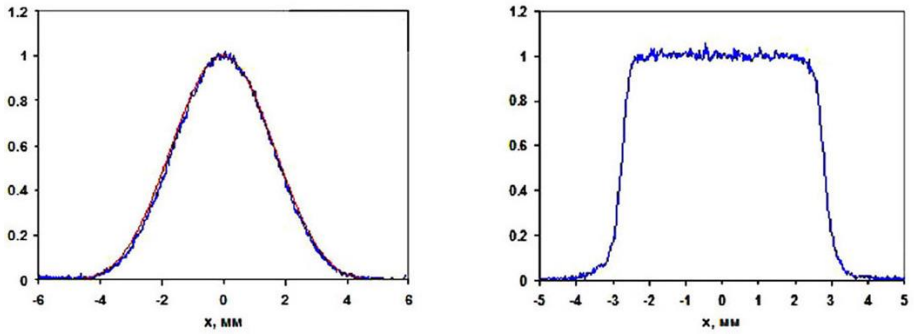

Figure 2.1: Intensity profiles of Gaussian (left) and tophat (right) beams

All experiments were performed for each set of conditions on at least 50 samples keeping in mind the stochastic nature of the nucleation process.

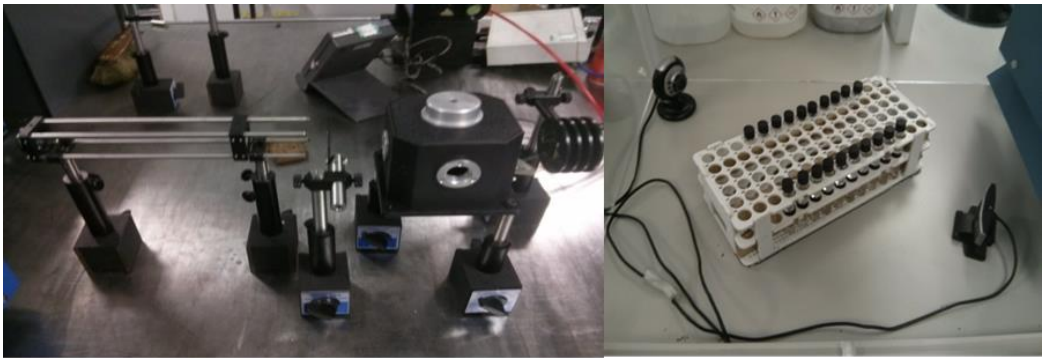

Figure 2.2: Images of irradiation (left) and monitoring set up inside an incubator for temperature control (right).

2.3. Imaging and Data Processing

All samples were placed in a temperature controlled bath immediately after irradiation and were then transferred to a vial rack in an incubator set at 298 K. Images of all the vials were recorded every 2 minutes for four days (~5000mins) using a webcam with borrocam (freeware) software. Induction times were obtained from the analysis of

image files by filtering and using a threshold intensity to identify crystals and estimate their size. The induction time is defined here as the period between the laser irradiation of samples under isothermal conditions for given supersaturation and the detection of crystals at constant temperature (298 K). Detection of crystals was based on time when the size of a crystal reached 1 mm.

The cumulative probability distribution function of the induction time can be determined from a large number of induction time measurements at given supersaturation and constant temperature as described by Jiang and ter Horst.[40] For N individual samples in repeated experiments, the cumulative probability P(t) that an induction time is between zero and time t is defined as

$$P(t) = \frac{N(t)}{N} \qquad \textbf{Eq.1}$$

where N (t) is the number of samples where crystals have been detected up to a given time t.

2.4. Sample filtration

The procedure outlined in sample preparation was followed. Both syringes and sterile PES syringe filters of 0.2, 0.4, 0.8, 1.2 and 5µm pore size were also kept in the incubator at 333K to ensure they were heated and prevent any crashing out during the filtration process. Solution was then filtered into the HPLC vials or DLS tubes at 333 K after each filter used had 10ml of solution passed through it as a 'flush'.

2.5. 50% Filtered samples

Two bottles of equally supersaturated aqueous glycine solution were prepared as described in solution preparation (section 2.1). At 333K 40ml was hot syringe filtered with a sterile 0.2µm or 1.2µm PES filter into 40ml of unfiltered solution then magnetically stirred for 10 hours. Samples for irradiation made with the mixed filtered/unfiltered solution were then made as described previously.

2.6. Filtered water

Deionised water used to make some of the solutions was passed through a sterile 0.2µm PES filter at room temperature with either a 10 or 20ml 'flush' that was discarded to remove any trace chemical on the membrane. The 'filtered' deionised water was then used to make supersaturated solution as described in solution preparation.

2.7. Recrystallized filtered glycine

Some experiments were performed using glycine that was recrystallized after nanofiltration to investigate possible impurities that may have been removed. Glycine was dissolved in de-ionised water, and then filtered through a sterile 0.2µm PES filter at 333K with a 10ml flush that was discarded, to remove any trace chemical on the membrane. The solution was then recrystallized in an ice bath and filtered under reduced pressure. This recrystallized glycine was then used to make solution as described solution preparation (section 2.1).

2.8. Dynamic light scattering (DLS)

Measurements using DLS were carried out with an ALV/LSE– 5004 instrument using scattering angle $\theta = 90°$ and laser light wavelength $\lambda = 632.8$ nm. Hydrodynamic radius was calculated using the cumulate method and the Einstein Stokes equation from the autocorrelation function.

Samples tested by DLS were made the same way as irradiated samples and can be considered to be representative of them.

2.8.1. Dynamic light scattering theory

Light scattering is the result of interactions between light waves and an object, which in DLS is a particle or change in density such as aggregates of molecules. The light interacts with the electrons orbiting the molecules; this interaction induces a shift in the electric field inducing a dipole. The oscillating induced dipole results in scattering light.[94]

For scattered light to be used to gain information there needs to be differences in the density medium that light is passed through resulting in different degrees of light scattering. If there are stationary particles in suspension then the differences in light

scattering will result in a static speckle pattern, if the particles are moving then the dark spots will move around, and if the light is scattered onto a detector then the change in the scattered light intensity can used to get information about the movement of the particles.

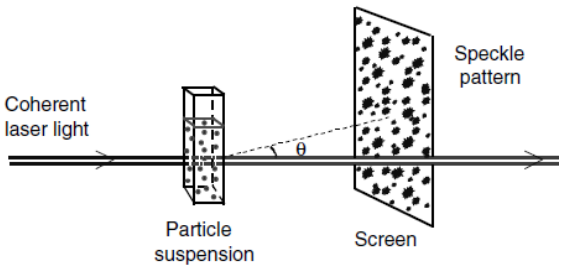

Figure 2.3: Speckle patter of a static suspension.[95]

Scattering can be quantified as a scattering vector (q) which is the difference in intensity between the initial laser light and the scattered light, calculated using eq2, from the refractive index (n), wavelength (λ) and the angle of detection (θ).

$$q = \frac{4\pi n}{\lambda} sin\left(\frac{\theta}{2}\right) \qquad \textbf{Eq.2}$$

In dynamic light scattering the change in the intensity is measured as a function of time (figure 2.3) and converted into an autocorrelation function from which size information can be calculated. The fluctuations in the scattered intensity are the result of Brownian motion of particles. Brownian motion is the random movement of a particle caused by collisions with solvent molecules.[96]

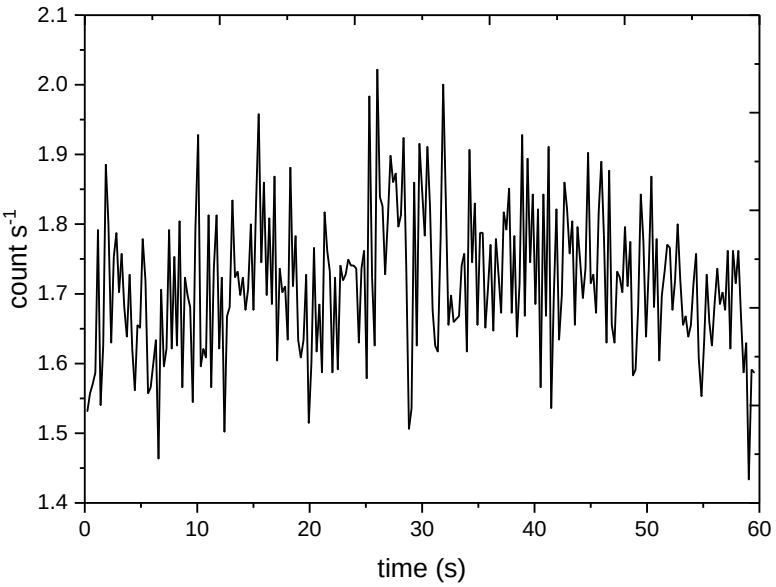

Figure 2.4: Example of fluctuations in intensity with time

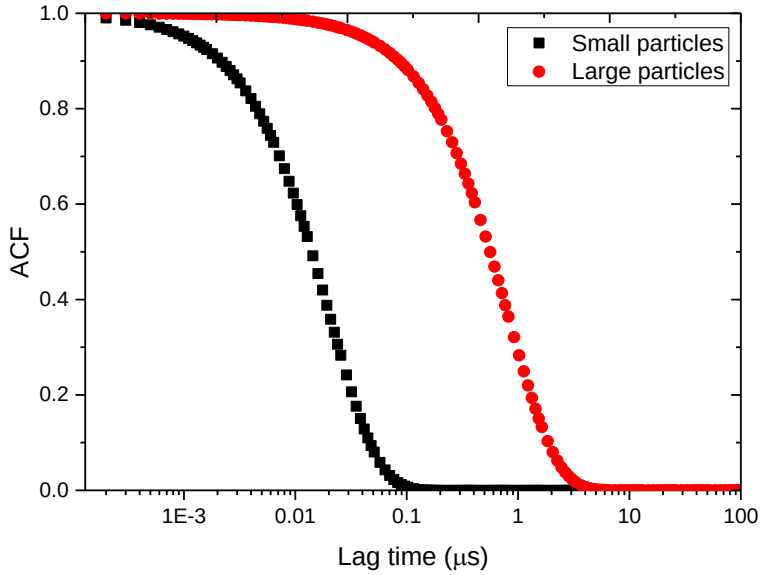

Figure 2.5: Example of autocorrelation functions of homogeneous samples.

The auto correlation function is the comparison between the scattered intensity function and a delayed version of itself, the time delay between the scattered light and the delayed intensity value.[97] Values for the auto correlation function (ACF) are how much correlation there is between the two scattering intensities; in short delays the

scattering is highly correlated, for long decays the scattering is poorly correlated and a low value of ACF. The rate of decay in the auto correlation function (Γ) is related to the diffusion coefficient by using the scattering vector (q)

$$\Gamma = Dq^2 \qquad \textbf{Eq.3}$$

The hydrodynamic radius (R_h) can be calculated form the diffusion coefficient using the stokes-Einstein equation;[98]

$$R_h = \frac{k_B T}{6\pi\eta D} \qquad \textbf{Eq.4}$$

where K_b is the Boltzmann constant, T is absolute temperature. The diffusion coefficient is related to the Brownian motion of a particle. Small particles have high Brownian motion and a high diffusion coefficient, and a shorter lag time and larger particles have low Brownian motion, smaller diffusion coefficient and longer lag times.

In the past, dynamic light scattering has been used to demonstrate the presence of solute-rich clusters of self-aggregating solute monomers. Previously it has been shown that glycine solutions have clusters in them around 250nm, the optical Kerr's effect requires the presence of these clusters to interact with the electric field (35, 54, 62). Filtration has been shown to remove these clusters, so the suppression seen in chapter 4 could be a result of the removal of the clusters from solution. (75, 76)

2.9. Rotary evaporation

Deionised water was placed on a rotary evaporator (Buchi R-215) and evaporated under reduced pressure until approximately 2/3 had evaporated off. Then both the residue water and the distillate water were collected respectively.

2.10. Distillation

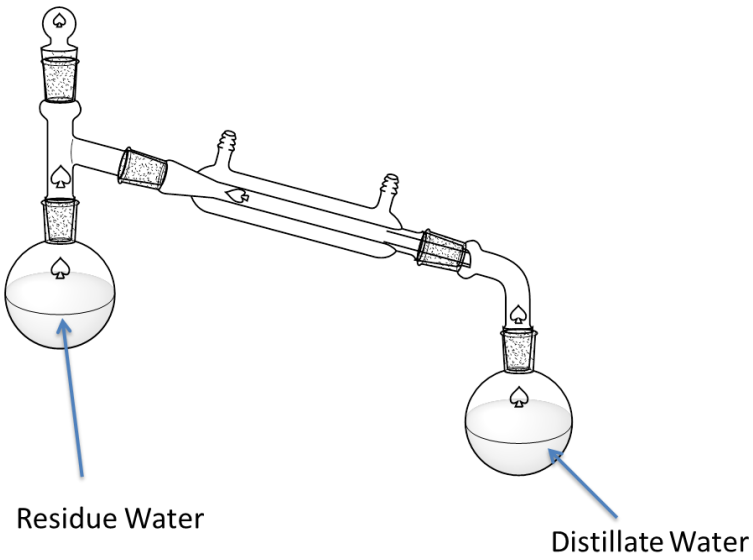

Figure 2.6: Distillation diagram

Deionised water was distilled using virgin glassware purchased from Scientific Glass Laboratories Limited. In the first experiment 2/3 was evaporated off, and the second experiment ½ was evaporated off. Both residue and distillate were collected, and samples made for irradiation using this water.

2.11. Reflux

Deionised water was refluxed for 5 hours using a heating mantel and the same glassware from distillation, with the water being used to make the solution.

2.12. Degassed

Deionised water in a bottle was placed in an ultrasound bath at 50°C on the degas setting for 5 hours. When finished, supersaturated samples were made within the hour to avoid any gas reabsorption.

2.13. Tap and HPLC grade water

Water was collected from the tap in the lab, HPLC grade water was purchased from Sigma Aldrich.

2.14. ATR-IR

Crystals formed were extracted from the vials for solid form characterization using an ATR-FTIR spectrophotometer with a diamond cell (Clairet Scientific, MB 3000). For each spectrum, 16 scans were collected in absorption mode with a resolution of 4 cm-1 at room temperature and analysed in the range of 800–1100 cm-1 for polymorph characterization. Reference spectra (air) were recorded under identical conditions.[92]

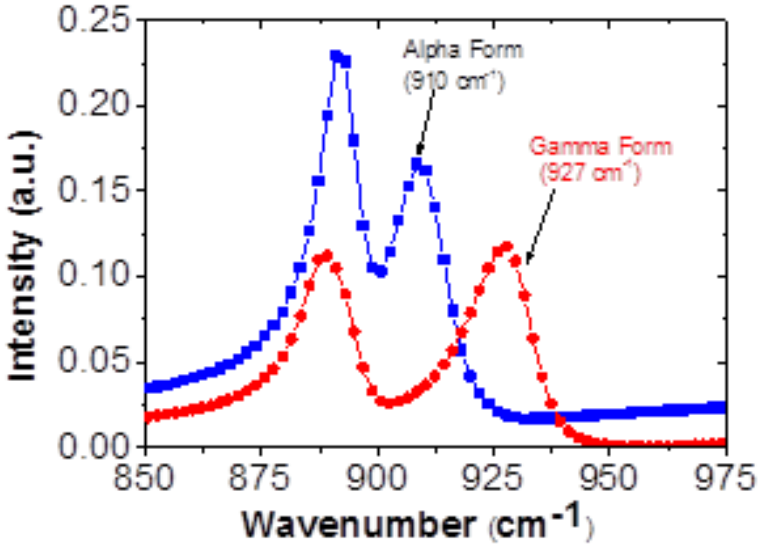

Figure 2.7: ATR-IR spectra for alpha and gamma glycine

3. Effect of laser intensity and duration time, and bimodal model function estimation of nucleation rates.

3.1. Aims of these experiments

- To build a high throughput set up that would allow for statistical testing of multiple factors on laser induced nucleation.
- To test some well-established experiments to confirm the validity of the set up.
- Quantitatively demonstrate the effect changes in peak laser intensity has on nucleation efficiency of laser induced nucleation.
- Quantify the effect of changes in supersaturation have on nucleation efficiency on laser induced nucleation in glycine and urea compared to non-irradiated samples.
- Investigate the effect various irradiation times and input powers has on nucleation efficiency as an indicator of whether the mechanism is related to cumulative energy input or probability of interaction.

3.2. Laser induced nucleation in glycine and urea

The first system that NPLIN was demonstrated on was aqueous urea in 1996, most of subsequent experiments were carried out using aqueous glycine solutions. Observation in these systems allowed the establishment of the optical Kerr's effect as a proposed mechanism by which NPLIN works. Observation in these experiments include the alignment of urea crystals formed with the polarization of the laser light, a dramatic reduction in induction time an increase in nucleation probability with increasing irradiation density and supersaturation. Furthermore, the establishment of an intensity and supersaturation threshold in NPLIN is not possible. It was also demonstrated that polarized switching control of the polymorph of glycine crystals formed.

Since aqueous glycine and urea are the most widely studied system for NPLIN experiments, these systems were chosen for this investigation.

3.3. Experimental

See chapter 2 for experimental procedure on sample preparation, laser irradiation, and image analysis.

3.4. Results and Discussion

3.4.1. Effect of laser intensity and irradiation duration on glycine nucleation

These experiments compare the effect of two different peak laser power densities and irradiation times on aqueous glycine solutions with a supersaturation 1.5. Low power irradiation (LP) has an intensity of 0.11 GW cm^{-2}; high power irradiation (HP) has an intensity of 0.47 GW cm^{-2} ;approximately 4X higher.

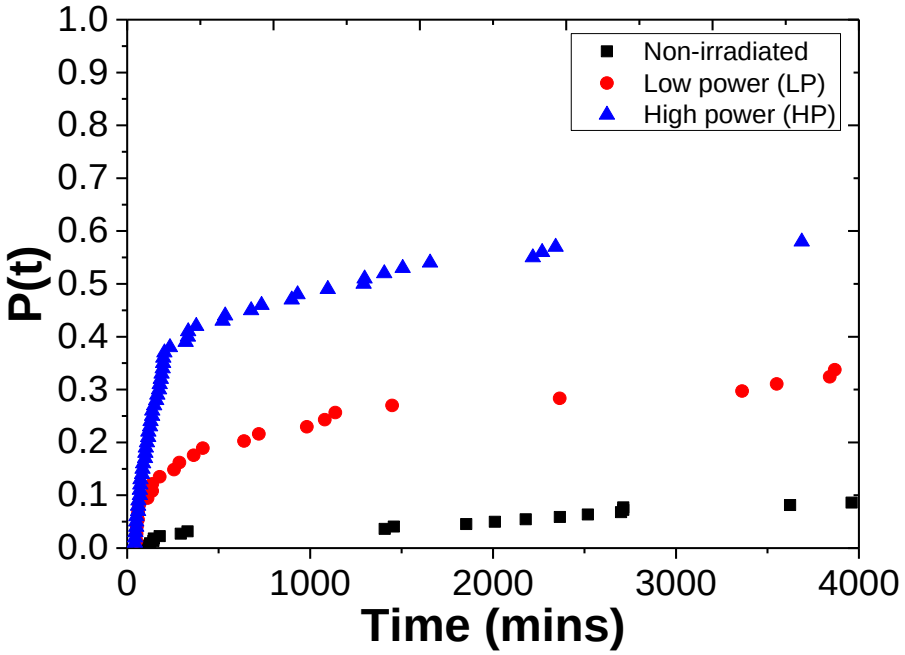

Figure 3.1: Cumulative probability distribution of induction times for 2 peak laser powers in aqueous glycine solutions with a supersaturation of 1.5. Black squares: non-irradiated; red circles: low power (LP)(0.11 GW cm^{-2}), blue triangles: high power (HP)(0.47 GW cm^{-2}).

Induction times (the time of appearance of a visible crystal after laser irradiation) for samples with 2 different irradiation powers were determined by analysing the digital images and were used to calculate the cumulative probability distribution functions of induction time; the results are shown in in Figure 3.1. The probability of nucleation in samples not irradiated was 8% irradiated, LP was 30%, irradiated with HP was 60% after 4000 minutes. The probability of nucleation is low in the absence of laser irradiation; this provides a base line for comparison with irradiated samples. The probability of nucleation is far greater in irradiated samples compared to non-irradiated samples. The cumulative probability of nucleation increases with increasing peak power density. This observation has been made in previous studies[61] however, it was observed that the increase is non-linear as a 4X increase in power only resulted in a 2X increase in nucleation probability

The cumulative probability distribution functions for the irradiated samples appear to show two distinct regimes of nucleation, which will be discussed in section 3.4.3.

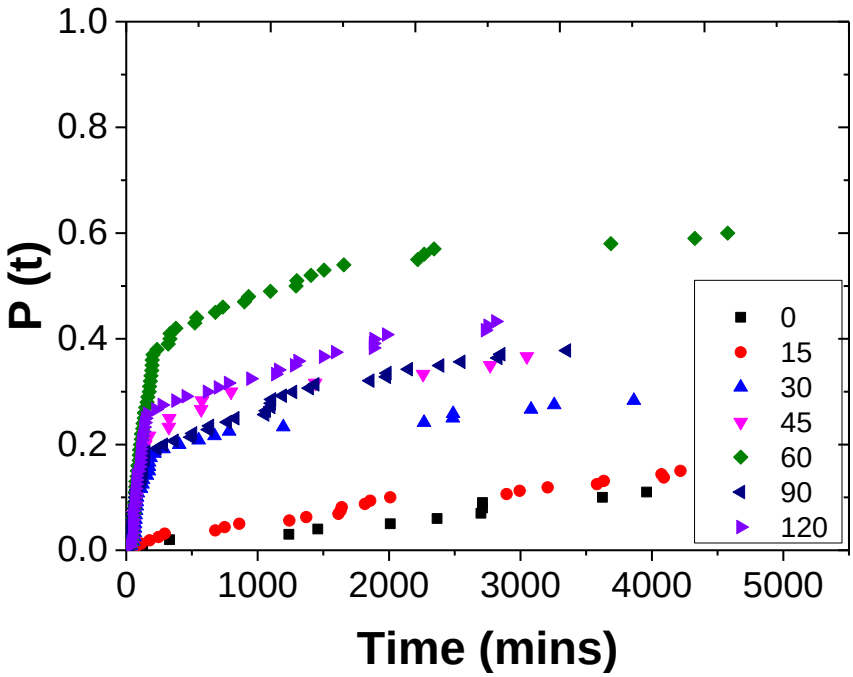

Figure 3.2: Cumulative probability distribution of induction times for various irradiation times in 1.5 supersaturated aqueous glycine solutions. Black squares: no irradiation; red circles: 15s; blue triangles: 30s; pink triangles: 45s; green diamonds: 60s; dark blue triangles: 90s; purple triangles: 120s irradiation time.

Experiments investigating irradiation duration on nucleation probability were carried out using 1.5 supersaturated solutions with high power intensity (0.49 GW/cm2). The probability of nucleation after 15 seconds is like samples that are not irradiated. Nucleation probability was significantly higher in samples that were irradiated for 30 seconds or longer compared to 15 seconds and not irradiated, this observation indicated that there is an irradiation duration threshold. Nucleation probability increases as irradiation duration increases, 30 seconds of irradiation 28%, 45 seconds of irradiation 36% and 60 seconds of irradiation 60% after 5000 mins. However longer irradiation than 60 seconds resulted in lower nucleation probability, 90 seconds 38% and 120 seconds 43% respectively.

The decrease in the nucleation probability of laser induced nucleation over the 60 second duration could be attributed to localised heating by absorption of the laser pulses by the water, stabilising supersaturation. This absorbance is accounted for in the presence of an intensity threshold being different between 1064nm and 532nm [65].

Whilst calculations show that the heating through absorption can be considered negligible at t<60, the increased number of pulses could be sufficient to cause heating which would stabilize the supersaturation. A way of testing this would be to repeat these experiments using 532nm wavelength where the absorption coefficient for water is significantly lower than 1064nm; however, this has not been carried out.

The presence of a minimum irradiation duration threshold can result in conclusions of either, 1) there needs to be a minimum amount of energy transferred into the solution in order for nucleation to occur e.g. minimum amount of energy needed to align molecules via the optical Kerr's effect. 2) there is a probability of interacting with an initiator particle, e.g. photoactive impurities.

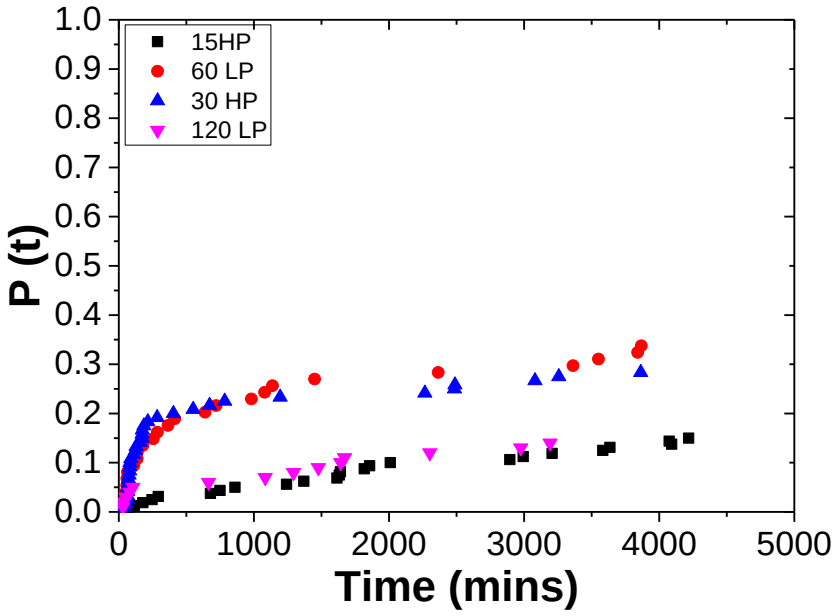

Figure 3.3: Cumulative probability distribution of induction times for different input powers of aqueous glycine solution. 15 seconds at HP is equal to 60 seconds LP black squares and red triangles, and 30 seconds HP is equal to 120 seconds LP, blue triangles and pink triangles.

A way of testing both of these observations is to irradiate samples with two powers for different irradiation durations so that the total power input into the system is equal, the only difference being the number of pulses experienced. The use of the telescope increased the pulse power by ~4X thus the irradiations would need to be 4X different for the input powers to be the same. Irradiation times chosen were 15 seconds HP

and 60 seconds LP, and 30 seconds HP and 120 seconds LP. The results show 15s HP 15%, 60 seconds LP 36%, 30 seconds HP 28% and 120 seconds LP 14% after 5000 minutes. The results show that even though the power put into the system is equal the nucleation probabilities are not, and suggest that the 60 seconds LP and 30 seconds HP are equivalent. This result indicates that the mechanism maybe the result of a probability of interacting with a particle or cluster rather than a cumulative effect.

3.4.2. Effect of supersaturation of glycine and urea

The effect of changing the supersaturation on the nucleation probability of NPLIN has been studied extensively. It has been shown that increasing supersaturation in most systems results in a higher probability of laser induced nucleation. However, previous experiments were conducted in a way that did not track the induction time of crystallisation rather the number of samples crystallised at the end of their experiment. Presented here are the results investigating the effect supersaturation has on NPLIN and how it influences the induction time.

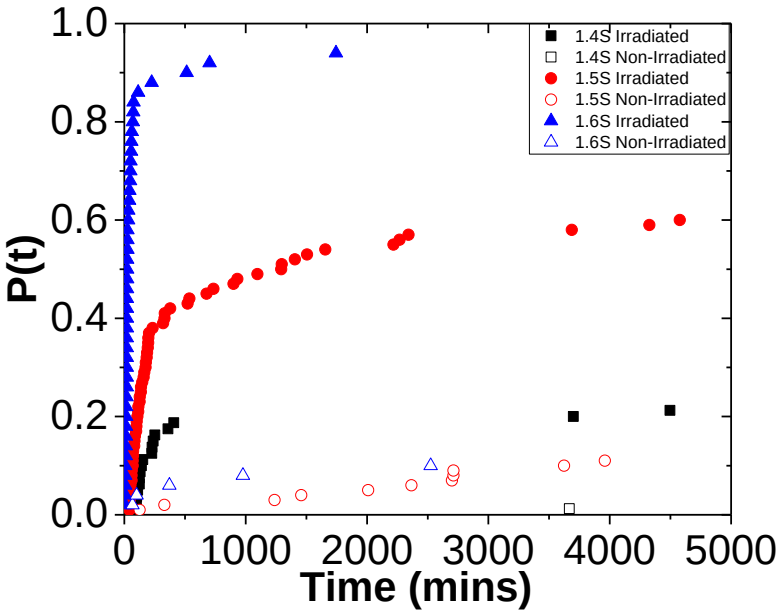

Figure 3.4: Cumulative probability distribution of induction times for different supersaturation of aqueous glycine solution, black squares 1.4, red circles 1.5 and blue triangles 1.6 supersaturations. Filled in symbols are irradiated and hollow symbols are non-irradiated.

Like previous studies it was observed the increase in nucleation as a result of an increase in supersaturation. However, using the setup it was possible to track the induction times of the samples and by plotting using the ter Horst method. it was shown that the induction time was very broad for all three supersaturations

Supersaturation	Induction time range (mins)
1.4	60-400
1.5	30-300
1.6	6-80

Table 3.1: Induction time spreads of the initial sharp increase in vials crystallising for different supersaturations.

The first measured induction time is consistent with the growth time of a 1 cm crystal from solution using published growth rates[77] for each supersaturation respectively. The presence of this broad induction time suggests that the mechanism may not be instantaneous, that a delay time may exist between activation by laser pulse and nucleation. One proposed explanation for the broad induction times is the variance in growth rates for glycine, that the longer induction times could be the result of slow growth rates. This can be tested through experiments on a system with a very high growth rate, such as urea in deionised water.

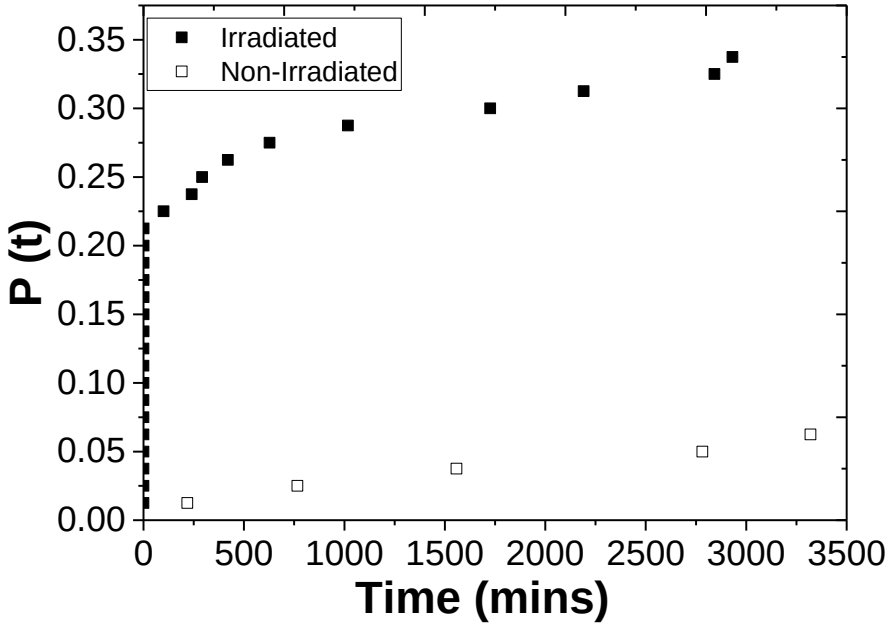

Figure 3.5: Cumulative probability distribution of induction times of, 1.4 supersaturation aqueous urea solution, filled black squares irradiated, hollow black squares non-irradiated.

Experiments were carried out using supersaturated aqueous urea solution. The growth time of aqueous urea solutions is very short (<1 second) because of the high solubility of urea in water, so it would be possible to see when nucleation occurs. It was found that samples that underwent laser induced nucleation were induced during the irradiation period, noticed by the rapid drop in laser intensity on the power meter. It can be seen (table 3.2) that the spread of induction times observed in glycine, is seen in the spread of nucleation during the irradiation period. Due to the high growth kinetics these times can be considered as nucleation time. Nucleation during the irradiation suggests that the spread of induction times after the irradiation seen in glycine are not related to the probability of irradiation interacting with an object but could be related to another factor such as variance in growth rates.

Supersaturation	Induction times (seconds)
1.4	10, 15, 20(2X), 30(2x) 40 45 50

Table 3.2: Induction times for 1.4 supersaturated urea

3.4.3. Estimation of nucleation kinetics

Estimation of nucleation kinetics was done using the bimodal equation outlined in the section 1.5 using equation 18.

The cumulative probability distribution functions of induction times for irradiated samples are shown with a logarithmic time scale in Figure 3.6. The delay time required for the first crystal to be observed increases as the supersaturation is reduced. As described above, in the case of irradiated samples a bimodal nucleation regime is observed. This consists of an initial fast regime which identified that as laser induced nucleation regime, which is absent from non-irradiated samples, and a second slower spontaneous nucleation regime. In order to describe the bimodal nucleation kinetics quantitatively, a function based on a weighted sum of two exponential distributions with different time constants was used, as shown in chapter 1.5.

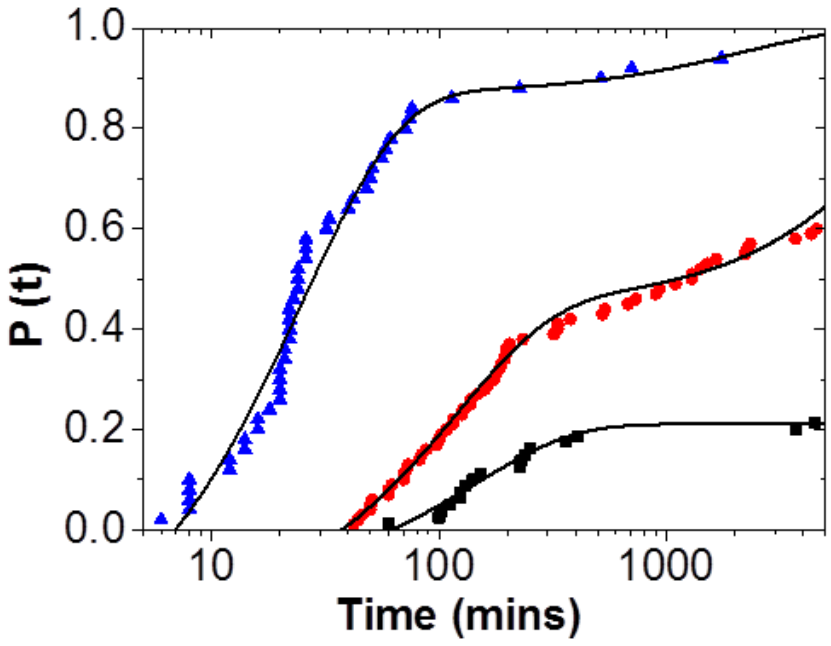

Figure 3.6: Fitting of biexponential model to cumulative probability distribution of induction times for supersaturations 1.4 (squares), 1.5 (circles) and 1.6 (triangles) for non-filtered, irradiated samples. (see figure 3.6 and table 3.1)

Values for the proportion of samples that underwent laser induced nucleation (A), characteristic times for both laser-induced (τ_1) and spontaneous (τ_2) nucleation regimes, and the delay time (t_d) representing the time required after nucleation for the

incipient crystal to grow large enough to be detected by image analysis, were estimated by fitting a function to the experimental data by the method of non-linear least squares. Fitted delay times should correspond to growth times for crystals to reach about 1 mm at a given supersaturation and temperature. Times were estimated for both the α- and γ-polymorphs of glycine using previously published crystal growth rate data.[99] It was found that they vary between approximately 10 and 25 minutes for the α-polymorph and 30 to 80 minutes for the γ-polymorph over the range of supersaturations investigated, in a reasonable agreement with estimated delay time values.

In the fitting process 95% confidence intervals for the estimated values were calculated based on the assumption that the experimental errors in evaluating each point in the cumulative distribution are Gaussian, uncorrelated and have a uniform standard deviation. Although it is difficult to be certain if these assumptions are strictly valid, the values nevertheless give an indication of the levels of uncertainty in the parameters extracted from the fits.

It can be seen from Table 3.3 that there is a strong increase in the proportion of samples that undergo laser-induced nucleation with increasing supersaturation: the value of A roughly doubles as supersaturation increases from 1.4 to 1.5 and doubles again from 1.5 to 1.6. The characteristic time for laser induced nucleation regime (τ_1) decreases as supersaturation increases indicating a higher nucleation rate. There is also a decrease in the characteristic time for spontaneous nucleation regime (τ_2) with increasing supersaturation as expected, and these characteristic times are about two orders of magnitude longer than those for laser induced nucleation. This means that laser induced nucleation kinetics is about two orders of magnitude faster than spontaneous primary nucleation in this system.

Supersaturation ratio	A	τ_1 (min)	τ_2 (min)	t_d (min)
1.4	0.21(±0.017)	143(±36.6)	$1.48X10^6$ (*)	62.3(±12.2)

1.5	0.45(±0.012)	117(±8.6)	$1.14(\pm0.16)X10^4$	37.4(±2.8)
1.6	0.87(±0.06)	24.7(±4.0)	$2.17X10^3$(*)	6.9(±1.4)

Table 3.3: Estimated values of parameters from fitting a biexponential model to cumulative probability distribution functions of induction times for non-filtered irradiated samples. *A* is the proportion of samples that underwent laser induced nucleation, t_d is the delay time between laser irradiation and appearance of the first crystals, τ_1 is the characteristic time for laser induced nucleation, τ_2 is the characteristic time for spontaneous nucleation. Quoted uncertainties represent 95% confidence intervals evaluated in the fitting process. Values marked with (*) are not statistically significant due to an insufficient number of data points.

In order to compare the characteristic time of the second nucleation regime; τ_2, observed in non-filtered, laser irradiated samples; with the spontaneous nucleation rate observed in non-irradiated samples, and both were fitted a single-exponential function to the data for non-filtered non-irradiated samples. Due to an insufficient number of data points caused by expected slow nucleation, this was only done for samples with supersaturation 1.5. The value of the spontaneous nucleation characteristic time is shown as τ_{spont} in Table 3.4 and the fit to the data is shown in Figure 4. The characteristic time for spontaneous nucleation τ_{spont} for non-irradiated samples appears to be higher than the value of τ_2 for the corresponding irradiated samples but the values are of a similar magnitude. To determine whether the cumulative probability distribution function of induction times for laser induced nucleation was consistent with a second regime governed by the rate of spontaneous nucleation, the bimodal fitting was repeated with τ_2 fixed to be equal to τ_{spont}. The new fit to the data is shown in Figure 4 along with the original one. Although the new fit does not agree with the data quite as well, the results seem broadly consistent with a model in which the second nucleation regime has a rate that is equal to the rate of spontaneous nucleation. The values of the parameters, A', τ_1' and t_d ', resulting from the new fit are shown in Table 3.4 and can be seen to have similar values to the fit in which τ_2 was varied.

Supersaturation	A'	τ_1' (min)	τ_{spont} (min)	t_d' (min)
1.5	0.49(±0.01)	145.7(±12.9)	3.43(±0.26) X10^4	34.0(±5.0)

Table 3.4: Estimated values of parameters A', t_d' and τ_1' from fitting a biexponential model to cumulative probability distribution function of induction times with a fixed value of $\tau_2 = \tau_{spont}$ for non-filtered irradiated samples at supersaturation 1.5.

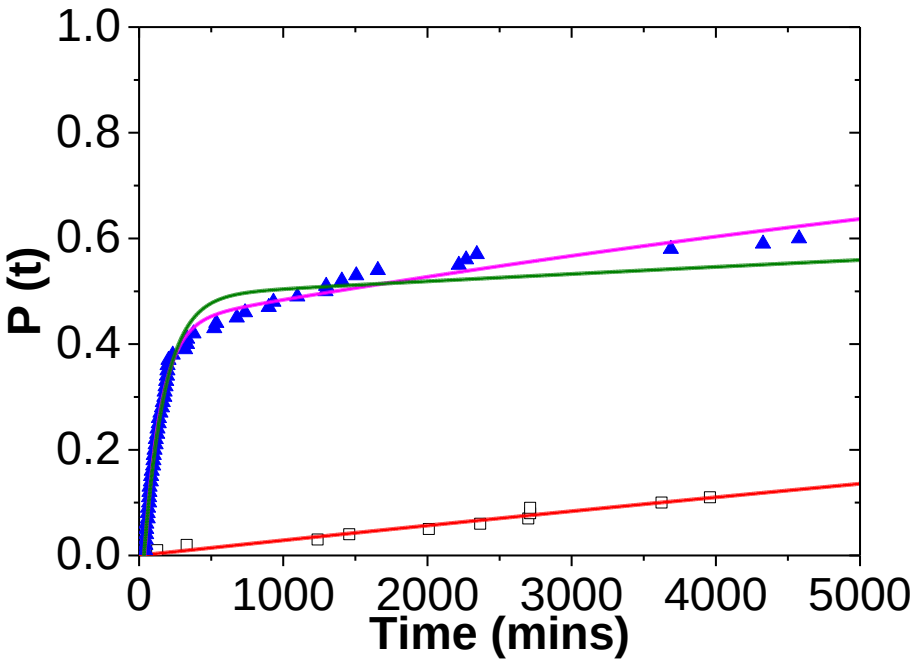

Figure 3.7: Cumulative probability distribution of induction times for irradiated and non-irradiated samples that had not been filtered, with supersaturation of 1.5. Best fits of single-exponential (non-irradiated samples) and biexponential (irradiated samples) models are shown. The single-exponential fit was used to estimate τ_{spont} for non-filtered non-irradiated samples (black line). The biexponential fit has been performed both with τ_2 fitted (pink line) and fixed (green line) to the value of the spontaneous nucleation characteristic time τ_{spont}.

3.5. Conclusions

In conclusion, experiments investigating the effects that changing the peak power density, irradiation duration, and supersaturation have on nucleation efficiency of laser induced nucleation in aqueous glycine and urea solutions has been conducted. Investigating the effect of changing the peak pulse energy revealed a non-linear relation to the nucleation efficiency in aqueous 1.5 supersaturated aqueous glycine solutions; that a 4X increase in peak intensity resulted in a 2X increase in laser induced nucleation. These experiments also showed two nucleation regimes, the initial fast laser-induced and the slower spontaneous. Further experiments investigating the effect of irradiation duration has showed an optimum irradiation duration that shorter irradiation period reduced nucleation efficiency, and longer durations than 60 seconds resulted in a decrease, which could be the result of localised heating stabilizing the supersaturation. When samples were exposed to equal input power by changing the peak intensity and irradiation duration, it was shown that there was no correlation to input power at different peak intensities which indicates that it is not a cumulative effect. Additionally, experiments have demonstrated qualitatively the effect increasing supersaturation has on increasing laser induced nucleation in aqueous glycine and urea solutions. Furthermore, the presence of a distribution of induction times for the laser induced regime was confirmed in both systems. A bimodal function was used to identify the associated time of laser induced nucleation which could be used to estimated nucleation rates.

4. Suppression by nanofiltration

4.1. Aims of these experiments

- Test the optical Kerr’s and isotropic polarizability effect through nanofiltration.
- Investigate the role mesoscale solute clusters play in laser induced nucleation using a combination of dynamic light scattering and irradiation experiments.
- Based on observations in nanofiltration irradiation experiments identify the possible source of initiators.

4.2. Experimental

See chapter 2 on sample preparation, laser irradiation and imagine analysis, dynamic light scattering, sample filtration, and production of 50% filtered and filtered water and recrystallized filtered glycine solution.

4.3. Results and Discussion

4.3.1. Nanofiltration in various supersaturations

A)

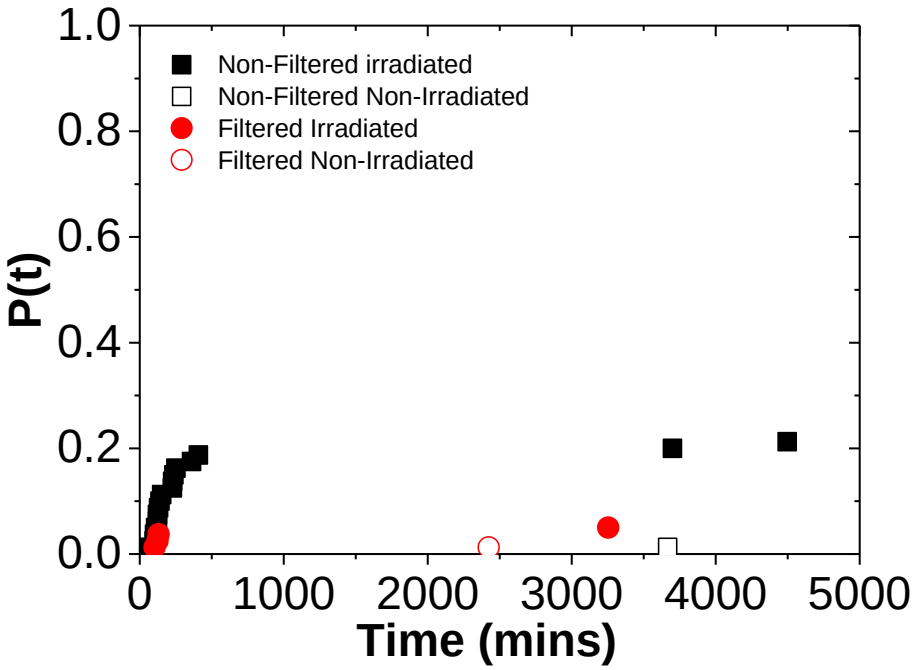

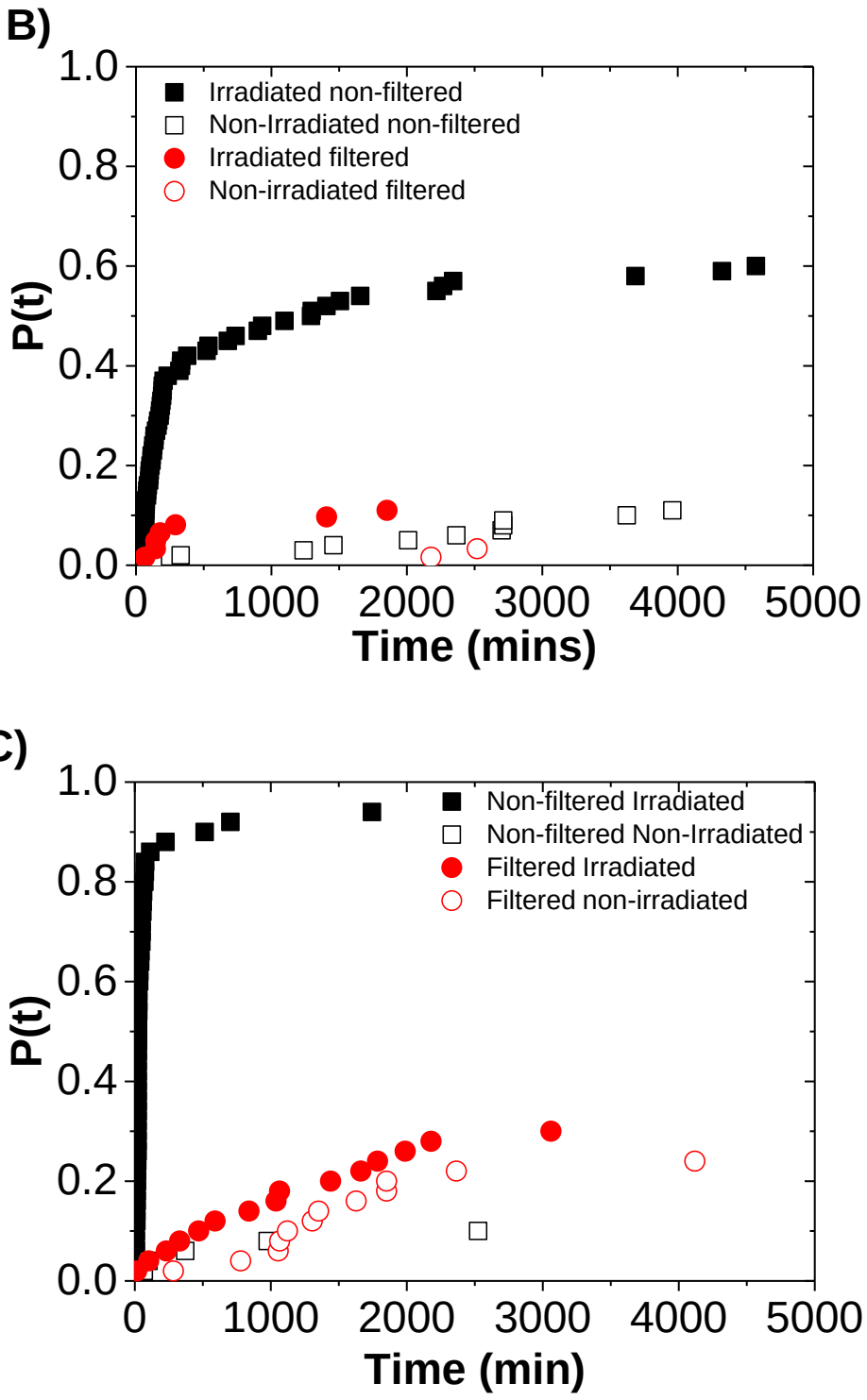

Figure 4.1: Cumulative probability distribution of induction times for supersaturated glycine aqueous solutions at three different supersaturations: A) 1.4, B) 1.5, C) 1.6, where filled symbols represent irradiated samples and hollow symbols represent non-irradiated samples, squares represent non-filtered samples and circles represent filtered samples.

As described in Methods section, the glycine solutions were hot filtered at 333 K with PES filters having pore size of 0.2 μm. This procedure therefore cannot remove glycine molecules from solution but is expected to filter out particulates with size larger than filter pore size or remove molecular or particulate impurities that can be absorbed on the filter membrane. Surprisingly, the nanofiltration of glycine solutions resulted in a massive decrease in the probability of laser induced nucleation at all supersaturations (figure 4.1). It is clear that the first fast nucleation regime is greatly suppressed in these filtered samples. The results therefore point to a mechanism for laser induced nucleation that is strongly dependent on the presence of impurities or particulates, in solute or solvent, or external origin, that can be removed by filtration.

4.3.2. Dynamic light scattering

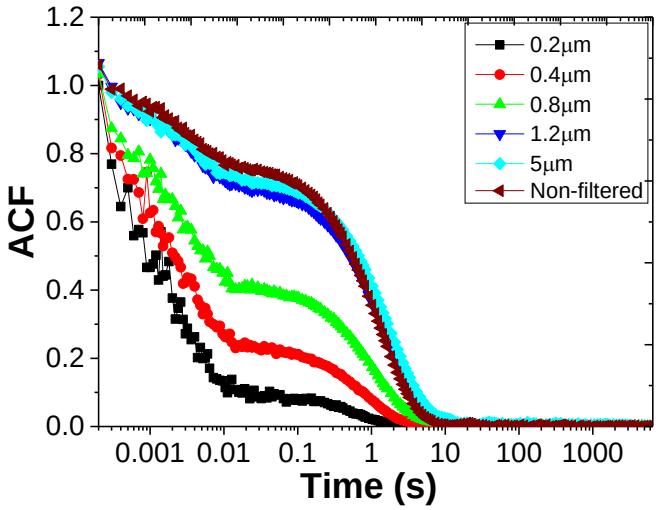

Figure 4.2: Normalised auto correlation function; 1.5 supersaturation at 25°C. Non filtered (brown, left facing triangles), 0.2μm PES filtered (black squares), 0.45μm PES filtered (red, circles), 0.8μm PES filtered (green, upwards triangles), 1.2μm PES filtered (Dark Blue. downwards triangles), 5μm PES filtered (light blue, diamonds)

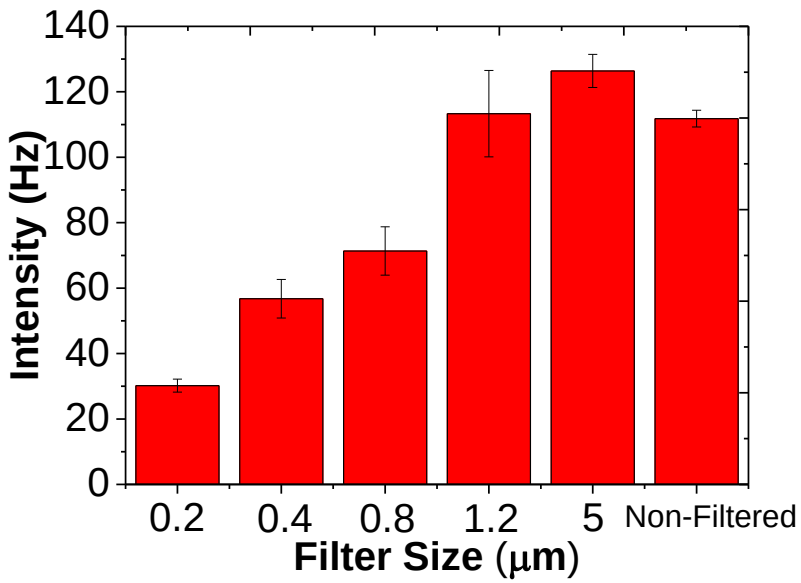

Figure 4.3: Average scattered light intensity and estimated mean hydrodynamic radius from DLS measurements for various filter sizes with standard errors from repeat measurements.

Pore size	Hydrodynamic radius (nm)	Intensity (a.u.)
0.2 Micron	130±3	34±6
0.4 Micron	131±6	57±7
0.8 Micron	162±6	79±13
1.2 Micron	234±15	96±5
5 Micron	264±6	115±3
Non-Filtered	257±18	101±2

Table 4.1. Values of mean hydrodynamic radius and scattered light average intensity of the tested PES pore sizes from DLS.

Using dynamic light scattering non-filtered samples the presence of liquid like nanodroplets with a calculated hydrodynamic radius approximately ~250nm and an associated scattering intensity of ~100s^{-1} which, for a fixed concentration can be considered proportional to the number of nanodroplets present in solution. When samples were passed through a 0.2 µm PES syringe filter, it was observed a dramatic reduction in calculated cluster size from 250 to 130 nm demonstrated by the change in the second decay of the autocorrelation function (figure 1). A reduction is also observed in intensity from 100 to 33 s^{-1} which, for samples of same concentration can be proportional to number of nanodroplets in solution. This observation about the change in the size and number of these nanodroplets by the act of nanofiltration with 0.2µm PES filter corresponds to the optical Kerr's effect theory of laser induced nucleation. That alignment of molecules within the liquid-like nanodroplets causes laser induced nucleation and by removing the majority from solution the suppression was observed. Various pore sizes of PES filter were tested to determine a critical size where the liquid-like droplets are unaffected by the filtration. The sizes tested were 0.4, 0.8, 1.2 and 5µm PES filters and it was observed there was an increase in average hydrodynamic radius to 131, 162, 234 and 264nm respectively, seen in the growth of the second decay in the auto correlation. It was concluded that the critical pore size where the liquid like nanodroplets are unaffected by the filtration is 1.2µm, and this pore size and the larger 5µm would be used to make samples which are irradiated to see if the suppression is present.

4.3.3. Irradiation after filtration of various filter pore sizes

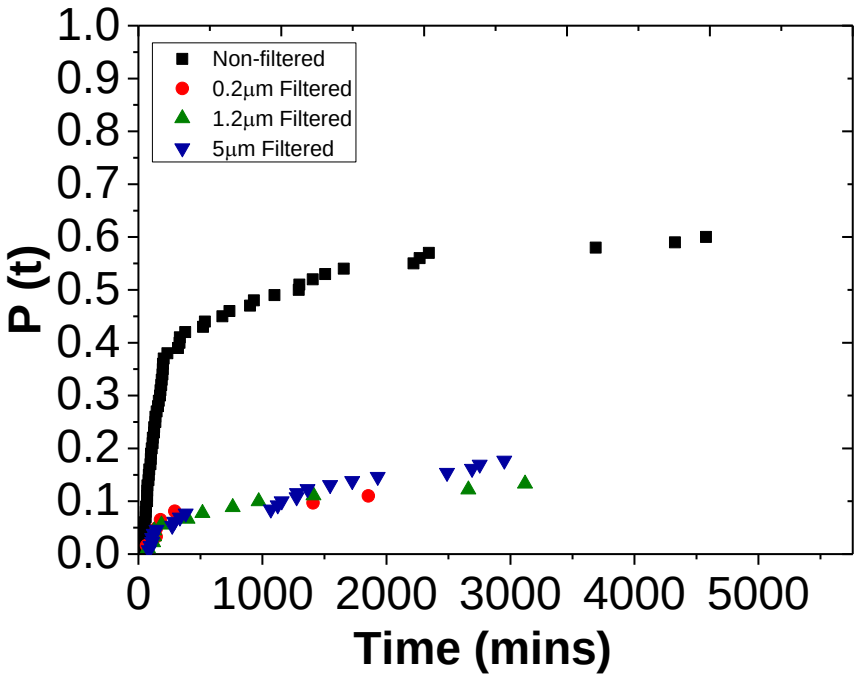

Figure 4.4: Cumulative probability distribution of induction times in 1.5 supersaturated aqueous solutions with various PES filter pore sizes. Non-filtered (squares), 0.2μm (circles), 1.2μm (upwards triangles), 5μm (downwards triangles).

The DLS results demonstrate that the critical pore size for PES syringe filters was 1.2μm, so 1.5 supersaturated aqueous glycine solutions was filtered using this pore size, cooled, irradiated, and then monitored for induction times to investigate if the suppression is still present. It was observed that when solution is filtered through 1.2μm PES filter and then irradiated there still is a suppression of the laser induced nucleation regime, similar to the suppression effect observed with 0.2μm filters (figure 3). When samples were filtered with the larger 5μm PES syringe filter then irradiated the suppression of the laser induced nucleation regime can still be seen, similarly to 0.2 and 1.2μm. These unexpected results are inconsistent with proposed mechanisms that solely involve liquid like nanodroplets as the cause of laser induced nucleation, such as the alignment of molecules within clusters due to the optical Kerr's effect that had been proposed previously.[68] These clusters may still play a role in the mechanism but they are not the cause/trigger of laser induced nucleation. Furthermore, it can suggested that from these the results that the initiators of laser induced nucleation could be binding to the material thus removing them from solution

as anything larger than 5 µm would have been visible in the DLS of non-filtered samples.

4.3.4. Irradiation of 50% filtered samples

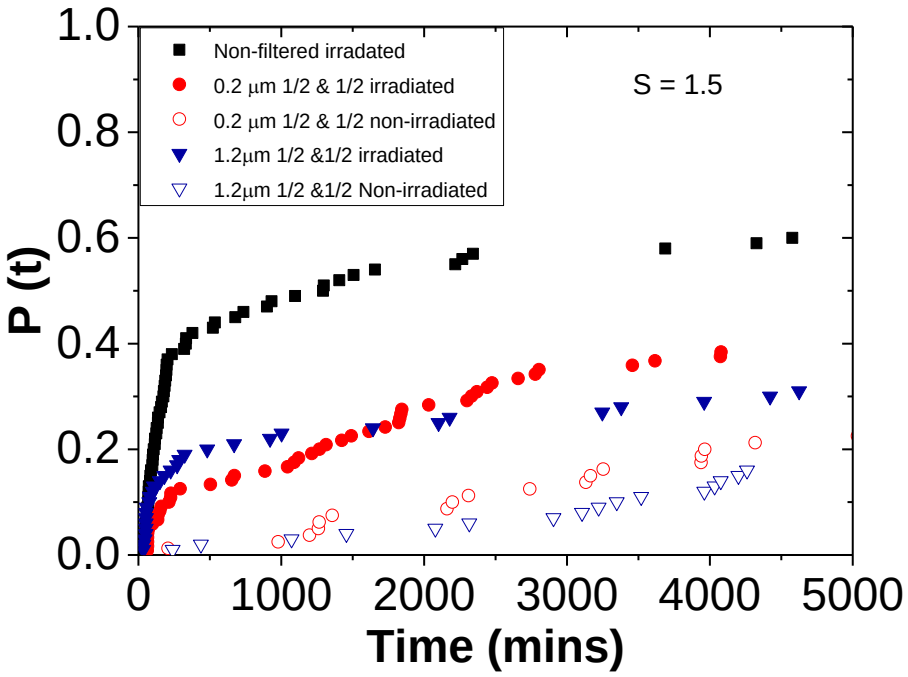

Figure 4.5: Cumulative probability distribution of induction times in 1.5 supersaturated aqueous solutions of 50% filtered with PES filter and 50% unfiltered. 100% unfiltered (black squares), 50% 0.2µm Filtered (circles, solid for irradiation, open control), 50% 1. 2µm Filtered (downward triangles, solid irradiated, open controls)

Having observed the suppression of laser induced nucleation in solutions that were filtered with PES membrane filter of any pore size further experiments were performed to gather evidence about the possible nature of this effect. Since the PES filters removed the initiators of laser induced nucleation, it is possible to investigate what effect concentration of these initiators has on nucleation efficiency of laser induced nucleation by mixing equal amounts of filtered and non-filtered solution of the same supersaturation (1.5 aqueous glycine) effectively halving the concentration of initiators. It was observed that when these mixture solutions with either 0.2 or 1.2µm are irradiated, the nucleation efficiency decreases by 50%, indicating that the

concentration of initiators is potentially directly related to nucleation efficiency. This was confirmed by using the bimodal exponential function that was reported previously (section 1.5), [90] when comparing the values of *A* (proportion of vials crystallised in laser induced nucleation regime) the values of non-filtered and 50% filtered with the critical pore size of 1.2µm is approximately half, whilst the value for 0.2µm is about ¼ ½ of non-filtered irradiated which might indicate that the smaller pore size is removing more of the initiators.

4.3.5. Component nanofiltration

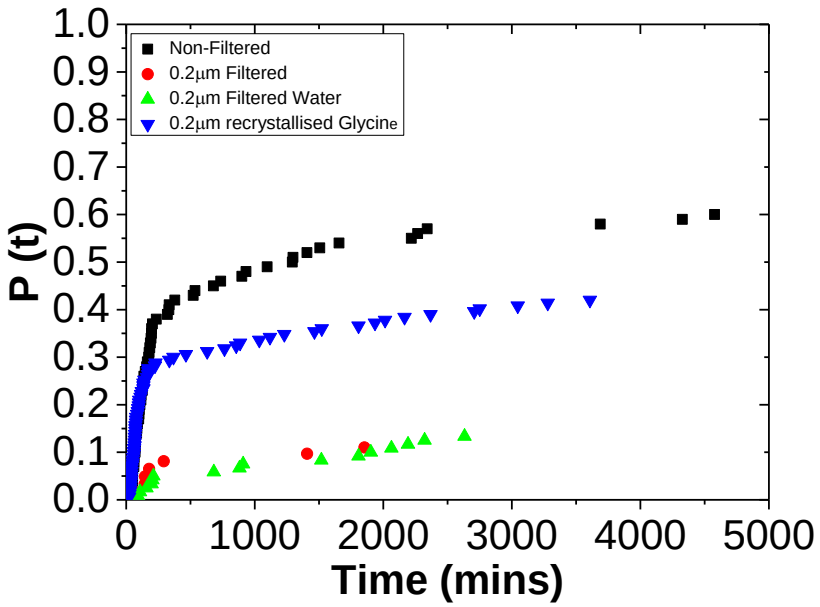

Figure 4.6: Cumulative probability distribution of induction times in 1.5 supersaturated aqueous solution Non-filtered (black squares) Filtered aqueous solution (red circles) Solution that was made with water passed through 0.2µm PES filter (green upward triangles) and recrystallized glycine from filtered (0.2µm PES) aqueous glycine solution (blue downwards triangle).

The results seem consistent with the presence in solution of initiators that can be removed by filtration. Further experiments were performed with the aim of identifying where these initiators originated, in the glycine solute or in the deionised water solvent. To test the solvent, it passed deionised water through 0.2µm PES filter at room temperature (~23°C) then made solutions using this 'filtered water'. When these

samples were irradiated it was observed that the suppression occurs similarly in magnitude, supported by comparing the values of *A* from the biexponential fitting (table 4.4), to when aqueous solution was filtered using the 0.2µm PES filter which indicates that the source of these initiators is the deionised water. To confirm the observations of suppression were not the result of chemical leaching from the filter experiments a 'flush' was used. The 'flush' is the amount of filtrate passed through the filter and discarded before the filter is used in experiments. In experiments listed previously a 10ml 'flush' was used, and when this was used on the deionised water the suppression was present, ruling out the possibility of chemical leaching off the membrane being the cause of the suppression. This was confirmed further with a 20ml 'flush' to ensure that any chemicals in trace amounts that could be the cause of the suppression of laser induced nucleation was removed (figure 4.7)

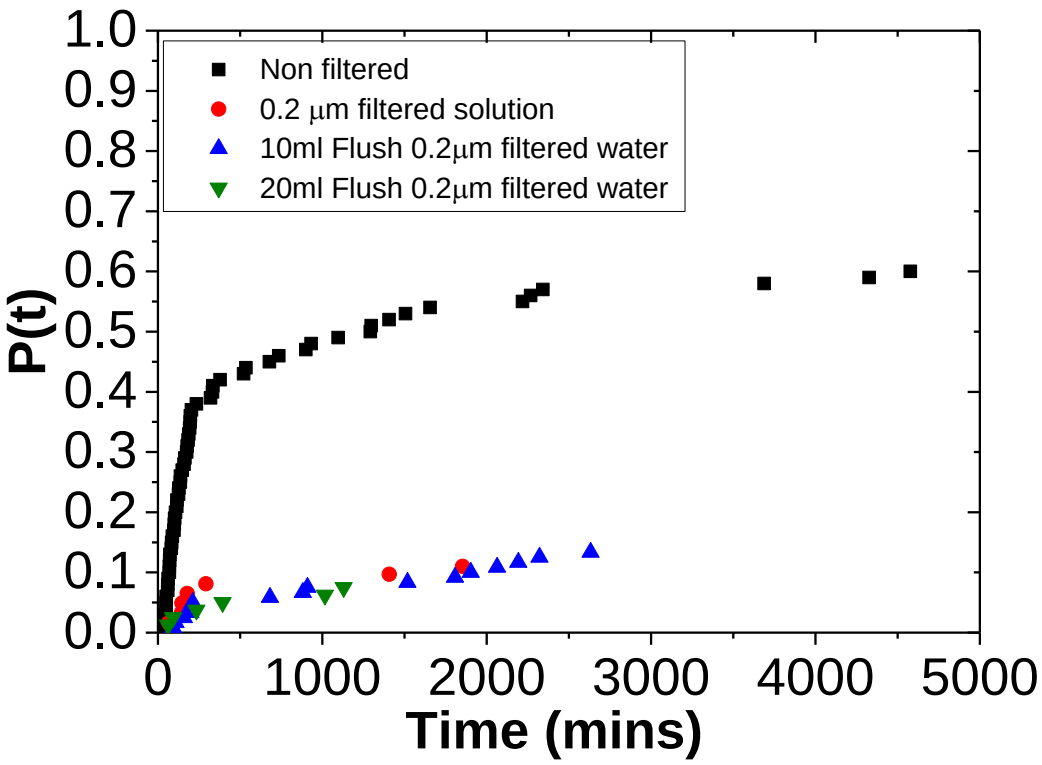

Figure 4.7: Cumulative probability distribution of induction times in 1.5 supersaturated aqueous glycine solutions. Non-filtered solution (Black squares), filtered solution (red circles), made with filtered water after a 10 ml flush (blue triangles), made with filtered water after a 20ml flush (green triangles)

In order to confirm that the solute was not the source of the impurities/initiators, the glycine was recrystallized after being filtered whilst in solution. This 'recrystallized glycine' was then dissolved in unfiltered deionised water for samples to be irradiated. When the resulting solutions were irradiated, the laser induced nucleation regime was still present. This allows for the exclusion of the solute as the majority source of the initiators.

4.3.6. Estimation of nucleation kinetics

This section will use the biexponential function model to investigate the effect nanofiltration has on the nucleation efficiency.

Conditions	A	τ_1 (min)	τ_2 (min)	t_d (min)
1.4S	0.21(±0.02)	62.3(±12.2)	$1.48X10^6$(*)	143.4(±36.6)
1.4S Filtered*	N/A	N/A	N/A	N/A
1.5S	0.45(±0.01)	117.0(±8.6)	$1.14(\pm0.16)X10^4$	37.4(±2.8)
1.5S filtered	0.09(*)	142.4(*)	$1.13X10^5$	44.4(*)
1.6S	0.87(±0.06)	6.9(±1.4)	$2.17X10^3$(*)	24.7(±4.0)
1.6S filtered*	N/A	N/A	N/A	N/A

Table 4.2: Estimated values of biexponential model parameter for different irradiated supersaturated samples filtered and non-filtered, * (too few data points to estimate error values); N/A too few data points to give a value reliably

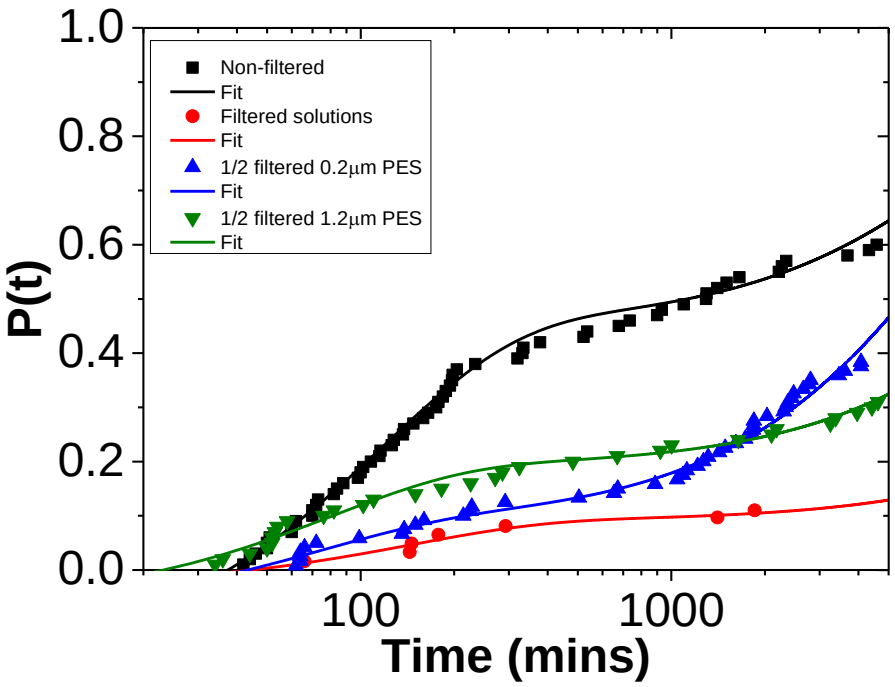

Figure 4.8: Fitting of biexponential model to cumulative probability distribution of induction times of 1.5 supersaturation for non-filtered (black squares), filtered solutions (red circles), ½ filtered with 0.2μm PES filter (blue triangles), ½ filtered with 1.2μm PES filter (green triangles).

50% filtered samples of 1.5 supersaturation, * too few data points to get error values.

Conditions	A	τ_1 (min)	τ_2 (min)	t_d (min)
Non-filtered	0.45(±0.01)	117.0(±8.6)	1.14(±0.2)X10^4	37.4(±2.8)
filtered solutions	0.09(*)	142.37(*)	1.13(*)X10^5	44.37(*)
½ filtered with 0.2μm filters	0.09(±0.01)	68.3(±42.8)	9.31(±0.6)X10^3	43.3(±17)
½ filtered with 1.2μm filters	0.19(±0.01)	79.9(±21)	2.74(±0.6)X10^4	23.2(±7.6)

Table 4.3: Estimated values of biexponential model parameter for different irradiat

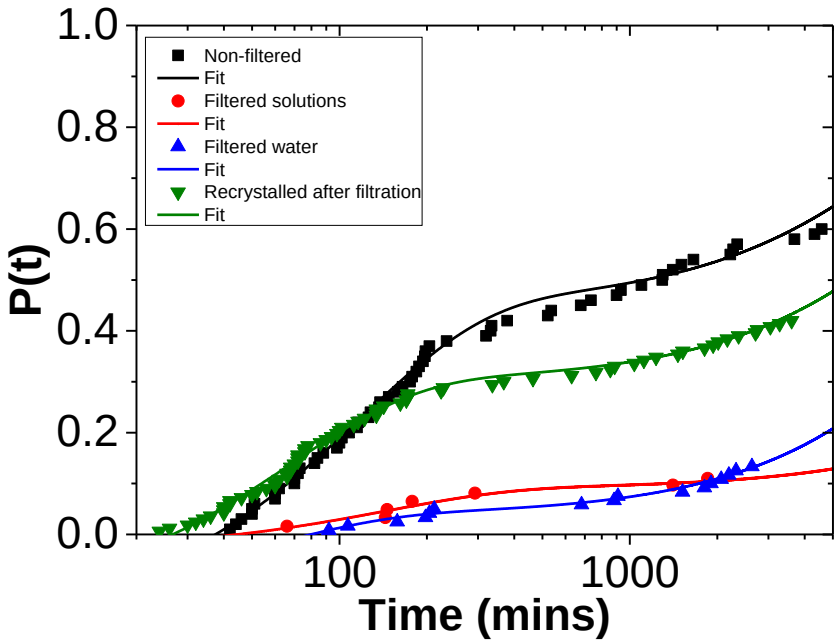

Figure 4.9: Fitting of biexponential mode to cumulative probability distribution of induction times of 1.5 supersaturation for non-filtered (black squares), filtered solutions (red circles), filtered water (blue triangles), recrystallized after filtration glycine (green triangles).

Conditions	A	τ_1 (min)	τ_2 (min)	t_d (min)
Filtered water	0.04(±0.01)	55.5(±67.6)	2.56(±0.45)X10^4	79.8(±27.1)
Recrystallized glycine after filtration	0.3(±0.06)	68.1(±3.9)	1.7(±0.15)X10^4	26.7(±1.3)
Nonfiltered	0.45(±0.012)	117.0(±8.6)	1.14(±0.16)X10^4	37.4(±2.8)
Filtered solution	0.09(*)	142.4(*)	1.13(*)X10^5	44.4(*)

Table 4.4: Estimated values of biexponential model parameter for different irradiated 1.5 supersaturated for component filtration. * too few data points to get error values.

From the biexponential function analysis of the 1.5 supersaturated solutions both filtered and non-filtered, (table 4.2) it is possible to see that the filtration is suppressing the laser induced nucleation rather than turning it off as a small percentage of vials still show laser induced nucleation.

The ½ filtered solutions with the 1.2μm PES syringe filter shows a reduction of the probability of laser induced nucleation by approximately half. The probability of laser induced nucleation is reduced from 0.45 to 0.19 suggesting a link between laser induced nucleation and concentration of the initiators. Furthermore, when filtered with 0.2μm PES syringe the decrease is larger which indicates that the smaller pore size is better at removing the initiators (table 4.3).

Biexponential analysis of the component filtering suggests the initiators source is the solvent because the reduction in laser induced nucleation is the same as when solutions were filtered, with A value of 0.04 and 0.09 respectively. (table 4.4)

4.4. Conclusions

In conclusion it has been demonstrated that pre-nucleating clusters are not the sole cause of the laser induced nucleation mechanism. This was achieved by continuing our investigation of the suppression effect nanofiltration has on the laser induced nucleation mechanism. By using DLS it was identified a pore size where clusters were unaffected and upon irradiation suppression still occurred. This new evidence casts serious doubt over the favoured optical Kerr effect mechanism where clusters are the sole component. It can be asserted that there is a need for a second initiator component, initiators whose concentration is potentially linked to the nucleation efficiency demonstrated by mixing filtered and unfiltered solutions. Through component analysis it was observed that the suppression of laser induced nucleation when samples were made with water after nanofiltration. The nature of these initiators is unknown, but these results identify where future research will be focused.

5. Water treatment and sources

5.1. Aims of these experiments

- Investigate the nature of initiators in the solvent
- Investigate the possibility of increasing laser induced nucleation probability through treatment of solvent

5.2. Experimental

See chapter 2 on sample preparation, laser irradiation and image analysis, rotavap, distillation, reflux and degassing water.

5.3. Results and Discussion

5.3.1. Distillation and Rotavap

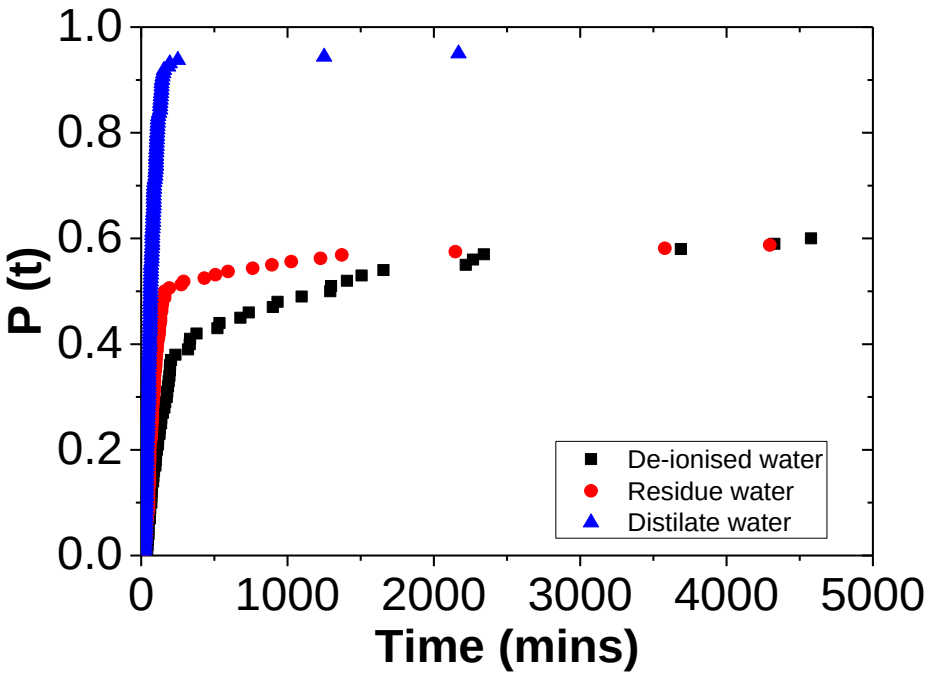

Figure 5.1: Cumulative probability distribution of induction times for 1.5 supersaturated aqueous glycine solutions made with deionised (black squares), residue (red circles) and distillate (blue triangles) from the rotavap.

Previously it was identified the need for an initiator to be in solution for laser induced nucleation. Further work identified that the source of these initiators was the solvent, deionised water (figure 4.6). The experiments in this section will investigate the nature of these initiators, with the goal of increasing the probability of laser induced nucleation occurring. The results in figure 5.1 show surprisingly that samples made with either the residue or distillate both showed the increase in laser induced nucleation probability, with the distillate increasing by over 2X. This increase in laser induced nucleation probability in both distillate and residue fraction is unexpected. If

the initiator was volatile, then you would expect an increase in laser induced nucleation probability in the distillate fraction and a decrease in nucleation probability in the residue water. The increase in both fractions would seem to indicate that more initiators have been introduced or created in the water. The introduction of impurities which could be initiators is a possibility as the rotary evaporator even when clean, can still leach trace chemicals from previous samples run on it. A way of testing this theory is to repeat the distillation process using virgin glassware which has not been used before to avoid any possibility of impurities being introduced. The results of these experiments are shown in figures 5.2 and 5.3.

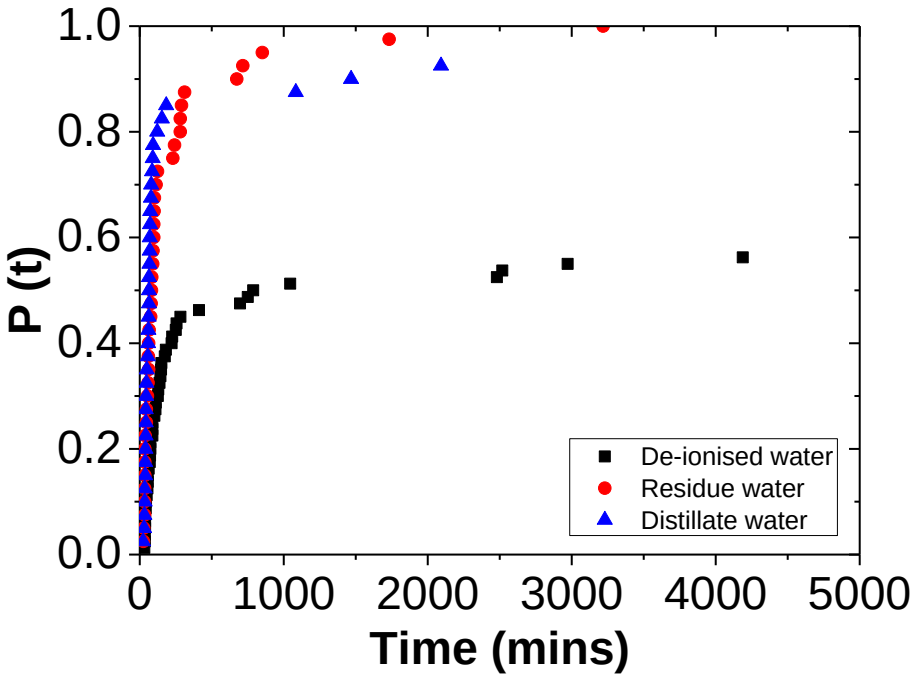

Figure 5.2: Cumulative probability distribution of induction times for 1.5 supersaturated aqueous glycine samples made with deionised (black squares), residue (red circles) and distillate (blue triangles) from the virgin glassware. Volume reduction by distillation was 50%.

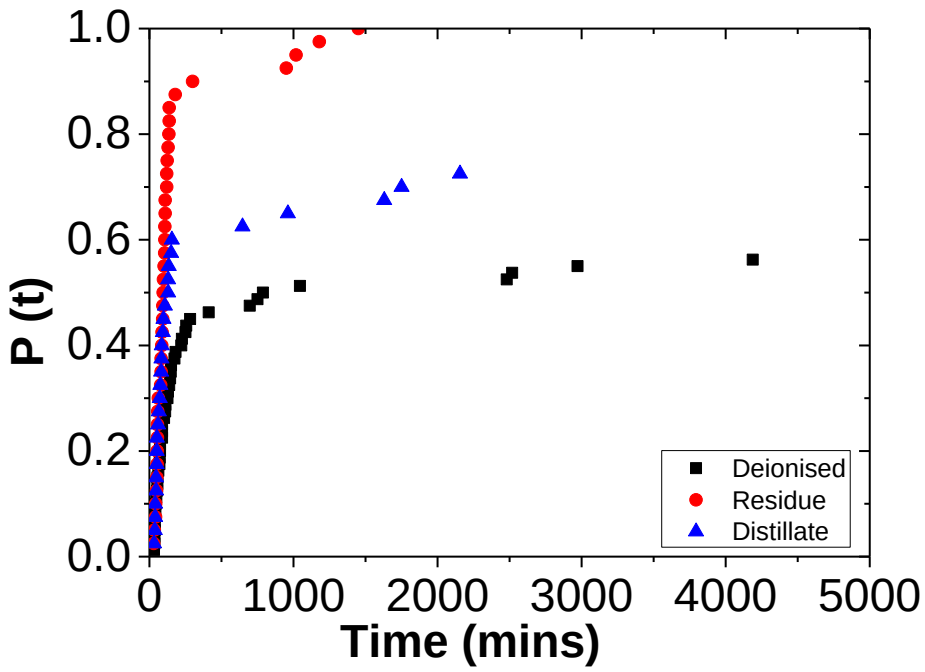

Figure 5.3: Cumulative probability distribution of induction times for samples made with deionised (black squares), residue (red circles) and distillate (blue triangles) from the virgin glassware. Volume reduction by distillation was 60%.

The experiments investigating the role distillation has on laser induced nucleation probability, whilst excluding the possibility of new impurities being introduced, were carried out by making supersaturated aqueous glycine samples after a benchtop distillation of deionised water using virgin glassware. The distillation showed a dramatic increase, over 2X, in laser induced nucleation probability of both distillate and residue fractions. When repeated again there was a dramatic increase in the residue water fraction and a slight increase in the distillate water fraction. The unexpected result raises question as to what the distillation process is actually doing to the initiators. Since new ones are not being added, they could be being created or the distribution of them in solution is changing, making the probability of laser induced nucleation more likely.

5.3.2. Reflux

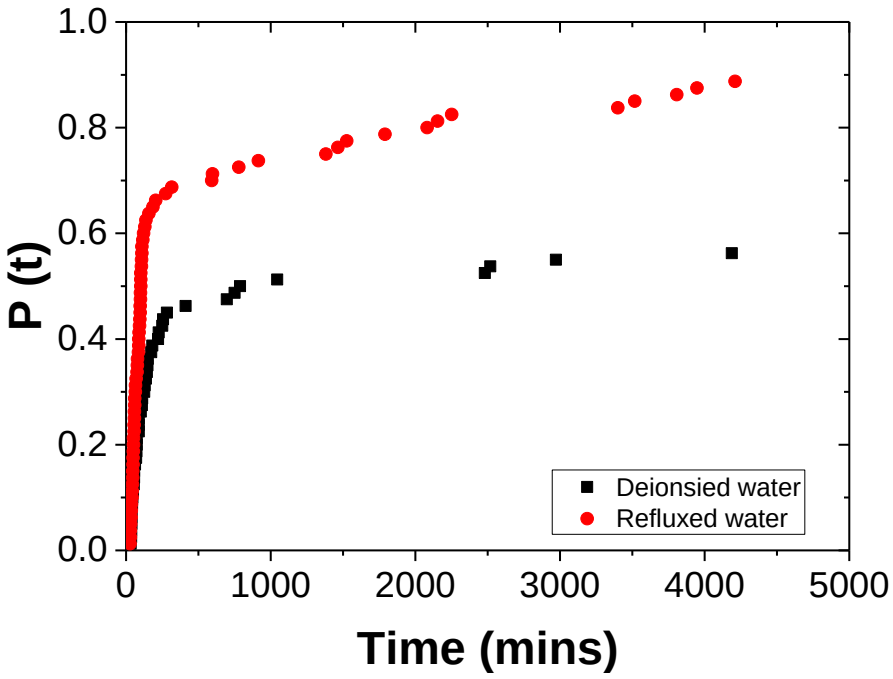

Figure 5.4: Cumulative probability distribution of induction times for samples made with deionised water, black squares, and water that had been refluxed for 3 hours in virgin glassware.

Deionised water was refluxed in virgin glassware for 4 hours. Supersaturated aqueous glycine samples were made using this refluxed water and irradiated and monitored noting induction times after irradiation. These experiments were carried out based on observation in the distillate and residue water and aim to identify if the effect of distillation is producible by refluxing. Samples made with deionised water that was refluxed expressed a higher laser induced nucleation probability than standard deionised water. This result shows that the observations in the distillation process are also visible in refluxing water suggesting that the increase seen in the distillation is a result of the heat treatment of the water.

5.3.3. Degassed water

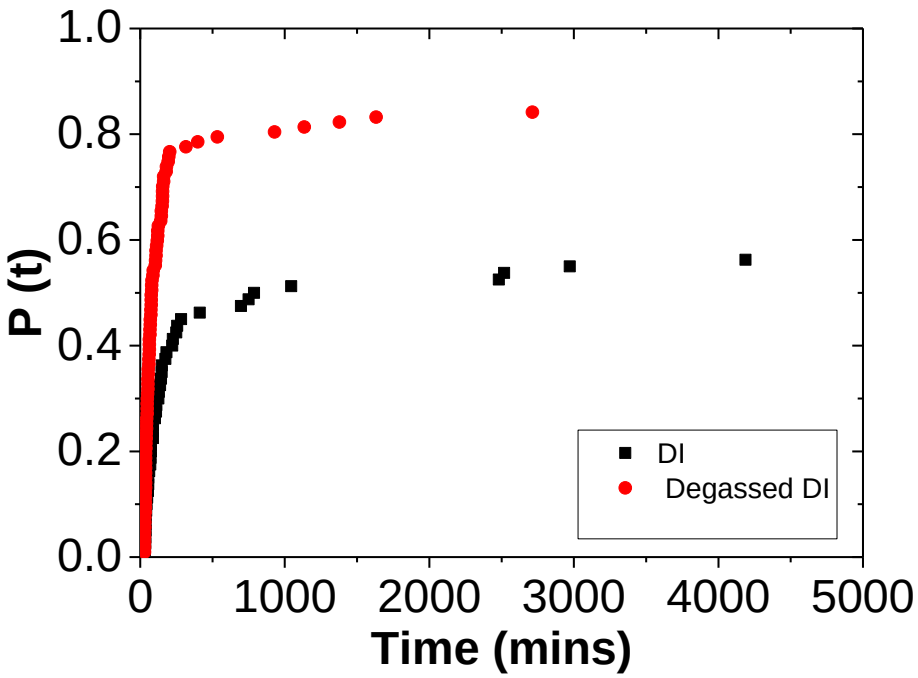

Figure 5.5: Cumulative probability distribution of induction times for samples made with deionised water (black squares) and degassed deionised water (red circles) water.

One possible action that is happening in both the distillation and refluxing of deionised water is degassing. This was tested by placing deionised water into a ultrasound bath on degas mode at 50°C for 5 hours then making supersaturated aqueous glycine samples and irradiating them. The results show the process of degassing of deionised water increases the laser induced nucleation probability by approximately 2X.

These series of experiments showed that various processing of deionised water can have a dramatic effect on increasing the probability of laser induced nucleation. The previous time laser induced nucleation probability has been increased was by doping with nanoparticles i.e. the introduction of known photoactive impurities. However, in this case nothing has been added and nothing has been taken away other than gasses which would not interact with the laser pulses. Since it is unlikely that it is creating new initiators in the deionised water through reflux, distillation, and degassing the distribution of initiators is improving resulting in a greater probability of interacting

with the laser pulses and a higher nucleation probability. This could be as a result of the initiators being attached to gas in solution. As the gas is removed, the initiators are able to freely move and improve distribution. An alternative is that the degassing is breaking up initiators which become smaller and more dispersed. This observation would still be in line with the idea of photoactive nanoparticle impurities as the initiator of laser induced nucleation.

5.3.4. Tap and HPLC grade water

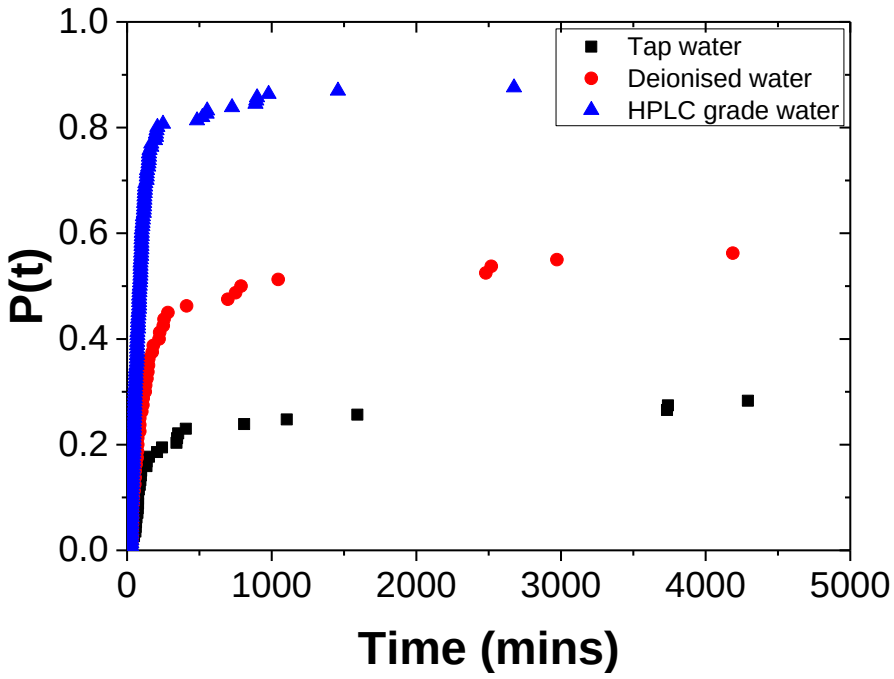

Figure 5.6: Cumulative probability distribution of induction times made with t (black squares), deionised (red circles) and HPLC grade (blue triangles) water.

The previous section had identified the need for initiators in the solvent to be present in order for laser induced nucleation to happen. It was demonstrated that processing the solvent resulted in a greater probability of laser induced nucleation without the need of additional initiators. However, there are several different sources/qualities of water which could have their own respective concentrations of initiators. These experiments aim to investigate this. Supersaturated aqueous glycine samples were made with three different sources of water; tap water, deionised water from an

Millipore ion exchange column, and HPLC grade water purchased from Sigma Aldrich, then irradiating them and noting the induction time.

The results of these experiments show that samples made with tap water resulted in a nucleation probability of 30%, deionised water 60%, and HPLC grade water 85% after 5000mins respectively. This suggests that there are a greater number of initiators in deionised water compared to tap water, and there are more initiators in HPLC grade water. This similar increase in nucleation probability between deionised water and HPLC grade water can also be seen in samples of urea made with deionised water and HPLC grade water (figure 5.7), another well investigated system for NPLIN confirming that the solvent is the source of these initiators.

The results coupled the observations in the processing of water, distillation reflux and degassing, suggest that the further purification of water results in the greater probability of laser induced nucleation. This would be contradictory with the proposed mechanisms involving photoactive nanoparticles unless they are being introduced by the purifying process from tap water to deionised water.

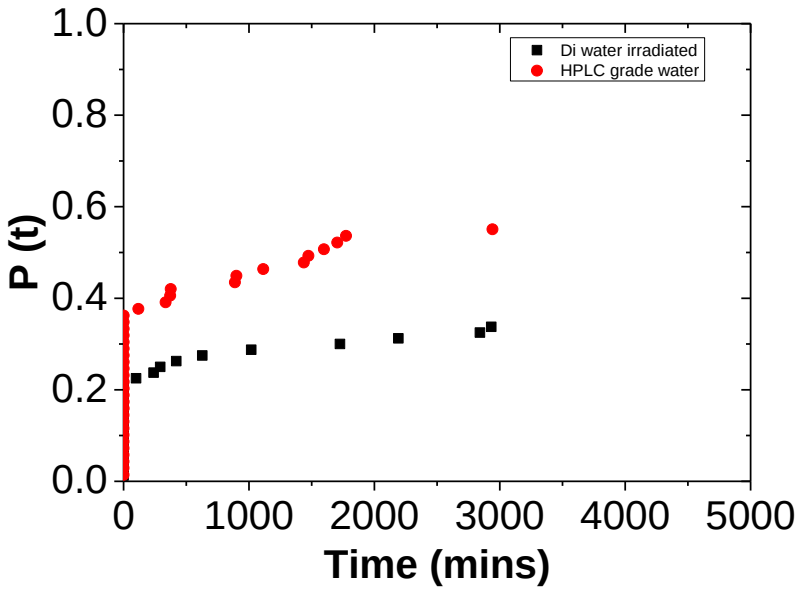

Figure 5.7: Cumulative probability distribution of induction times of 1.4 supersaturated aqueous urea solutions made with deionised (black squares), HPLC grade (red circles) water.

Water source	Induction time (s)
Deionised	10, 15, 20X2, 30X2, 40, 45, 50
HPLC grade	10X2, 20, 25X4, 30X3, 40X3, 45X3, 50X2, 60X7

Table 5.1: Induction times during irradiation for 1.4 supersaturated urea samples made with deionised and HPLC grade water respectively

5.3.5. Estimation of nucleation kinetics

This section will apply the biexpoential function to the cumulative probability distribution of induction times for different water treatments and water sources to investigate the effect they have on the nucleation efficiency and rate of the laser induced nucleation.

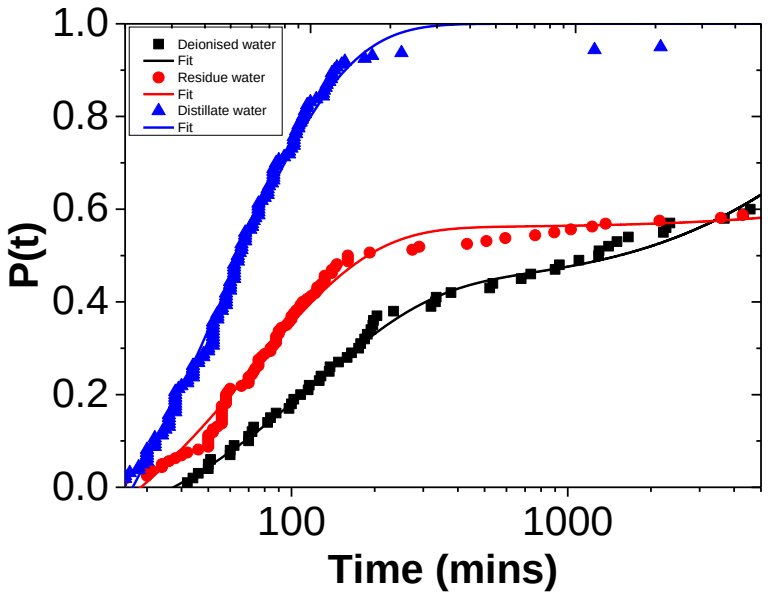

Figure 5.8: Fitting of biexponential model to cumulative probability distribution of induction times of 1.5 supersaturation for deionised water (black squares), residue water (red circles), distillate water (blue triangles). (fitting of data shown in figure 5.1)

Conditions	A	τ_1 (min)	τ_2 (min)	t_d (min)
Deionised	0.43(±0.04)	117.0(±0.04)	1.14(±0.2)X10^4	37.4(±2.8)
distillate	1.0(±0.01)	56.4(±2.5)	N/A	26.6(±0.5)
residue	0.56(±0.02)	72.1(±5.6)	9.93(N/A)X10^4	28.5(±1.6)

Table 5.2: Values of biexponential for different irradiated supersaturated samples filtered and non-filtered

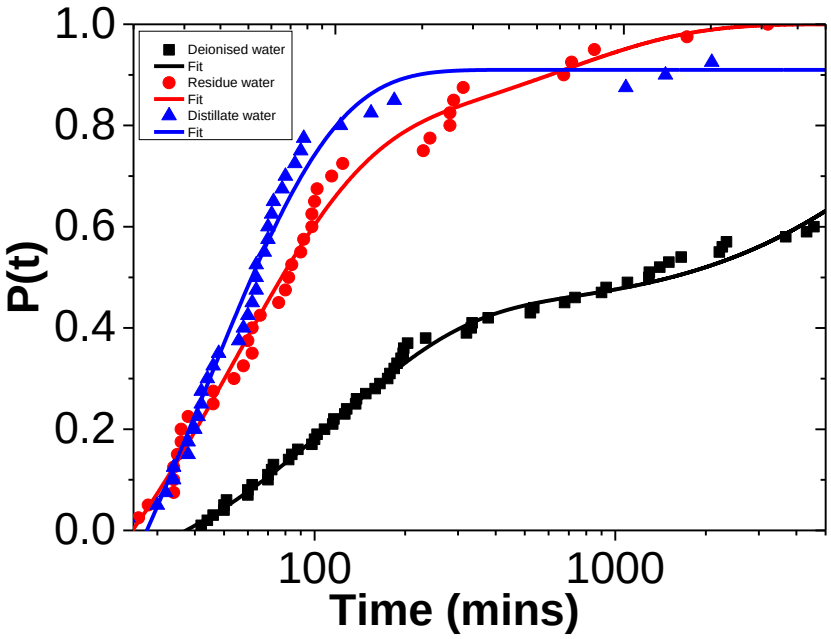

Figure 5.9: Fitting of biexponential model to cumulative probability distribution of induction times of 1.5 supersaturation for deionised water (black squares), residue water (red circles), distillate water (blue triangles). (fitting of data in figure 5.2)

Conditions	A	τ_1 (min)	τ_2 (min)	t_d (min)

Deionisesd	0.43(±0.04)	117.0(±0.04)	1.14(±0.15)X10^4	37.4(±2.8)
distillate	0.76(±0.08)	52.7(±9.6)	6.64(±0.2)X10^4	24.8(±2.2)
residue	0.91(±0.03)	42.8(±5.0)	8.19(±2.2)X10^9	27.7(±1.7)

Table 5.3: Values of biexponential for different irradiated supersaturated samples filtered and non-filtered

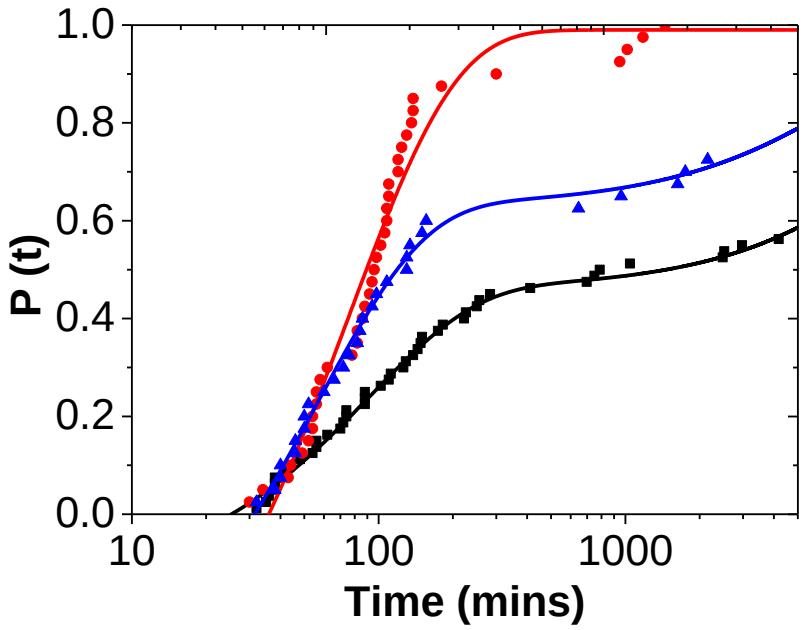

Figure 5.10: Fitting of biexponential model to cumulative probability distribution of induction times of 1.5 supersaturation for deionised water (black squares), residue water (red circles), distillate water (blue triangles). (Fitting of data in figure 5.3)

Conditions	A	τ_1 (min)	τ_2 (min)	t_d (min)
Deionised	0.43(±0.04)	117.0(±0.04)	1.14(±0.15)X10^4	37.4(±2.8)

Distillate	0.99(±0.02)	75.88(±5.64)	N/A	35.9(±1.7)
Residue	0.63(±0.04)	56.3(±8.13)	8.86(±0.8)X10^4	31.4±(2.0)

Table 5.4: Values of biexponential for different irradiated supersaturated samples filtered and non-filtered

Biexponential analysis of the residue and distillate fractions after distillation show that in all cases those fractions of vials that undergo laser induced nucleation (A) increases and have an associated nucleation time between 42-75 which suggests that the mechanism is the same and the nucleation rate is similar as expected with solutions of the same supersaturation.

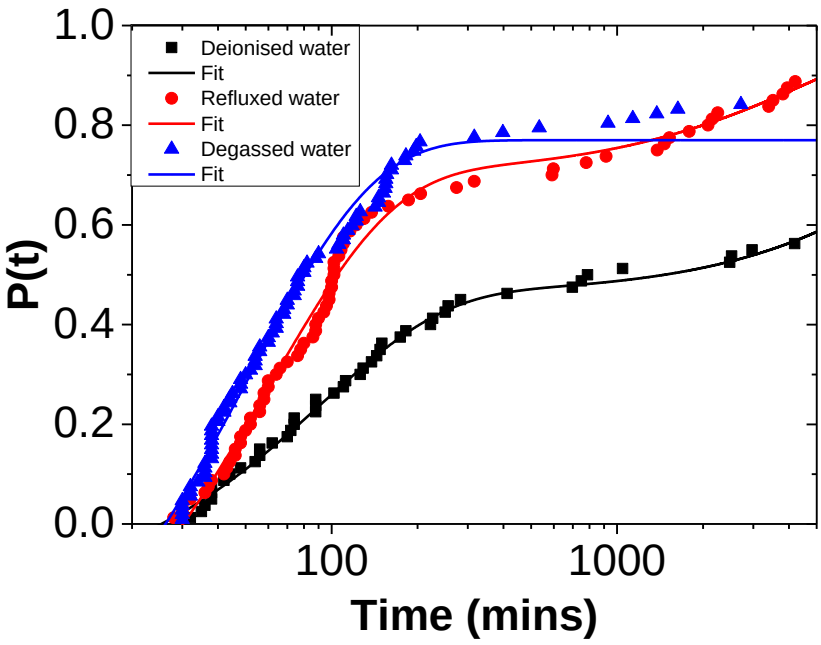

Figure 5.11: Fitting of biexponential model to cumulative probability distribution of induction times of 1.5 supersaturation for deionised water (black squares), refluxed water (red circles), degassed water (blue triangles).

Conditions	A	τ_1 (min)	τ_2 (min)	t_d (min)

Deionised	0.43(±0.04)	117.0(±0.04)	1.14(±0.15)X10^4	37.4(±2.8)
Reflux	0.7(±0.02)	60.57(±5.03)	4.85(±1.17)X10^3	30.2(±1.5)
Degassed	0.77(±0.02)	52.1(±3.3)	N/A	26.2(±0.6)

Table 5.5: Values of biexponential for different irradiated supersaturated samples filtered and non-filtered

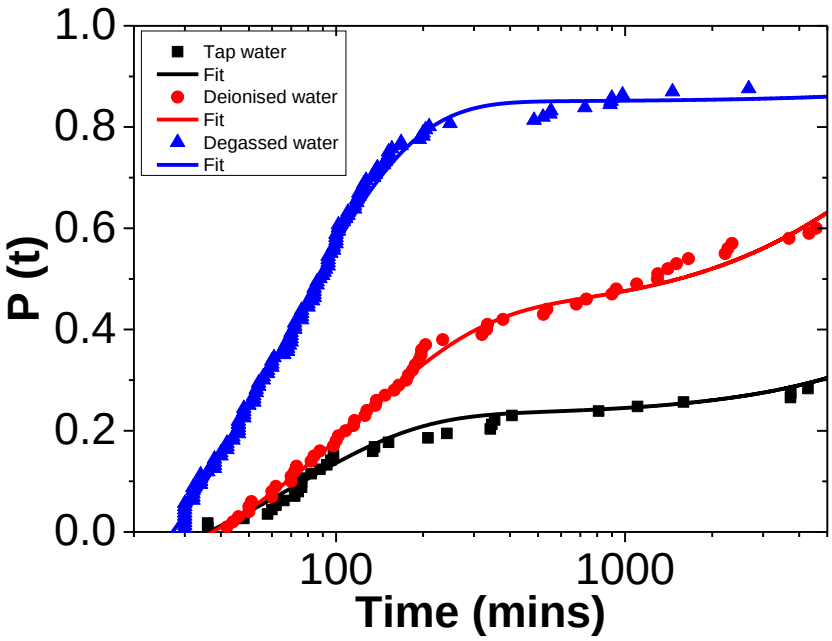

Figure 5.12: Fitting of biexponential model to cumulative probability distribution of induction times of 1.5 supersaturation for tap water(black squares), deionised water (red circles), HPLC grade water (blue triangles).

Conditions	A	τ_1 (min)	τ_2 (min)	t_d (min)
Deionised	0.43(±0.04)	117.0(±0.04)	1.14(±0.15)10^4	37.4(±2.8)

HPLC Grade	0.85(±0.01)	66.2(±1.8)	7.2(±0.01)X10^4	27.2(±0.01)
Tap	0.23(±0.02)	72.2(±13.3)	4.9(±1.8)X10^4	36.1(±4.95)

Table 5.6: Different water supplies

It is observed that despite the different water supplies having very different proportions of laser induced nucleation, they have similar associated nucleation time, so the mechanism is not changing, only the probability of it happening. By comparing the bimodal functions for all the different sources of water it is visible that the values of τ_1, associated with nucleation rate, are very similar (50-120 min). This suggests that the nucleation rate of laser induced nucleation is consistent, regardless of the type of water, and by changing the water source the probability of nucleation is changing but the mechanism is not.

5.3.6. Variation in experiments

In most cumulative probability distributions which are reported, the number of vials tested consists of at least 100 vials to ensure good statistics. However due to the limitation of the number of vials that can be tested at one time using the set up designed, typically two experiments needed to be run. In this section comparisons of the cumulative probability distribution between the two experiments of at least 50 vials is shown. The two data sets (runs) are experimentally the same, preparation; irradiation and monitoring are all constant, the only difference being that they come from different stock solutions made on different days.

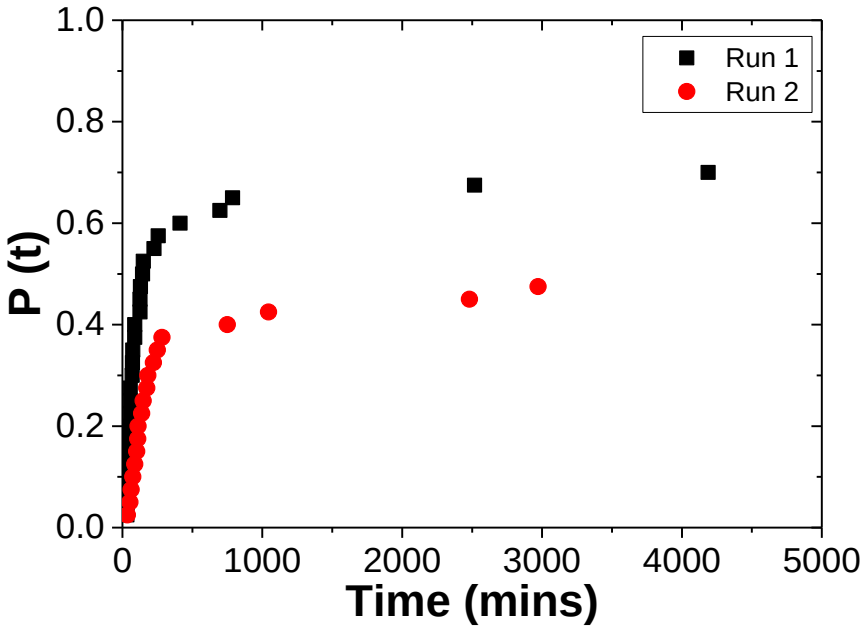

Figure 5.13: Cumulative probability distribution of induction times made with deionised water taken on different days

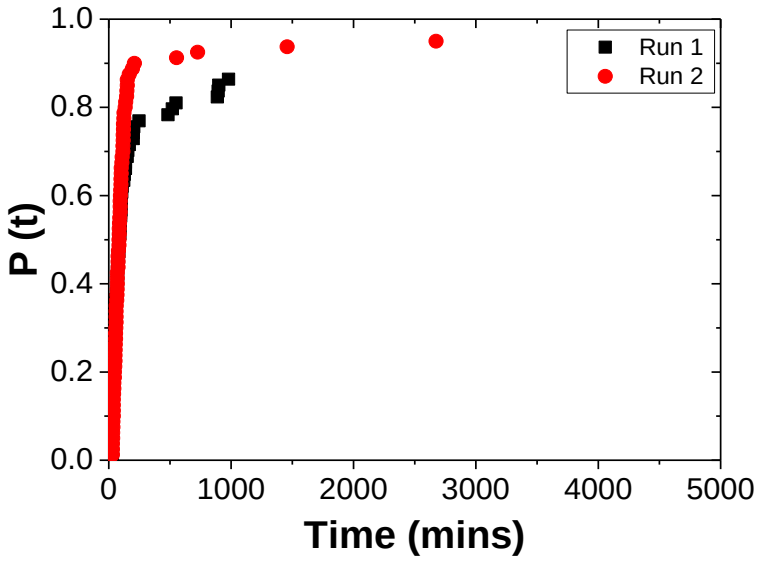

Figure 5.14: Cumulative probability distribution of induction times for samples made with HPLC grade water made on different days

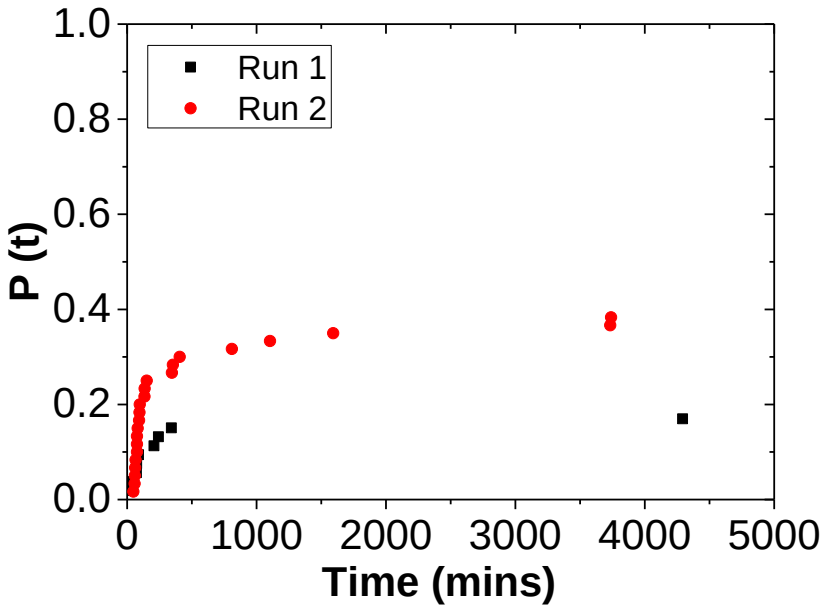

Figure 5.15: Cumulative probability distribution of induction times for samples made with tap water made on different days

In the experiments using different sources of water to make supersaturated glycine solutions samples were prepared on different days, so by investigating how the nucleation probability varies from batch to batch, it might be possible to learn about the underlining statistics of laser induced nucleation in different water sources.

The analysis of the two individual runs that make up the data set reported in previous chapters for deionised water, it is observed that there is a difference of ~0.2 (0.41-0.58) for the probability of laser induced nucleation occurring, but the nucleation rate is similar in magnitude (40-120). This indicates that the underlying mechanism is the same in both runs, but the probability of that mechanism occurring is varied. Furthermore, comparing this result to the variance seen in the tap water subsets it is observed that similarly, the variance in laser induced nucleation probability is approximately 0.2 (0.14-0.29) This suggests that the water supply from the tap has this concentration of initiators that varies from time to time, and that when the water is fed into the deionised water machine that variance still occurs but the probability of laser induced nucleation is increased overall by the treatment. The variance in the HPLC grade water which is a stock water supply also has this variance of ~0.2 (0.74-0.97). A separate supply of water also displays this 0.2 variance in probability which could indicate the variance is intrinsic to the mechanism rather than concentration of initiators.

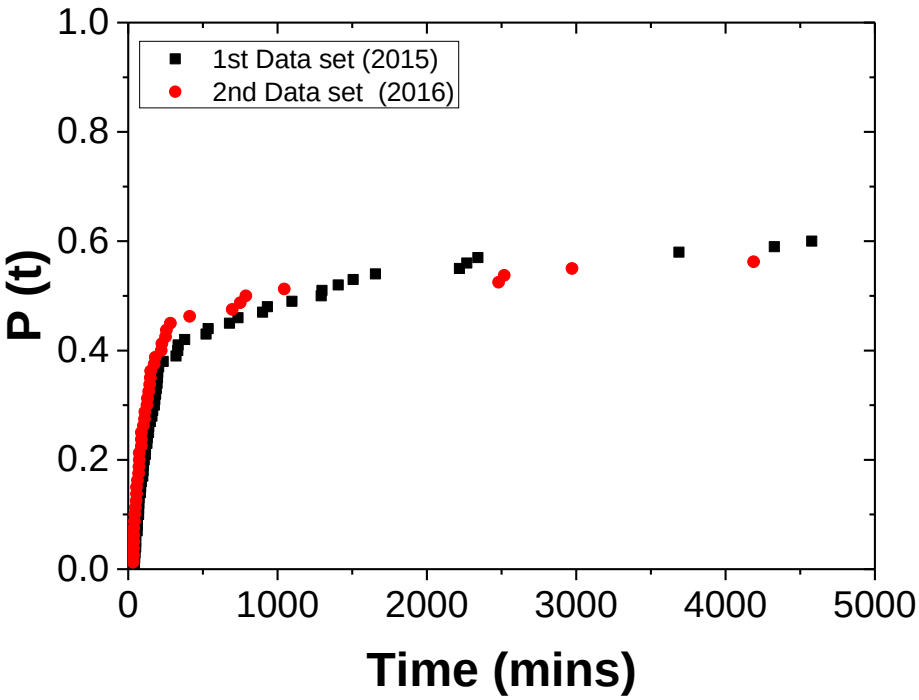

Figure 5.16: Cumulative probability distribution of induction times for different sets of data consisting of over 100 vials taken a year apart.

Comparison of the two raw data sets of over 100 vials of the sample solution and irradiation parameters, shows that the there is a large overlap. Despite there being an underlying variance between runs, shown previously, the average of the runs is consistent when the number of vials tested is significant. This would seem to indicate that the average probability of laser induced nucleation occurring is the same, and the possibly the concentration of the initiators in solution are the same, despite being made a year apart.

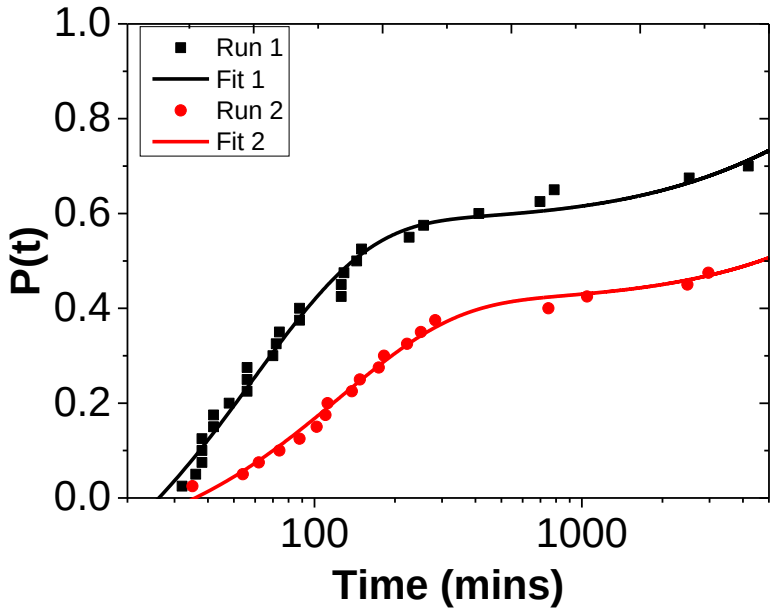

Figure 5.17: Fitting of biexponential model to cumulative probability distribution of induction times of 1.5 supersaturation for deionised water taken of different weeks, run 1 (black squares), run 2 (red circles).

Conditions	A	τ_1 (min)	τ_2 (min)	t_d (min)
Run 1	0.58(±0.03)	58.6(±9.8)	1.1(±0.6)X10^4	26.2(±2)
Run 2	0.41(±0.03)	123.5(±21.1)	2.78(±2.13)X10^4	35.8(±6.2)

Table 5.7: Values of biexponential for different irradiated supersaturated of deionised water

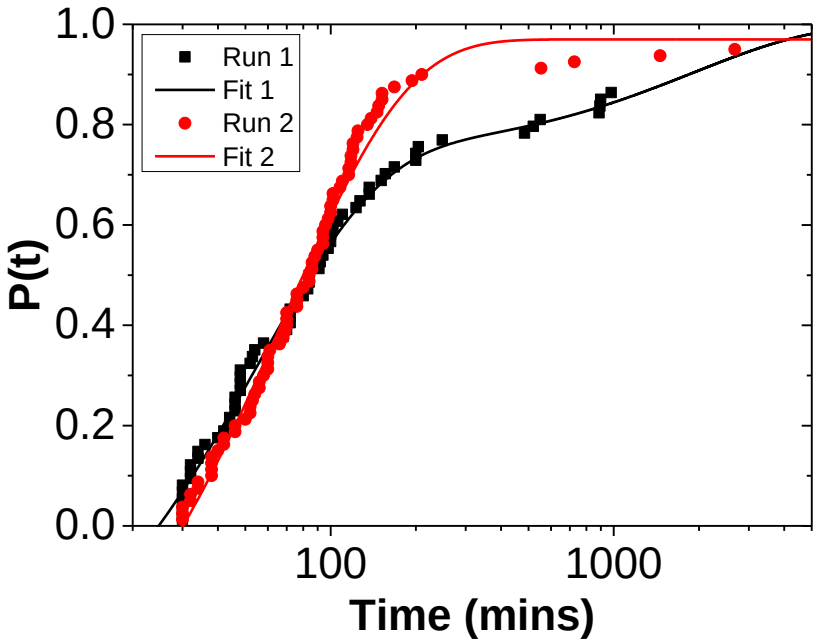

Figure 5.18: Fitting of biexponential model to cumulative probability distribution of induction times of 1.5 supersaturation for HPLC grade water taken of different weeks, run 1 (black squares), run 2 (red circles).

Conditions	A	τ_1 (min)	τ_2 (min)	t_d (min)
Run1	0.74(±0.03)	54.8(±5)	1.9(±0.8)X10^3	24.7(±1)
Run 2	0.97(±0.02)	68.9(±4)	N/A	30.1(±1)

Table 5.8: Values of biexponential for different irradiated supersaturated of HPLC grade water

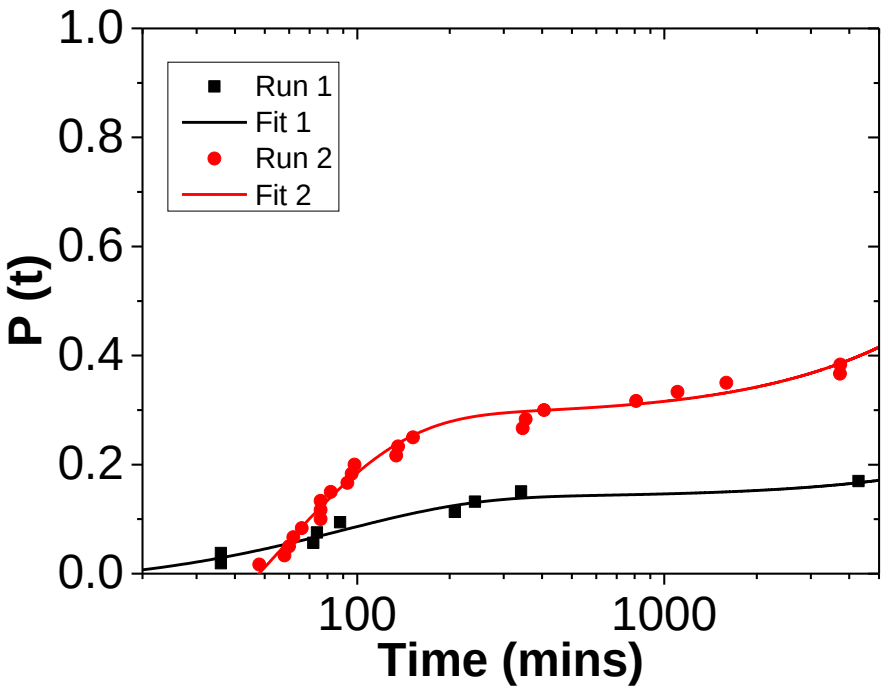

Figure 5.19: Fitting of biexponential model to cumulative probability distribution of induction times of 1.5 supersaturation for tap water taken of different weeks, run 1 (black squares), run 2 (red circles).

Conditions	A	τ_1 (min)	τ_2 (min)	t_d (min)
Run 1	0.14(±0.04)	89.1(±8.0)	1.35(±2.7)X10^5	15.4(±3.0)
Run 2	0.29(±0.02)	52.1(±9.9)	2.55(±0.8)X10^4	47.9(±3.9)

Table 5.9: Values of biexponential for different irradiated supersaturated of tap water

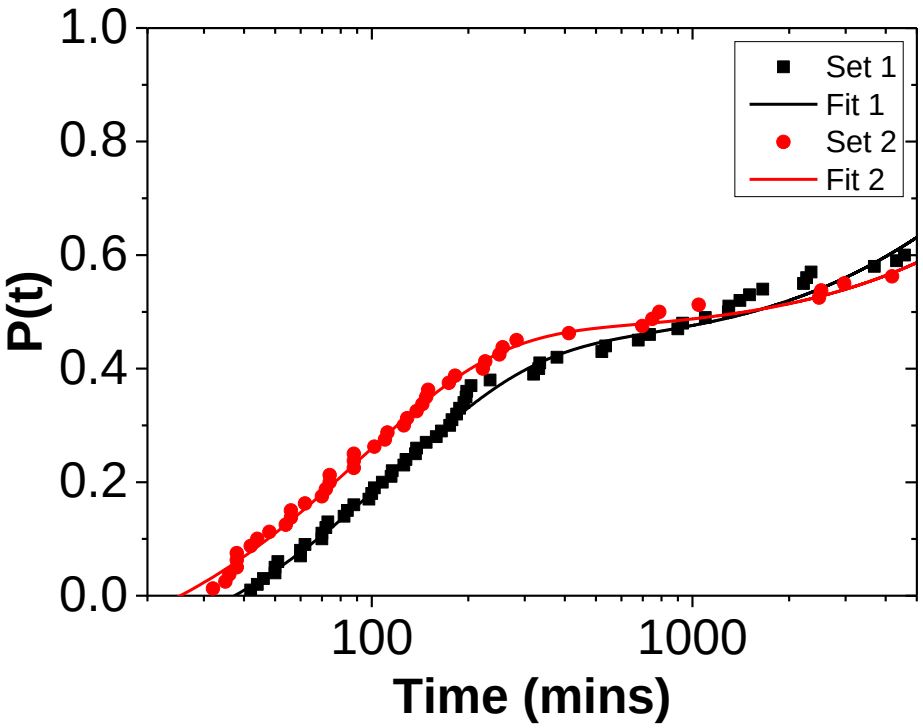

Figure 5.20: Fitting of biexponential model to cumulative probability distribution of induction times of 1.5 supersaturation for deionised water reported take a year apart (figure 5.16), set 1 (black squares), set 2 (red circles).

Conditions	A	τ_1 (min)	τ_2 (min)	t_d (min)
Set 1	0.46(±0.01)	91.1(±8.6)	1.86(±0.16)X10^4	25.3(±2.8)
Set 2	0.43(±0.04)	117.0(±0.04)	1.14(±0.15)X10^4	37.4(±2.8)

Table 5.10: Values of biexponential for different irradiated supersaturated samples filtered and non-filtered

For the 1.5 supersaturation deionised water two different sets of data consisting of at least 100 vials. Comparison of these two data sets allows for testing how repeatable the results are. These two data sets are very similar, the associated τ_1 and A are, 91.1 and 117 and 0.46 and 0.43 respectively. These values demonstrate that the

observations made regarding the probability and associated nucleation rate is consistent and repeatable.

5.4. Conclusions

In conclusion, evidence has been gathered for the need of an initiator to be present for laser induced nucleation to occur, and through a series of experiments investigating the effect different sources of water have on nucleation probability, that the source of these initiators is the solvent. The processes tested were distillation using a rotary evaporator and a bench top distillation using virgin glassware, reflux, and degassing. All resulted in a significant increase in nucleation probability. Observation in the increase nucleation probability of degassed water indicated that this is the key process that is happening in the distillation and refluxing of water. This increased nucleation probability by degassing is an interesting result considering it has previously been shown to be increased through doping with photoactive nanoparticles, however, in this case nothing has been added. It is suspected that the prcessing for the removal of gas from the solvent is resulting in a more favourable distribution of initiators or nanoparticles in solution.

6. Polymorphism observations

6.1. Aims of these experiments

- Investigate the role laser pulses have on polymorphism in glycine
- Investigate how increasing laser induced nucleation efficiency influences resultant polymorphism

6.2. Experimental

See chapter 2 section on FT-IR.

6.3. Results and Discussion

6.3.1. Spontaneous nucleation

In order to determine the effect laser induced nucleation has on polymorphism, it is important to have a background of spontaneous nucleation polymorphic result.

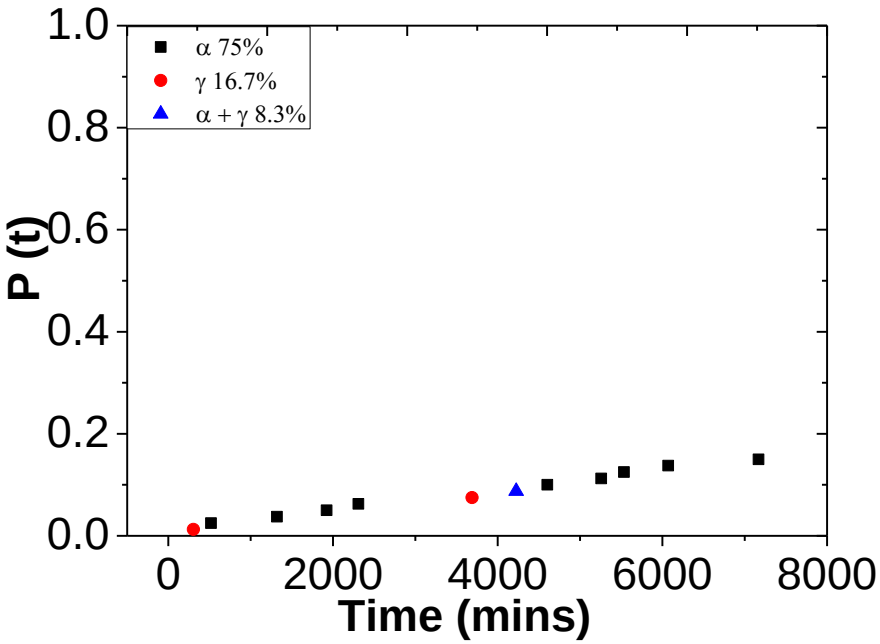

Figure 6.1: Cumulative probability distribution of induction times of spontaneous nucleation for 1.5 supersaturation, α-polymorph (black squares), γ-polymorph (red circles), α+γ polymorph mix (blue triangles)

As expected, the nucleation rate for the supersaturations used in experiments is very low, which means that the number of vials that crystallise is few even after 8000 minutes, so it is difficult to draw conclusions. However, they can be used as an indication what polymorphic result to expect in samples not irradiated with laser pulses. It can be seen that when using aqueous glycine solutions of 1.5 supersaturation, 75% crystallised the α-polymorph, 16.7% the γ-polymorph, and 8.3% α+γ polymorph. It is clear that the great majority of samples that did crystallise were in the alpha form as expected. Using this result, it is possible to draw comparison to

the proportion of vials which formed the γ-form when irradiated to identify the effect the laser pulses have.

6.3.2. Effect of supersaturation

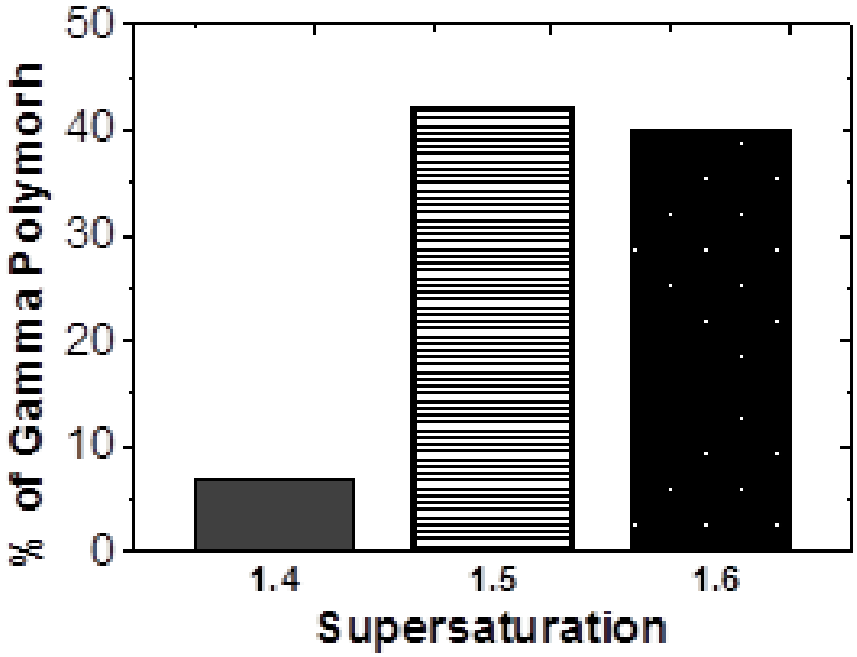

Figure 6.2: Percentage of gamma polymorph obtained for nonfiltered irradiated glycine solutions at supersaturation 1.4, 1.5 and 1.6.

Polymorphism analysis of the glycine crystals was performed using an ATR-FTIR spectrophotometer in the spectral range of 800 cm^{-1} to 1200 cm^{-1} at ambient temperature. The characteristic spectra of the α- and γ-polymorphs are shown in the section 2.14. The α-polymorph exhibits a distinct absorption peak at 910 cm^{-1}, and the γ-polymorph shows a characteristic peak at 927 cm^{-1}.[92]

Differential polymorphism behaviour in irradiated samples of different supersaturations is observed. At low supersaturations (1.4) the α-polymorph is strongly predominant, and only one vial out of 14 which crystallized showed the γ-polymorph. By increasing the supersaturation to 1.5 and 1.6, the probability of formation of the γ-polymorph increases significantly to about 40% of the vials which crystallized. From a preliminary analysis on a limited number of samples, it was noted that both the α- and γ- polymorph were formed in the fast laser-induced regime, which

indicates that nucleation of both polymorphs is enhanced by laser irradiation. However, crystals formed in the slow regime were almost exclusively the α-polymorph, which is consistent with a spontaneous nucleation regime, as samples which were not irradiated similarly yielded almost exclusively the α- polymorph. In order to further confirm the solid form identification single-crystal X-ray diffraction patterns were recorded for the crystals obtained from solutions at supersaturation 1.5, and it was observed that a similar percentage of the γ- polymorph as was determined by ATR-FTIR experiments. Clair *et al*.[100]have shown in a recent study that glycine solutions at 290 K irradiated with linearly polarized laser radiation with power density of 0.9 GW/cm^2 produced 20−25% of the γ polymorph for supersaturations of 1.4 and 1.6.

These results quantitatively differ from the observations reported by Sun *et al*. [19] where 100% of the α-polymorph is observed for supersaturation 1.4, and 100% of the γ-polymorph is observed for supersaturations 1.5 and 1.6 for linearly polarized light. However, it was observed just 40% of the γ-polymorph for supersaturations 1.5 and 1.6, in contrast to 100% observed by Sun *et al*.[62] This could be due to intensity of laser pulses (our value is 0.4 GW/cm^2 and they reported 0.7 GW/cm^2). Our observations also differ from those of Clair *et al*. [100] but some of these differences may be because Clair *et al*. used a different irradiation geometry in which the laser beam exits the solution through the air−solution interface and the nucleation they observe occurs at that interface, while Sun *et al*. used a similar geometry to that used here where the laser beams enters and exits the solution through glass walls and nucleation occurs in bulk solution. Because of the small number of nucleating samples, for cases without laser irradiation or with filtration, there were too few results to give reliable information for numerical probabilities of polymorphic outcomes. Nevertheless, in all cases without laser irradiation or with filtration, the vast majority of crystals formed were α-polymorphs at all supersaturations.

Comparing the polymorphic outcome of samples that were irradiated and non-irradiated, it is clear there is a pronounced effect on the fraction of gamma formed in the irradiated samples.

6.3.3. Effect of different water types, processing and polarization

This section will investigate the polymorphic outcome of changing laser polarisation and water processing and sources by plotting the cumulative probability distribution of induction times and noting what the resultant polymorph was. It could be suggested that enhanced gamma polymorph formation was primarily seen in the laser induced regime. Plotting the polymorphic results this way will look to address this claim.

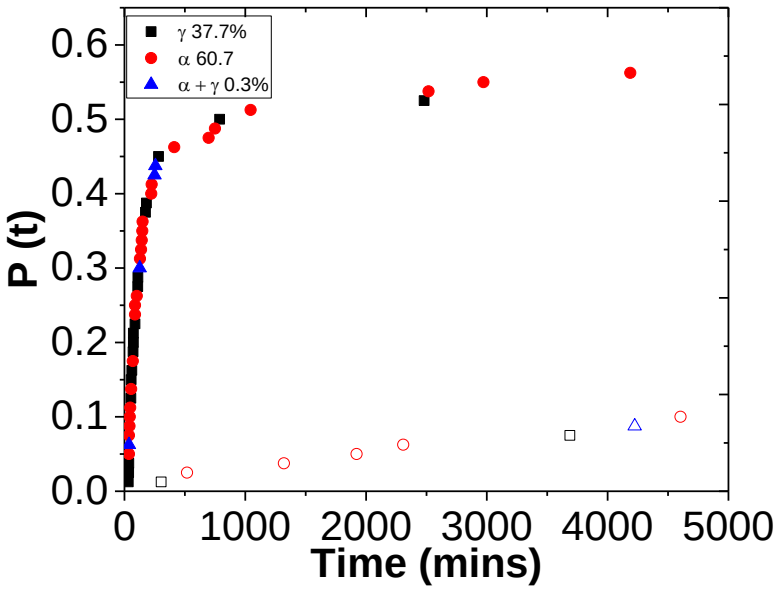

Figure 6.3: Cumulative probability distribution of induction times for deionised water showing polymorphism for linear polarised light

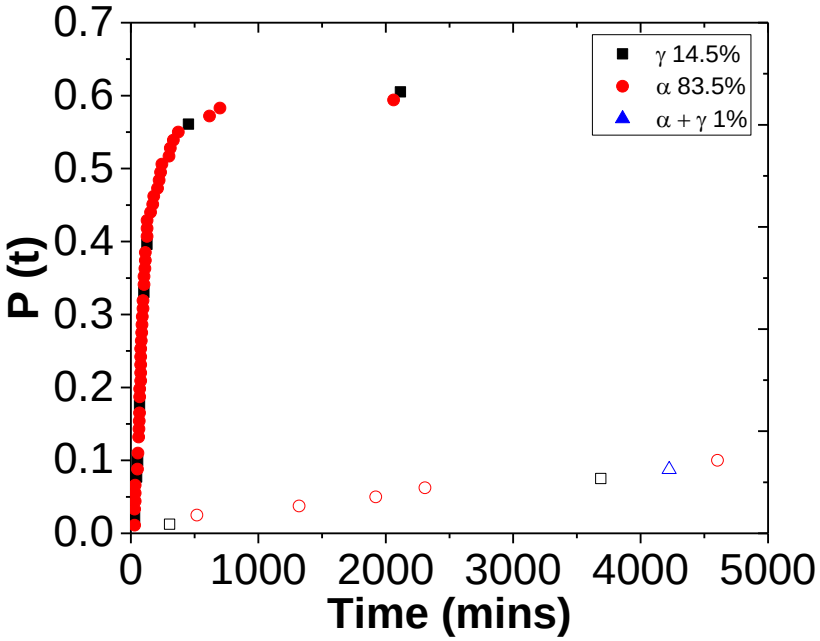

Figure 6.4: Cumulative probability distribution of induction times showing polymorphism for circular polarised light

The effect polarization of the laser pulses on the polymorphic outcome of laser induced nucleation is disputed. Previously Garetez *et al*[19, 62] were able to obtain exclusively the α-form from circular polarized light, and the γ-form from linear polarized light for 1.5 supersaturation. However, this result has not been reproduced, and the results presented here are only able to achieve 40% gamma formation for linear polarized light.[91]

When a second set of over 100 vials was tested with linear polarized light a dramatic increase in the gamma polymorph is noted, to the same extent as the previously reported value. When the sample conditions of solution and irradiation are the same, but the polarisation of light is circular, a dramatic reduction of the gamma polymorph is observed, reducing from ~37% to 14.5%. From table 6.1 it is possible to see the results obtained for both the LP and the CP are close to those reported by Alexander *et al* [22] but are very different from Garetz *et al* [19] which reported the polarized switching at the 1.5 supersaturation. Differences from the values reported by Garetz *et al* could be the result of the vials used; the curvature of the vials acting as a lens and focusing the laser. Different shaped vials would act as a different strength lens changing the effective laser power.

	Report	α-polymorph %	γ-polymorph %
LP	Kendall *et al*	60	40
	Garetz *et al*	0	100
	Alexander *et al* (20˚C)	50	30
	Alexander *et al* (25˚C)	100	0
CP	Kendall *et al*	84.5	15.5
	Garetz *et al*	100	0
	Alexander *et al*	80	20

Table 6.1: Various reported percentage values of polymorphic results for 1.5 supersaturation, with comparable irradiation intensity (~0.4GW/cm^2) for linear polarized (LP) and circular polarized light (CP).
Alexander *et al* experimental conditions 20˚C, 0.5GW/cm^2
Garetz *et al* experimental conditions 15-25˚C, 0.46GW/cm^2

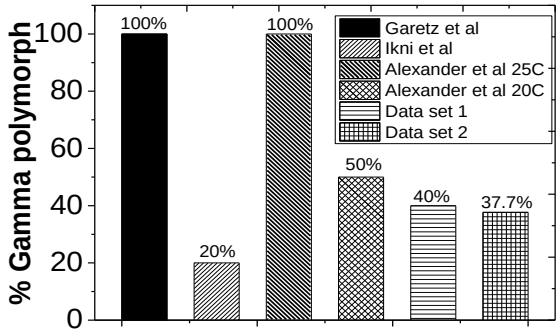

Figure 6.5: Reported percentage of gamma polymorphism reported for 1.5 superstation with deionised water irradiated with linear polarized light. It should be noted that the Ikni uses a higher intensity (0.91GW/cm^2) and irradiation is through the interface not the bulk. It should be noted that the experiments conducted by Alexander *et al* had a recrystallization and dissolution step before irradiation.

Polymorphism was measured for various types of waters, 1.5 supersaturation after irradiation, taking note of their induction time. As discussed in chapter 5, treatment of deionised water with distillation resulted in an increased nucleation probability of both the residue and the distillate fractions. The use of purchased HPLC grade water also had this effect.

In a previous set of experiments of approximately 100 vials, it was demonstrated that for 1.5 supersaturated solution made with deionised water that there was an increase in nucleation rate of both the α and γ form, and the resulting ratio was 60:40. This experiment set was repeated, similarly with approximately 100 vials, and the same observation can be seen. There is an increase in the nucleation rate of both the α and γ polymorph to a similar ratio as previously demonstrated, 55:37, and by plotting the polymorph result as a function of time (figure 6.6), it is possible to see that the less likely γ-polymorph forms in both initial laser induced nucleation phase and the slower spontaneous phase, suggesting that the influence on the polymorphism happens even if the nucleation is not induced by the laser pulse.

In the previous chapter it was shown that these two results for the cumulative probability are similar, demonstrated through the biexponential function values, and the polymorphic outcome suggest that the results of laser induced nucleation is repeatable and consistent.

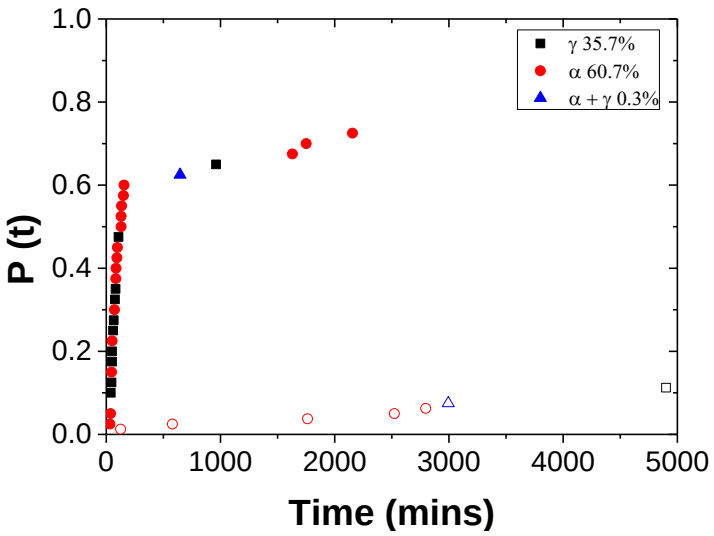

Figure 6.6: Cumulative probability distribution of induction times for samples made with residue water showing polymorphism

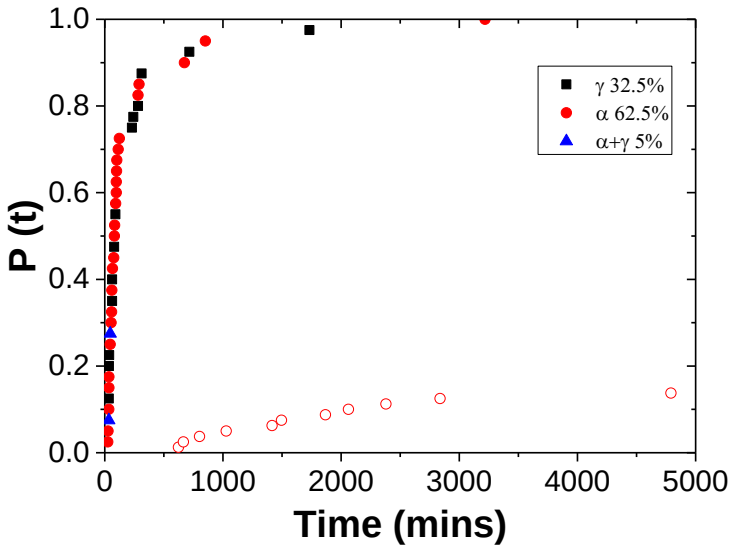

Figure 6.7: Cumulative probability distribution of induction times for samples made with distillate water showing polymorphism

In chapter 5 it was demonstrated that the processing of deionised water by distillation resulted in an increase in the probability of laser induced nucleation in both the distillate and the residue fractions, and here the resulting polymorphs of the crystals formed, and what they could mean for the potential mechanism, will be discussed.

The results for both the residue and distillate show an increase in % γ polymorphic form compared to non-irradiated samples. Similarly, the results of the deionised water show there is the unfavoured γ-polymorph being formed in the second spontaneous nucleation regime, which further suggests that there is a residual effect of the laser pulses that influence the polymorph even if nucleation by the laser pulse does not occur. Furthermore, the increase in nucleation rate compared to non-irradiated samples of the individual polymorphs is increased to a similar proportion as the deionised water. The residue fraction resulted in a 64:36 alpha:gamma split and the distillate fraction showed a 63:33 split compared to the ~60:40 in the standard deionised water.

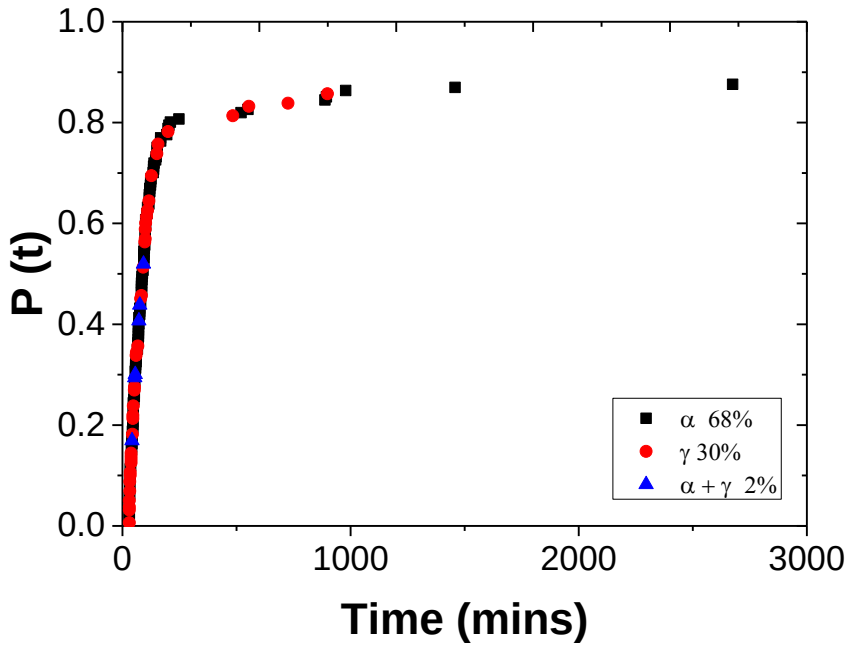

Figure 6.8: Cumulative probability distribution of induction times for samples made with HPLC grade water showing polymorphism

This surprising result indicates that the polymorphic influence on crystals formed after irradiation is independent of the probability of successful laser induced nucleation. In these cases, the probability of laser induced nucleation is increased from the deionised water suggesting that the concentration of initiators is different, but their polymorphic outcome is very similar, suggesting that the mechanism could consist of 2 components; an initiator entity with which there is a probability of a laser pulse interacting with, and a polymorphic influence that is separate from the initiator.

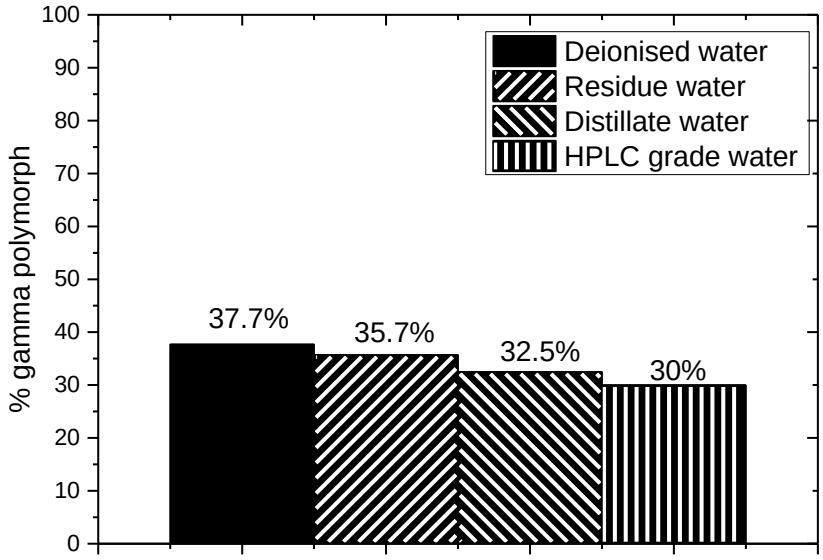

Figure 6.9: Percentage of gamma polymorphism reported for 1.5 superstation with different water types

Similar results can be seen in the different source of water used, HPLC grade, to make the glycine samples for irradiation. The HPLC grade water demonstrated an increase in the laser induced nucleation probability compared to the deionised water with an increase of the γ-form in both the laser induced and spontaneous regime. Similar to the other cases reported here, the ratio of the 2 polymorphs is again approximately 60:40 alpha:gamma split. This result, coupled with the others, strongly indicated an independent polymorphic influence of the laser pulses as part of the overall mechanism.

6.3.4. Recrystallized glycine

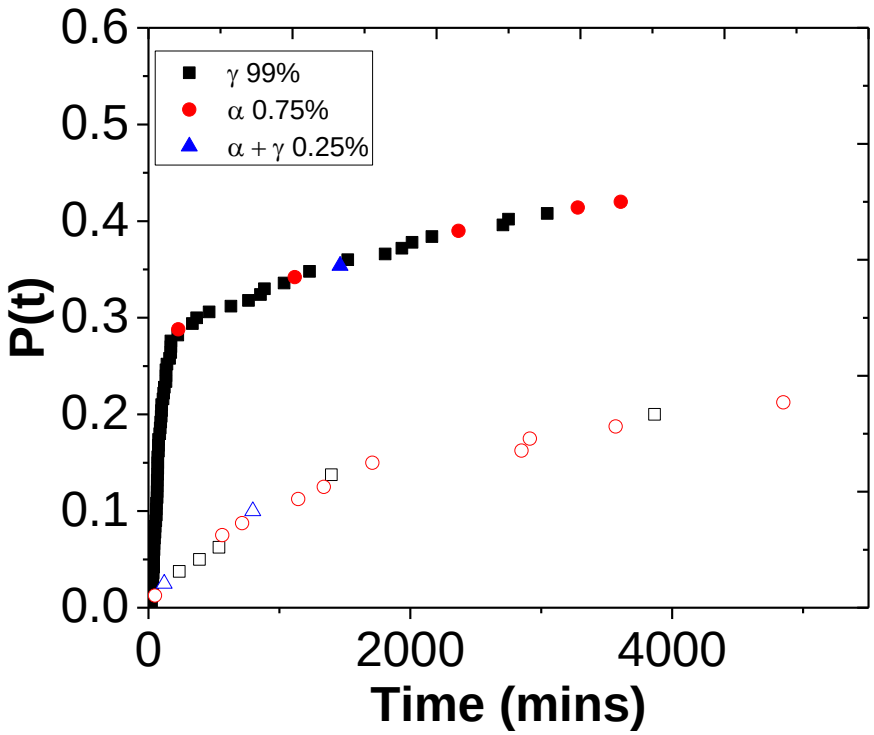

Figure 6.10: Cumulative probability distribution of induction times for 1.5 supersaturated aqueous glycine solutions made with recrystallized glycine after nanofiltration and with deionised water. Gamma polymorph (black squares), alpha polymorph (red circles), alpha and gamma polymorph (blue triangles), filled in symbols are irradiated, hollow symbols are non-irradiated.

In experiments made with glycine that had been recrystallized after nanofiltration it was found that 99% of vials that crystallised formed the less favoured gamma polymorph. This result appears to support the observations in polymorphic control demonstrated by Garetz *et al*[17, 71] and is in stark contrast to 40% gamma polymorphic formation results shown earlier.

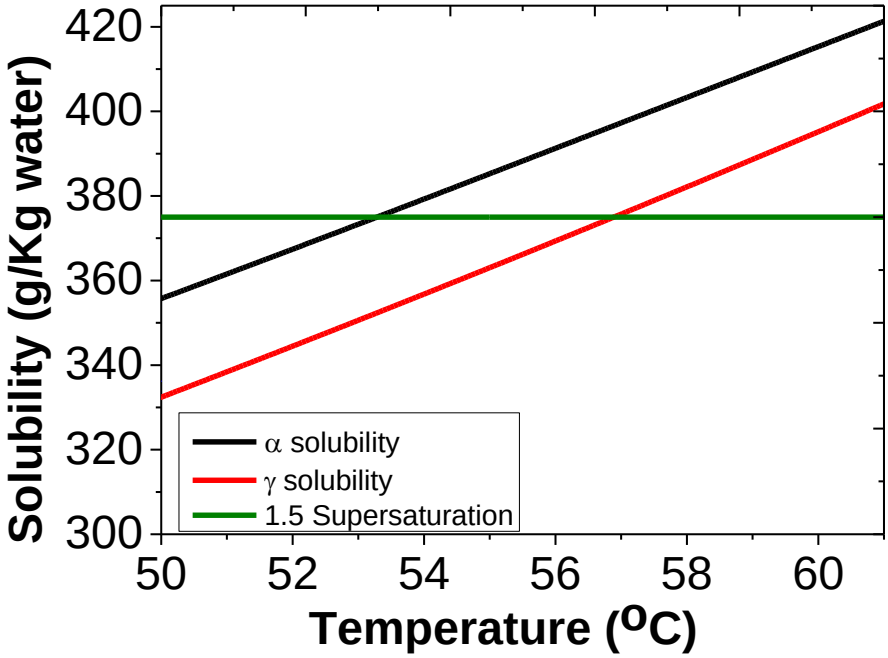

Figure 6.11: Solubility of α and γ glycine in water[92] and position of 1.5 supersaturation

The starting material was tested for its polymorphism, and the glycine purchased from Sigma Aldrich was only the alpha form, but when recrystallized after nanofiltration showed a mixture of both alpha and gamma glycine. All samples were made by dissolving the glycine in deionised water in an incubator at 60°C. However, inspection of the solubility of the individual polymorphs in water (figure 6.11) shows that at ~57°C the solubility becomes less than the concentration required to achieve 1.5 supersaturation. And whilst attempts can be made to ensure the temperature is above this value, there could be temperature fluctuations inside the incubator due to air flow and circulation, and heat transfer to the external environment. Therefore, it is possible that the gamma polymorph never completely dissolved in solution and the polymorphic outcome could be the result of unintentional seeding with the gamma polymorph. This observed difference in polymorphic starting material and its, respective solubilities could explain the polarized switching window. A way of testing this is to test a polymorphic mixture starting material with circular polarized light. Another experiment that should be carried out to investigate this explanation would be heating samples to above 60°C to ensure thorough dissolving of both polymorphs.

6.4. Estimation of nucleation kinetics of polymorphs

This section will investigate the effect different parameters have on the polymorphic outcomes. It has been suggested that the enhanced gamma formation observed is only found in the laser induced nucleation regime (initial fast). This is addressed by creating cumulative probability distribution of induction times indicating what the polymorph formed was. However, now because the individual polymorphs are being analysed the previous model is no longer applicable, as the value of P(t) will eventually equal 1, which is impossible for competing polymorphs. Thus P(t) of the raw data must equal the sum of the probabilities for each polymorph at time (t),P_α and P_γ. Furthermore, the sum of the probability must not exceed the total P(t) at the end of the experiment (~5000). To account for this the equation was modified by introducing K values, which act as a limiting factor and correspond to the fraction of samples that crystallised that polymorph and calculates the parameters for each polymorph at the same time (Eq. 6.3) where x can be either α or γ polymorph.

$$P(t) = K_\alpha P_\alpha + K_\gamma P_\gamma \quad \textbf{Eq. 6.1}$$

$$1 = K_\alpha + K_\gamma \quad \textbf{Eq. 6.2}$$

$$P_x = A_x(1 - exp^{\left(-\frac{t_x - t_{d,x}}{\tau_{1,x}}\right)}) + (1 - A_x)(1 - \exp^{\left(-\frac{t_x - t_{d,x}}{\tau_{2,x}}\right)}) \quad \textbf{Eq. 6.3}$$

However, in fitting of the individual polymorphs simultaneously the values of τ_2 gave poor fits so were fixed to $1.14X10^4$ which was calculated previously for 1.5 supersaturation.

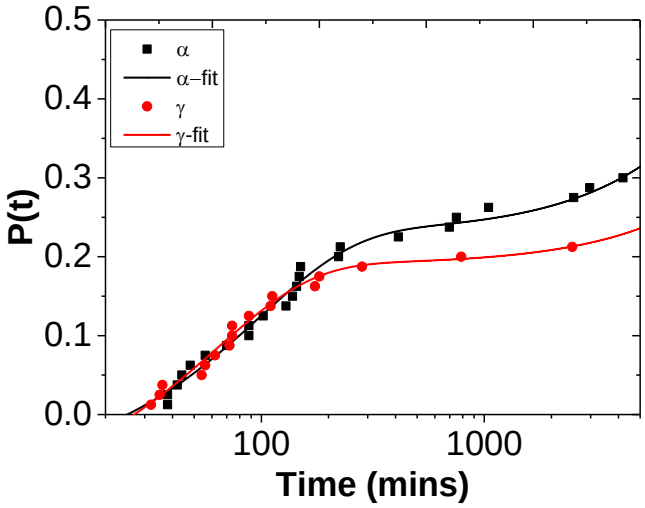

Figure 6.12: Bimodal fitting of the cumulative probability distribution of induction times of alpha and gamma polymorphism in sample made with deionised water and irradiated with linear polarised light

	K	A	τ_1 (min)	τ_2 (min)	t_d (min)
α-form	0.78	0.23	97.0	N/A	25.0
γ-form	0.22	0.19	62.7	N/A	26.9

Table 6.2: Values of biexponential for different polymorphs supersaturated solutions made with distillate water irradiated with linear polarized light

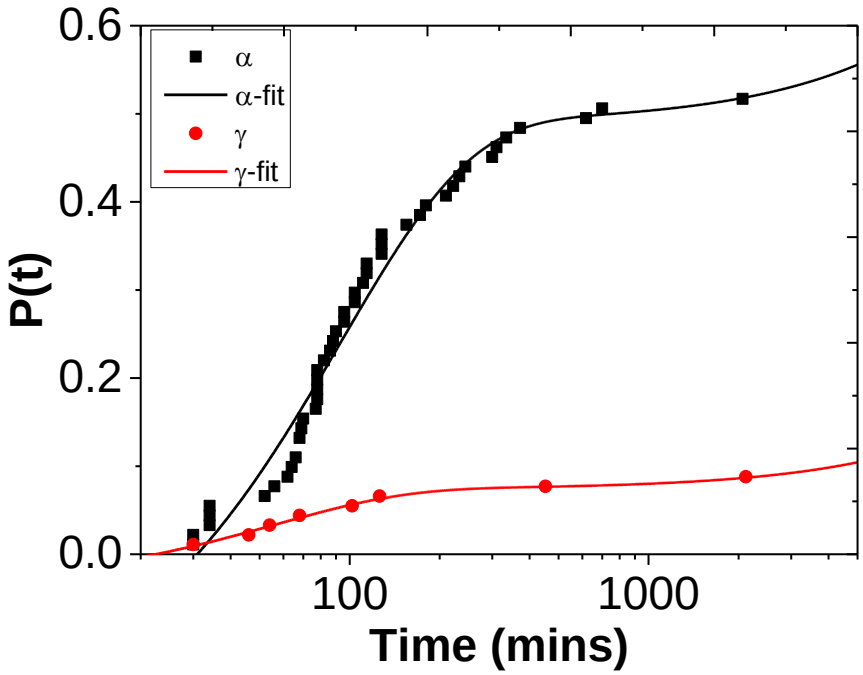

Figure 6.13: Bimodal fitting of the cumulative probability distribution of induction times of alpha and gamma polymorphism in sample made with deionised water and irradiated with circular polarised light

	K	A	τ_1 (min)	τ_2 (min)	t_d (min)
α-form	0.56	0.49	93.0	N/A	30.9
γ-form	0.44	0.074	56.3	N/A	22.5

Table 6.3: Values of biexponential for different polymorphs supersaturated solutions made with distillate water irradiated with circular polarized light

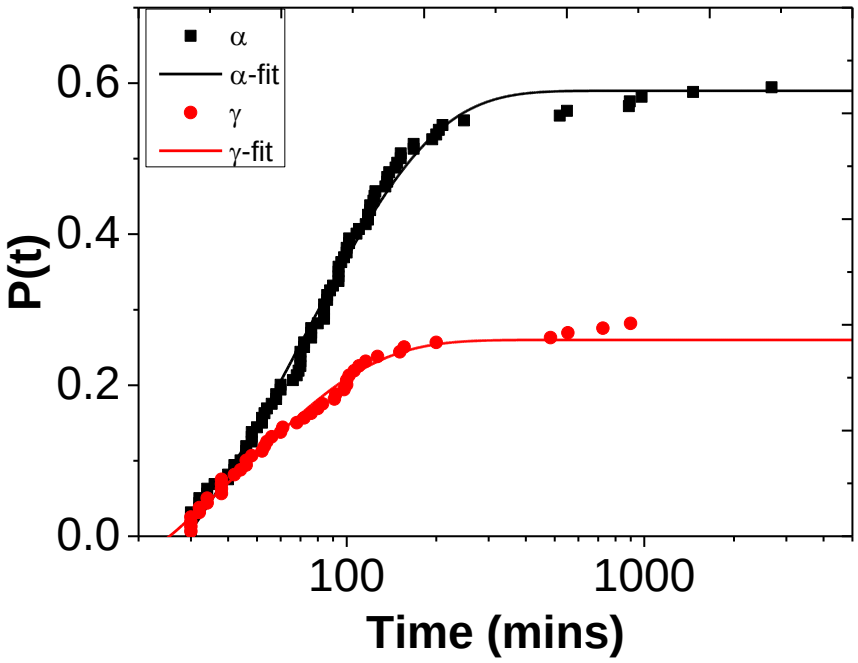

Figure 6.14 Bimodal fitting of the cumulative probability distribution of induction times of alpha and gamma polymorphism in sample made with HPLC grade water and irradiated with linear polarised light

	K	A	τ_1 (min)	τ_2 (min)	t_d (min)
α-form	0.65	0.59	72.5	N/A	29.0
γ-form	0.35	0.26	46.0	N/A	25.4

Table 6.4: Values of biexponential for different polymorphs of supersaturated solutions made with HPLC grade water

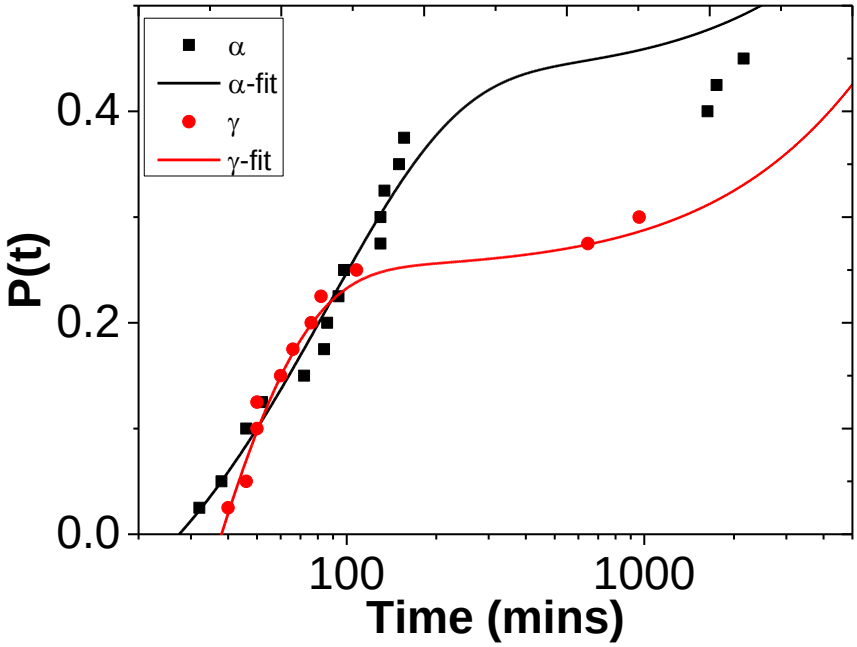

Figure 6.15: Bimodal fitting of the cumulative probability distribution of induction times of alpha and gamma polymorphism in sample made with residue water and irradiated with linear polarised light

	K	A	τ_1 (min)	τ_2 (min)	t_d (min)
α-form	0.62	0.43	85.4	N/A	27.4
γ-form	0.38	0.25	24.5	N/A	38.0

Table 6.5: Values of biexponential for different polymorphs of supersaturated solutions made with residue water irradiated with linear polarised light.

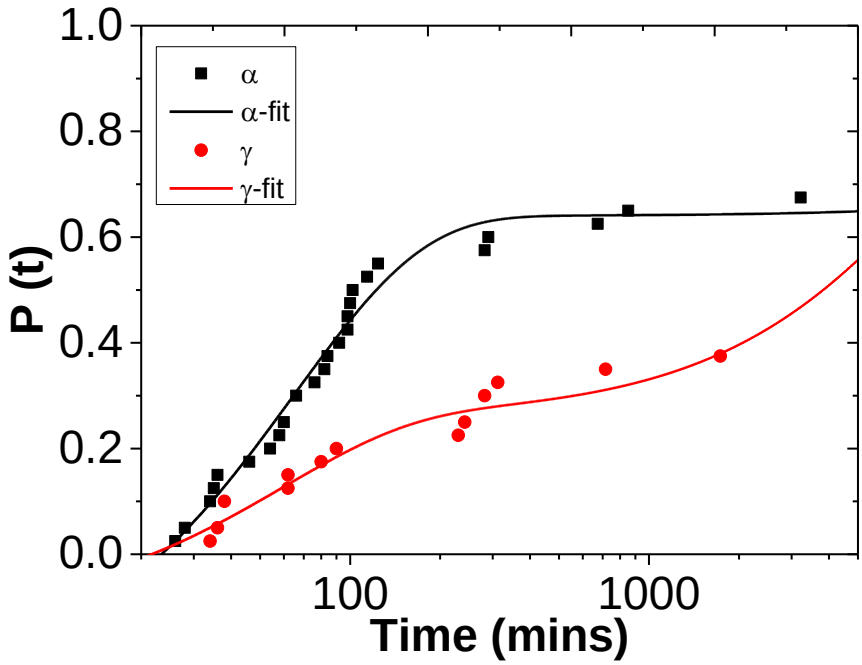

Figure 6.16: Bimodal fitting of the cumulative probability distribution of induction times of alpha and gamma polymorphism in sample made with distillate water and irradiated with linear polarised light.

	K	A	τ_1 (min)	τ_2 (min)	t_d (min)
α-form	0.06	0.64	65.2	N/A	23.4
γ-form	0.94	0.26	58.7	N/A	21.7

Table 6.6: Values of biexponential for different polymorphs of supersaturated solutions made with distillate water

The results of the biexponential analysis showed that despite the proportions of alpha:gamma spilt varying depending on the water used, the associated nucleation time for each polymorph are similar so the nucleation rate for the competing polymorphs are the same. It also shows that despite there being a large majority of

the gamma forming in the laser induced regime, there is some gamma being formed in the spontaneous regime, which from the baseline measurements should be entirely alpha.

It has been suggested [41] for a system of competing polymorphs the total nucleation rate should be equal to the sum of the nucleation rates of the individual polymorphs. However, in the experiments reported here this is not the case. An explanation for this could be because the laser is changing the energy barrier. Another possible explanation would be that some metastable alpha polymorph converts to the stable gamma form.[17, 18] This is because the gamma τ_1 is consistently lower than the alpha and the transformation of the alpha to the gamma form would result in fewer alpha and more gamma and a difference in the τ_1 values.

6.5. Conclusions

It is observed that as supersaturation increases from 1.4-1.5, there is an increase in the percentage gamma formation; the increase in the probability of the gamma polymorph is expected as supersaturation increases. There is a dramatic increase from 1.4-1.5, 20% to 40% gamma formation. The increase in the percentage of gamma formation could be the result of a localised supersaturation increase caused by cavitation

Laser irradiation has a pronounced influence on the polymorphic outcome of nucleation, enhancing both the alpha and gamma polymorph, depending on the polarization for 1.5 supersaturated aqueous glycine solutions. In the previously identified polarized switching zone, where it is possible to selectively form either the gamma for linear or alpha for circular polarized light, this work demonstrates that a 60:40 alpha: gamma split is possible for linear polarized and 80:20 for circular polarized light. This difference between circular and linear polarized light indicates that whilst the optical Kerr's effect is not responsible for the mechanism it still be having an influence on the alignment of molecules which could influence the resultant polymorph.

The observed 60:40 alpha:gamma split in linear polarised light was replicated by a second set of experiments including at least 100 vials, which were collected using the same irradiation and solution conditions. This result indicates that for a fixed set of

laser and solution parameters the polymorphic outcome can be reproduced. This is also the first time both polymorphic and probability outcome have been reproduced.

Furthermore, it is demonstrated that for all the different treatments of water, distillation, both distillate and residue waters and HPLC grade water, for the same irradiation and solution conditions the 60:40 alpha gamma-split is seen. It shows that whilst the overall nucleation probability increases, it is a similar enhancement of the polymorphic results each time. This can indicate that the polymorphic outcome is intrinsic to the laser irradiation and an independent aspect of the overall mechanism.

7. Final Conclusions and suggestions

Crystallisation is a commonly used technique for purification and processing used in several industries, and consists of two processes nucleation and growth. Of the two, nucleation is far less understood and controllable so many investigations have been undertaken on this issue. Laser induced nucleation offers a unique way of controlling both when and where the nucleation, event occurs and influencing the resultant polymorphism. It has the potential to be a useful tool for both fundamental understanding of nucleation and as an industrial tool for crystallisation. However, the mechanism is not well understood.

In chapter 3 the effect of intensity and irradiation duration was investigated. It has been demonstrated that an increase in pulse intensity results in an increase in nucleation probability four-fold. It also shows that nucleation peaks at the duration of 60 seconds. The decrease in the probability with reduced irradiation time could be explained by the reduced chance of interacting with an initiator, greater than 60 seconds, could be explained by an increase in temperature which would stabilise the supersaturation. This chapter also demonstrated the effect of increasing supersaturation; there is an increase in probability of nucleation from 1.4-1.5 and a larger increase from 1.5-1.6. Two nucleation regimes were observed; the first fast laser induced, and the second slower spontaneous regime. It is observable that in all three supersaturations there is a broad distribution of induction times starting from the time between when laser irradiation finished and the time when 1mm crystal appears according to published growth data. This distribution of induction times is also seen in urea, but due to its very high growth rate the nucleation occurs during the irradiation period.

Chapter 4 investigates the effect nanofiltration and solute cluster have on the laser induced nucleation mechanism. Using dynamic light scattering the presence of solute clusters was demonstrated with an average hydrodynamic radius of 250 nm. It was found that nanofiltration with poly (ether sulfone) membrane syringe filters of 0.2 µm

removed solute clusters and supressed laser induced nucleation. Several pore sizes were investigated, and it was found that 1.2 and 5µm were critical pore sizes where the clusters were not removed. However, when samples were filtered with these pore sizes, the suppression of laser induced nucleation was observed. This result suggests that solute clusters are not the cause of laser induced nucleation, there needs to be an initiator also, which means the optical Kerr's effect can be excluded as a viable mechanism as it solely requires solute clusters. Subsequent experiments investigated the source of the initiators, by irradiating samples made with filtered deionised water it was identified to be the source of the initiators. By mixing equal parts of filtered and non-filtered solutions it was observed that the nucleation probability effectively halved which links the concentration of initiators to the nucleation probability.

Investigating the nature of the initiators and attempting to isolate them to increase laser induced nucleation probability was the focus of chapter 5. This was done using a rotary distillation under vacuum, testing both distillate and residue. This was then repeated using virgin glassware in a bench top distillation. In all cases an increase in laser induced nucleation was observed in both the residue and distillate. This surprising result was followed up by treating deionised water by refluxing and degassing, and again, an increase in laser induced nucleation was observed. This suggests that the distillation is promoting nucleation by degassing the deionised water. The degassing of deionised water is not adding anything, and the only thing being removed is gas which would not interact with the laser pulse. This suggests the degassing is improving the distribution of initiators in solution by either breaking up groups of them or removing initiators that may have been stuck to the wall of the vessel. It was also found that HPLC grade water had a higher, and tap water a lower, probability than deionised water respectively. By analysing the individual experimental runs that make up the data set, it is possible to see the underlying probability in the mechanism. The typical variance in probability of laser induced nucleation was 20%, and can be seen in all types and sources of water.

The influence that polarized laser pulses have on aqueous glycine solutions has been greatly disputed. In chapter 6 it was demonstrated that there was a sharp increase in in the gamma polymorph percentage when increasing the supersaturation from 1.4-1.5. It is observed that there is a 40% probability of gamma formation at supersaturation1.5. This is in contrast to the values previously reported by Garetz *et*

al[19] 100% gamma polymorph formation under similar conditions. The 60:40 alpha:gamma split that was seen in this in one data set of 100 vials was reproduced in another data set of over 100 vials of the exact same experimental conditions over a year later. This is the first time that a polymorphic result for laser induced nucleation has been reproducible. Under the same irradiation and solution conditions but with circular polarized light instead of linear polarized light, the percentage gamma formation is reduced to <20%. This difference could be explained by an alignment of molecules with the polarisation of light. Furthermore, the 60:40 split can be seen in in the HPLC grade water and both the distillate and the residue water after distillation of deionised water. This trend indicates that for a fixed set of laser and solution parameters it is possible to have a consistent influence on the polymorphic outcome.

Considering the results reported in this thesis several recommendations can be made on what next steps would be needed to progress non-photochemical laser induced nucleation. To determine more information about the underlying mechanism of non-photochemical laser induced nucleation experiments should be conducted using a hydrophone, which has been used in the past to investigate cavitation induced by ultrasound. Its application here could be used to determine if laser induced cavitation is the cause of the observed nucleation. Another experiment that should be conducted is the use of an in situ form of particle tracking such Brownian microscopy, to trace solute clusters during, and immediately after, laser irradiation so as to understand their role in how the crystal is formed from irradiation. The identification of the need for an initiator in solution, and the source being in the solvent (water) it is suggested that elemental analysis be done on different water supplies and deionised water after processing, to determine what underlying element could be the initiator and then compare with the observations by Ward *et al*.[87]

There are several experiments that could be done to investigate the utility of non-photochemical laser induced nucleation as a potential industrial tool. Laser induced nucleation has been demonstrated at 1ml scale but how the observation seen at this scale changes with the volume of the experiments is something that has not been addressed. Another aspect of laser induced nucleation that has not been investigated is if the laser influences the growth rate of the resultant crystal. Other aspects which could be useful for the development of laser induced nucleation could be the combination of laser induced nucleation with other conditions such as high pressure,

co-crystals, ultrasound etc to understand the potential and limitations of this technique.

Recently it has been shown that after nanofiltration, laser induced nucleation activity can be brought back using nanoparticles. An interesting series of experiments which could be done is to dope systems that do not undergo laser induced nucleation and attempt to make them active. This could open the potential of laser induced nucleation to being considered alongside traditional crystallisation techniques.

8. Appendix A: Laser induced nucleation in continuous flow

This section will address the work that was undertaken to implement laser induced nucleation in a continuous flow environment. It will include designing and implementing a continuous flow set up and the results, and suggestion for improvements to resolve issues identified during operation of the system.

1. Designing flow set up

The designing of the flow setup consisted of 3 parts, 1) syringe pump, 2) irradiation cell, and 3) imaging cell (figure 8.1).

1) For this flow setup supersaturated aqueous potassium chloride (KCl) solution was chosen because it only required a single pulse to induce nucleation as opposed to glycine and urea which take up to 1 minute of irradiation to induced nucleation which is not always successful. Another reason this system was selected was it allows for the use of much lower supersaturation than required for glycine or urea which aided in the flow to avoid nucleation induced by the shear on the walls of the tubing.

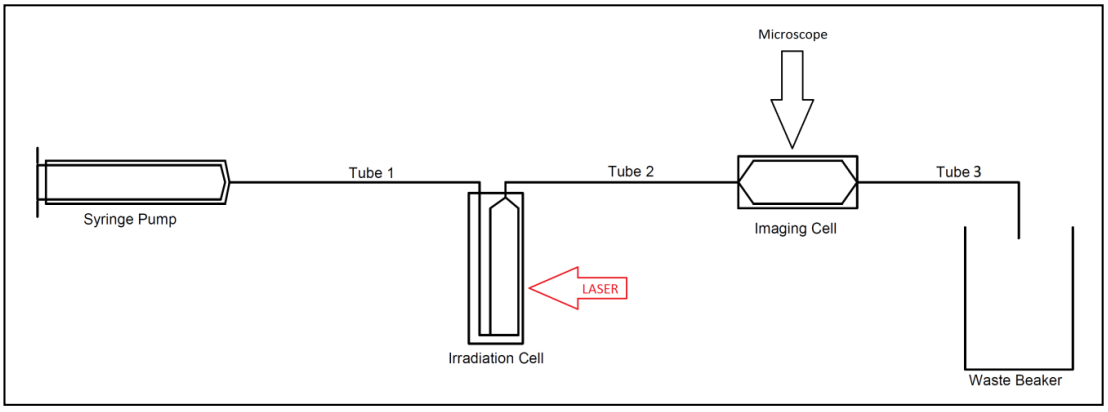

Figure 8.1: Schematic representation of the experimental set up. The three main parts are represented: Syringe Pump, Irradiation Cell and Imaging Cell

Design parameters that needed to be taken into consideration in this section were temperature control and flowrates. The role of temperature control in this flow set up

is to ensure there is no nucleation prior to the laser irradiation and to ensure the supersaturation is as expected with the point of irradiation so nucleation can be induced. Flow rate needs to be balanced so the experiment could run for a sufficient time to get results high enough to allow for the transport of a solid material formed, but not so high that shear induced nucleation could occur. To strike the balance needed for this design a calibrated syringe pump was used which could deliver an appropriate range of flow rates.

2) The purpose of the irradiation cell was to allow for isothermal laser induced nucleation to occur. This was done using a flow cuvette with polished windows to allow for the laser to pass through. This was held in a Peltier temperature-controlled block.

3) Imaging was performed post-irradiation, using a microscope and a flat flow cell designed to work with microscopes. The distance from irradiation and observation cell was tuned to be equal to the growth rate of 1mm at the chosen flow rate.

2. Temperature control

In order to achieve the temperature control required, a suitable temperature cooling profile was designed. This was achieved by keeping the syringe pump in an incubator at 36°C and allowing air convection currents to cool the solution as it passes through Tube 1 (figure 8.1). To optimize this cooling system, it was possible to change the length of the tubing between syringe pump and irradiation cell based on the flow rate to alter the cooling profile (see figure 8.2). Control of the cooling profile is necessary as rapid cooling can generate the supersaturation too fast and can result in spontaneous nucleation (crashing out). Excessively long tubing will increase the chance of nucleation when supersaturation is generated, and can be difficult to manage.

The cooling profile can be calculated using Eq.1 to get the heat transfer coefficient and then Eq.2 to calculate the temperature at a given distance

$$U = \frac{m\, C_p\, \Delta T}{A\, \Delta T_{lm}} \qquad \textbf{Eq.1}$$

Where:

U = Overall Heat Transfer Coefficient (W/m^2K)

m= Mass flowrate (kg/s)

C_p = Specific heat capacity (J/kgK)

ΔT = Temperature difference of liquid (K)

A = External Area of the tubing between the two thermocouples (m^2)

ΔT_{lm} = Log mean temperature difference along the tube. (K)

$$T_{out} = T_{air} + \left(\frac{T_{in} - T_{air}}{e^{\frac{UA}{Cpm}}} \right) \qquad \textbf{Eq.2}$$

T_{out} = output temperature of liquid (K)

T_{air} = Temperature of air (K)

T_{in} = Input Temperature of liquid (K)

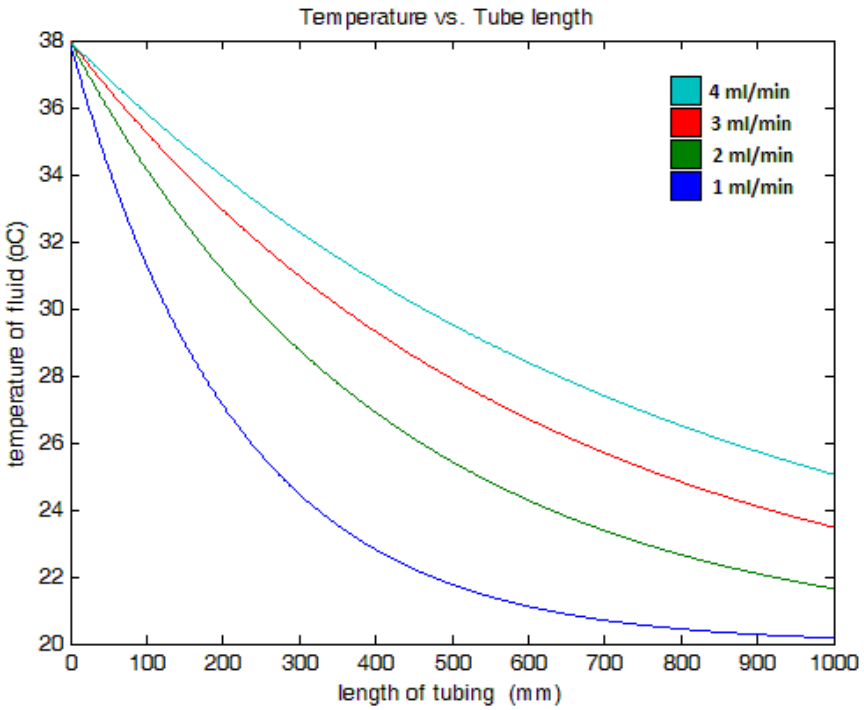

Figure 8.2: The relationship between the length of tube and the temperature drop based on an initial temperature of 38°C.

A flow rate of 2nl/min was selected and according to the predicted cooling profile it would require 550mm of tube between the temperatures controlled syringe pump and irradiation cell.

3. Particle sedimentation

A transportation issue with crystallisation in continuous flow is that if the flow rate is not fast enough then there is a possibility that the particle will sediment and could block the tubing. This issue becomes a greater problem in the tubing after the irradiation cell as eventually the crystal will grow to a size where buoyancy is no-longer sufficient to prevent the crystal from sedimentation. Using equation 3-7 it is possible to estimate this, figure 8.3 shows at what point this occurs for different flow rates, at the nucleation the laser point.

Firstly, the upward flow velocity (u_{fl}) is defined as shown (Q = total flow, A_{sec} Cross sectional area).

$$u_{fl} = Q/A_{sec} \quad \text{Eq.3}$$

Terminal settling velocity of particle (u_{ter}),(p_p =density of particle p_{fl}= density of fluid, μ = total flow rate, g = gravity , r_{KCl} = radius of crystal)

$$u_{ter} = \frac{2}{9}\left(\frac{\rho_p - \rho_{fl}}{\mu}\right) g\ (r_{KCl})^3 \qquad \text{Eq.4}$$

Where the particle size (r_{KCl}) (sphere-radius) after time (t), (G_{KCl} = growth rate of KCl)

$$r_{KCl} = G_{KCl} * t \qquad \text{Eq.5}$$

Actual particle velocity (u_p)

$$u_p = u_{fl} - u_{ter} \qquad \text{Eq.6}$$

Displacement of particle (d_p)

$$d_p = u_p * t \qquad \text{Eq.7}$$

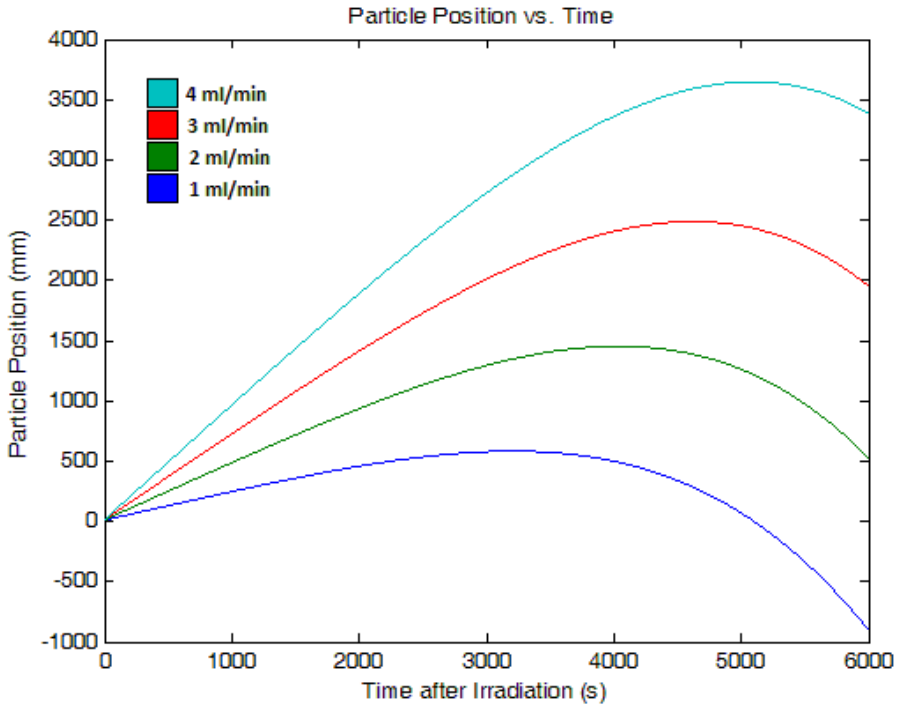

Figure 8.3: The movement of the crystal is plotted with time to determine after what time it begins to move downwards.

The graph shows for the 2 ml/min that the time for sedimentation starts to commence is 4500 seconds (75 mins) after irradiation which is beyond the time scales of this system so it is assumed that the sedimentation would not be problem.

4. Particle sedimentation

Supersaturation	1.0 ml/min	2.0 ml/min	3.0 ml/min	% Probability Nucleation
1.08	Y	N, Y	Y	25 %
1.102	N,Y	N, YYYY	Y	25 %
1.13		Y,N		50 %
1.17		NNN		100 %

Table 3: Summary of test runs with KCl and no laser. Y = No spontaneous nucleation occurred, N = spontaneous nucleation occurred.

Table 3 shows results where experiments were carried out without the laser pulses to ensure that there is no shear or spontaneous nucleation caused by the setup. The data in Table 3 suggest that despite its lower nucleation probability the conditions that should be used in future experiments are 1.102 supersaturation and a flow rate of 2ml/min.

5. Results of laser irradiation

Flow experiments were carried out in the presence of laser irradiation; however, no crystals were observed in the imaging cell even when the supersaturated solution was irradiated with multiple pulses. A possible explanation for this could be that the laser induced nucleation is not as effective as in stationary samples. Another reason could be that the crystals were too small to be seen by the microscope, or the position was wrong. Finally, it could be that the crystals did nucleate but became stuck between the laser irradiation cell and the monitoring cell.

A possible way of improving the continuous flow set up would be to increase the length of the tube between irradiation cell and monitoring cell to increase the residence time in this section to allow crystals to grow larger. Another improvement could be to implement a segmented flow set up. Introducing a carrier medium, liquid or gas, could solve the issue ofcrystals getting stuck or sedimentation.

(1) Braga, D.; Grepioni, F., Making crystals from crystals: a green route to crystal engineering and polymorphism. *Chem. Commun.* **2005**, (29), 3635-3645.

(2) Yu, L.; Reutzel-Edens, S. M.; Mitchell, C. A., Crystallization and Polymorphism of Conformationally Flexible Molecules: Problems, Patterns, and Strategies. *Org. Process Res. Dev.* **2000,** 4, (5), 396-402.

(3) Roy, S.; Aitipamula, S.; Nangia, A., Thermochemical Analysis of Venlafaxine Hydrochloride Polymorphs 1−5. *Crystal Growth and Design* **2005,** 5, (6), 2268-2276.

(4) Reutzel-Edens, S. M.; Bush, J. K.; Magee, P. A.; Stephenson, G. A.; Byrn, S. R., Anhydrates and Hydrates of Olanzapine: Crystallization, Solid-State Characterization, and Structural Relationships. *Crystal Growth and Design* **2003,** 3, (6), 897-907.

(5) Swarbrick, J.; Boylan, J. C., *Encyclopedia of Pharmaceutical Technology: Volume 9 - Liposomes as Pharmaceutical Dosage Forms to Microencapsulation*. ed.; Taylor and Francis: 1993.

(6) Pienaar, E. W.; Caira, M. R.; Lötter, A. P., Polymorphs of nitrofurantoin. I. Preparation and X-ray crystal structures of two monohydrated forms of nitrofurantoin. *Journal of Crystallographic and Spectroscopic Research* **1993,** 23, (9), 739-744.

(7) Stahly, G. P., Diversity in Single- and Multiple-Component Crystals. The Search for and Prevalence of Polymorphs and Cocrystals. *Crystal Growth and Design* **2007,** 7, (6), 1007-1026.

(8) Varughese, S., Non-covalent routes to tune the optical properties of molecular materials. *Journal of Materials Chemistry C* **2014,** 2, (18), 3499-3516.

(9) De Villiers, M. M.; van der Watt, J. G.; Lötter, A. P., Kinetic study of the solid-state photolytic degradation of two polymorphic forms of furosemide. *International Journal of Pharmaceutics* **1992,** 88, (1), 275-283.

(10) Brittain, H. G., *Polymorphism in Pharmaceutical Solids, Second Edition*. ed.; CRC Press: 2016.

(11) Dufour, F.; Stichel, B.; Grayson, J. I., Control of Crystal Modification and Crystal Shape by Control of Solid–Solid Transitions during Crystallization and Drying: Two Industrial Case Studies. *Org. Process Res. Dev.* **2013,** 17, (3), 568-577.

(12) Yu, L. X.; Furness, M. S.; Raw, A.; Outlaw, K. P. W.; Nashed, N. E.; Ramos, E.; Miller, S. P.; Adams, R. C.; Fang, F.; Patel, R. M., Scientific considerations of pharmaceutical solid polymorphism in abbreviated new drug applications. *Pharmaceutical research* **2003,** 20, (4), 531-536.

(13) Chemburkar, S. R.; Bauer, J.; Deming, K.; Spiwek, H.; Patel, K.; Morris, J.; Henry, R.; Spanton, S.; Dziki, W.; Porter, W.; Quick, J.; Bauer, P.; Donaubauer, J.; Narayanan, B. A.; Soldani, M.; Riley, D.; McFarland, K., Dealing with the Impact of Ritonavir Polymorphs on the Late Stages of Bulk Drug Process Development. *Org. Process Res. Dev.* **2000,** 4, (5), 413-417.

(14) Han, G.; Chow, P. S.; Tan, R. B. H., Salt-dependent growth kinetics in glycine polymorphic crystallization. *Crystengcomm* **2016,** 18, (3), 462-470.

(15) Park, K.; Evans, J. M. B.; Myerson, A. S., Determination of Solubility of Polymorphs Using Differential Scanning Calorimetry. *Crystal Growth and Design* **2003,** 3, (6), 991-995.

(16) Yu, L.; Ng, K., Glycine Crystallization during Spray Drying: The pH Effect on Salt and Polymorphic Forms. *Journal of Pharmaceutical Sciences* **2002,** 91, (11), 2367-2375.

(17) Boldyreva, E. V.; Drebushchak, V. A.; Drebushchak, T. N.; Paukov, I. E.; Kovalevskaya, Y. A.; Shutova, E. S., Polymorphism of glycine, Part I. *Journal of Thermal Analysis and Calorimetry* **2003,** 73, (2), 409-418.

(18) Boldyreva, E. V.; Drebushchak, V. A.; Drebushchak, T. N.; Paukov, I. E.; Kovalevskaya, Y. A.; Shutova, E. S., Polymorphism of glycine, Part II. *Journal of Thermal Analysis and Calorimetry* **2003,** 73, (2), 419.

(19) Sun, X. Y.; Garetz, B. A.; Myerson, A. S., Supersaturation and polarization dependence off polymorph control in the nonphotochemical laser-induced nucleation (NPLIN) of aqueous glycine solutions. *Crystal Growth and Design* **2006,** 6, (3), 684-689.

(20) Zaccaro, J.; Matic, J.; Myerson, A. S.; Garetz, B. A., Nonphotochemical, laser-induced nucleation of supersaturated aqueous glycine produces unexpected gamma-polymorph. *Crystal Growth and Design* **2001,** 1, (1), 5-8.

(21) Mullin, J. W., *Crystallization*. Fourth ed.; Butterworth-Heinemann: Oxford, 2001.

(22) Liu, Y.; van den Berg, M. H.; Alexander, A. J. Y., - Supersaturation dependence of glycine polymorphism using laser-induced nucleation, sonocrystallization and nucleation by mechanical shock. - *Physical Chemistry Chemical Physics*, (-), -.

(23) Vázquez Diosdado, J. A.; Ashwin, P.; Kohary, K. I.; Wright, C. D., Threshold switching via electric field induced crystallization in phase-change memory devices. *Applied Physics Letters* **2012,** 100, (25), 253105.

(24) Kordylla, A.; Krawczyk, T.; Tumakaka, F.; Schembecker, G., Modeling ultrasound-induced nucleation during cooling crystallization. *Chemical Engineering Science* **2009,** 64, (8), 1635-1642.

(25) Volmer, M.; Weber, A., *Physikal. Chemie* **1925,** 119, (227).

(26) Becker, R.; Döring, W., Kinetische Behandlung der Keimbildung in übersättigten Dämpfen. *Annalen der Physik* **1935,** 416, (8), 719-752.

(27) Gebauer, D.; Kellermeier, M.; Gale, J. D.; Bergstrom, L.; Colfen, H., Pre-nucleation clusters as solute precursors in crystallisation. *Chemical Society Reviews* **2014,** 43, (7), 2348-2371.

(28) Herrmann, E.; Lihavainen, H.; Hyvärinen, A.-P.; Riipinen, I.; Wilck, M.; Stratmann, F.; Kulmala, M., Nucleation Simulations Using the Fluid Dynamics Software FLUENT with the Fine Particle Model FPM. *The Journal of Physical Chemistry A* **2006,** 110, (45), 12448-12455.

(29) Vekilov, P. G., The two-step mechanism of nucleation of crystals in solution. *Nanoscale* **2010,** 2, (11), 2346-2357.

(30) Laaksonen, A.; McGraw, R.; Vehkamäki, H., Liquid-drop formalism and free-energy surfaces in binary homogeneous nucleation theory. *The Journal of Chemical Physics* **1999,** 111, (5), 2019-2027.

(31) Drenth, J.; Haas, C., Nucleation in protein crystallization. *Acta crystallographica. Section D, Biological crystallography* **1998,** 54, (Pt 5), 867-72.

(32) Knezic, D.; Zaccaro, J.; Myerson, A. S., Nucleation Induction Time in Levitated Droplets. *The Journal of Physical Chemistry B* **2004,** 108, (30), 10672-10677.

(33) Strey, R.; Viisanen, Y., Measurement of the molecular content of binary nuclei. Use of the nucleation rate surface for ethanol–hexanol. *The Journal of Chemical Physics* **1993,** 99, (6), 4693-4704.

(34) Myerson, A. S., Concluding remarks. *Faraday Discussions* **2015,** 179, (0), 543-547.

(35) Erdemir, D.; Lee, A. Y.; Myerson, A. S., Nucleation of Crystals from Solution: Classical and Two-Step Models. *Accounts of Chemical Research* **2009,** 42, (5), 621-629.

(36) Wolde, P. R. t.; Frenkel, D., Enhancement of Protein Crystal Nucleation by Critical Density Fluctuations. *Science* **1997,** 277, (5334), 1975-1978.

(37) Pan, W.; Vekilov, P. G.; Lubchenko, V., Origin of Anomalous Mesoscopic Phases in Protein Solutions. *The Journal of Physical Chemistry B* **2010,** 114, (22), 7620-7630.

(38) Lomakin, A.; Chung, D. S.; Benedek, G. B.; Kirschner, D. A.; Teplow, D. B., On the nucleation and growth of amyloid beta-protein fibrils: detection of nuclei and quantitation of rate constants. *Proceedings of the National Academy of Sciences of the United States of America* **1996,** 93, (3), 1125-9.

(39) Galkin, O.; Pan, W.; Filobelo, L.; Hirsch, R. E.; Nagel, R. L.; Vekilov, P. G., Two-Step Mechanism of Homogeneous Nucleation of Sickle Cell Hemoglobin Polymers. *Biophysical Journal* **2007,** 93, (3), 902-913.

(40) Jiang, S. F.; ter Horst, J. H., Crystal Nucleation Rates from Probability Distributions of Induction Times. *Crystal Growth and Design* **2011,** 11, (1), 256-261.

(41) Sun, W.; Ceder, G., Induction time of a polymorphic transformation. *CrystEngComm* **2017**.

(42) Price, S. L.; Braun, D. E.; Reutzel-Edens, S. M., Can computed crystal energy landscapes help understand pharmaceutical solids? *Chem. Commun.* **2016,** 52, (44), 7065-7077.

(43) Hancock, B. C., Predicting the Crystallization Propensity of Drug-Like Molecules. *Journal of Pharmaceutical Sciences* **2017,** 106, (1), 28-30.

(44) LaPlante, S. R.; D. Fader, L.; Fandrick, K. R.; Fandrick, D. R.; Hucke, O.; Kemper, R.; Miller, S. P. F.; Edwards, P. J., Assessing Atropisomer Axial Chirality in Drug Discovery and Development. *Journal of Medicinal Chemistry* **2011,** 54, (20), 7005-7022.

(45) Hursthouse, M. B.; Huth, L. S.; Threlfall, T. L., Why Do Organic Compounds Crystallise Well or Badly or Ever so Slowly? Why Is Crystallisation Nevertheless Such a Good Purification Technique? *Org. Process Res. Dev.* **2009,** 13, (6), 1231-1240.

(46) Threlfall, T. L.; De'Ath, R. W.; Coles, S. J., Metastable Zone Widths, Conformational Multiplicity, and Seeding. *Org. Process Res. Dev.* **2013,** 17, (3), 578-584.

(47) Kitamura, M., Controlling factor of polymorphism in crystallization process. *J. Cryst. Growth* **2002,** 237–239, Part 3, 2205-2214.

(48) Baird, J. A.; Van Eerdenbrugh, B.; Taylor, L. S., A Classification System to Assess the Crystallization Tendency of Organic Molecules from Undercooled Melts. *Journal of Pharmaceutical Sciences* **2010,** 99, (9), 3787-3806.

(49) Nurzyńska, K.; Booth, J.; Roberts, C. J.; McCabe, J.; Dryden, I.; Fischer, P. M., Long-Term Amorphous Drug Stability Predictions Using Easily Calculated, Predicted, and Measured Parameters. *Molecular Pharmaceutics* **2015,** 12, (9), 3389-3398.

(50) Nurzyńska, K.; Austin, R. P.; Fischer, P. M.; Booth, J.; Gommer, F., Survival of the Fittest: Time-To-Event Modeling of Crystallization of Amorphous Poorly Soluble Drugs. *Journal of Pharmaceutical Sciences* **2016,** 105, (6), 1858-1866.

(51) Mahlin, D.; Bergström, C. A. S., Early drug development predictions of glass-forming ability and physical stability of drugs. *European Journal of Pharmaceutical Sciences* **2013,** 49, (2), 323-332.

(52) Mullin, J. W.; Leci, C. L., Some nucleation characteristics of aqueous citric acid solutions. *J. Cryst. Growth* **1969,** 5, (1), 75-76.

(53) Murray, B. J., Inhibition of ice crystallisation in highly viscous aqueous organic acid droplets. *Atmos. Chem. Phys.* **2008,** 8, (17), 5423-5433.

(54) Okutsu, T., Photochemically-induced crystallization of protein. *Journal of Photochemistry and Photobiology C: Photochemistry Reviews* **2007,** 8, (3), 143-155.

(55) Rungsimanon, T.; Yuyama, K.-i.; Sugiyama, T.; Masuhara, H.; Tohnai, N.; Miyata, M., Control of Crystal Polymorph of Glycine by Photon Pressure of a

Focused Continuous Wave Near-Infrared Laser Beam. *The Journal of Physical Chemistry Letters* **2010,** 1, (3), 599-603.

(56) Yuyama, K.-i.; Rungsimanon, T.; Sugiyama, T.; Masuhara, H., Selective Fabrication of α- and γ-Polymorphs of Glycine by Intense Polarized Continuous Wave Laser Beams. *Crystal Growth and Design* **2012,** 12, (5), 2427-2434.

(57) Murai, R.; Yoshikawa, H. Y.; Takahashi, Y.; Maruyama, M.; Sugiyama, S.; Sazaki, G.; Adachi, H.; Takano, K.; Matsumura, H.; Murakami, S.; Inoue, T.; Mori, Y., Enhancement of femtosecond laser-induced nucleation of protein in a gel solution. *Applied Physics Letters* **2010,** 96, (4), 043702.

(58) Liu, T. H.; Uwada, T.; Sugiyama, T.; Usman, A.; Hosokawa, Y.; Masuhara, H.; Chiang, T. W.; Chen, C. J., Single femtosecond laser pulse-single crystal formation of glycine at the solution surface. *J. Cryst. Growth* **2013,** 366, 101-106.

(59) Garetz, B. A.; Aber, J. E.; Goddard, N. L.; Young, R. G.; Myerson, A. S., Nonphotochemical, Polarization-Dependent, Laser-Induced Nucleation in Supersaturated Aqueous Urea Solutions. *Phys. Rev. Lett.* **1996,** 77, (16), 3475-3476.

(60) Liu, Y.; Ward, M. R.; Alexander, A. J., Polarization independence of laser-induced nucleation in supersaturated aqueous urea solutions. *Phys. Chem. Chem. Phys.* **2017,** 19, (5), 3464-3467.

(61) Matic, J.; Sun, X. Y.; Garetz, B. A.; Myerson, A. S., Intensity, wavelength, and polarization dependence of nonphotochemical laser-induced nucleation in supersaturated aqueous urea solutions. *Crystal Growth and Design* **2005,** 5, (4), 1565-1567.

(62) Garetz, B. A.; Matic, J.; Myerson, A. S., Polarization switching of crystal structure in the nonphotochemical light-induced nucleation of supersaturated aqueous glycine solutions. *Physical Review Letters* **2002,** 89, (17).

(63) Alexander, A. J.; Camp, P. J., Single Pulse, Single Crystal Laser-Induced Nucleation of Potassium Chloride. *Crystal Growth and Design* **2009,** 9, (2), 958-963.

(64) Ward, M. R.; Ballingall, I.; Costen, M. L.; McKendrick, K. G.; Alexander, A. J., Nanosecond pulse width dependence of nonphotochemical laser-induced nucleation of potassium chloride. *Chem. Phys. Lett.* **2009,** 481, (1-3), 25-28.

(65) Ward, M. R.; Alexander, A. J., Nonphotochemical Laser-Induced Nucleation of Potassium Halides: Effects of Wavelength and Temperature. *Crystal Growth and Design* **2012,** 12, (9), 4554-4561.

(66) Ikni, A.; Clair, B.; Scouflaire, P.; Veesler, S.; Gillet, J. M.; El Hassan, N.; Dumas, F.; Spasojevic-de Bire, A., Experimental Demonstration of the Carbamazepine Crystallization from Non-photochemical Laser-Induced Nucleation in Acetonitrile and Methanol. *Crystal Growth and Design* **2014,** 14, (7), 3286-3299.

(67) Li, W. J.; Ikni, A.; Scouflaire, P.; Shi, X. X.; El Hassan, N.; Gemeiner, P.; Gillet, J. M.; Spasojevic-de Bire, A., Non-Photochemical Laser-Induced Nucleation

of Sulfathiazole in a Water/Ethanol Mixture. *Crystal Growth and Design* **2016,** 16, (5), 2514-2526.

(68) Garetz, B. A.; Aber, J. E.; Goddard, N. L.; Young, R. G.; Myerson, A. S., Nonphotochemical, Polarization-Dependent, Laser-Induced Nucleation in Supersaturated Aqueous Urea Solutions. *Phys Rev Lett* **1996,** 77, (16), 3475-3476.

(69) Soare, A.; Dijkink, R.; Pascual, M. R.; Sun, C.; Cains, P. W.; Lohse, D.; Stankiewicz, A. I.; Kramer, H. J. M., Crystal Nucleation by Laser-Induced Cavitation. *Crystal Growth and Design* **2011,** 11, (6), 2311-2316.

(70) Myerson, A. S.; Lo, P. Y., Cluster formation and diffusion in supersaturated binary and ternary amino acid solutions. *J. Cryst. Growth* **1991,** 110, (1), 26-33.

(71) Chemla, D. S.; Zyss, J., *Nonlinear Optical Properties of Organic Molecules and Crystals*. ed.; Academic Press: 1987.

(72) Liu, X. Y.; Boek, E. S.; Briels, W. J.; Bennema, P., Prediction of crystal growth morphology based on structural analysis of the solid-fluid interface. *Nature* **1995,** 374, (6520), 342-345.

(73) Huang, J.; Stringfellow, T. C.; Yu, L., Glycine Exists Mainly as Monomers, Not Dimers, in Supersaturated Aqueous Solutions: Implications for Understanding Its Crystallization and Polymorphism. *J. Am. Chem. Soc.* **2008,** 130, (42), 13973-13980.

(74) Srinivasan, K., Crystal growth of α and γ glycine polymorphs and their polymorphic phase transformations. *J. Cryst. Growth* **2008,** 311, (1), 156-162.

(75) JD, B., Short notifications and notes - The crystal structure of the natural amino acids and related compounds. *Zeitschrift Fur Kristallographie* **1931,** 78, (3/4), 363-369.

(76) Iitaka, Y., The crystal structure of γ-glycine. *Acta Crystallographica* **1961,** 14, (1), 1-10.

(77) Towler, C. S.; Davey, R. J.; Lancaster, R. W.; Price, C. J., Impact of molecular speciation on crystal nucleation in polymorphic systems. *J. Am. Chem. Soc.* **2004,** 126, (41), 13347-13353.

(78) Duff, N.; Dahal, Y. R.; Schmit, J. D.; Peters, B., Salting out the polar polymorph: Analysis by alchemical solvent transformation. *The Journal of Chemical Physics* **2014,** 140, (1), 014501.

(79) Sauter, E. G., *Nonlinear Optics*. ed.; Wiley: 1996.

(80) Orttung, W. H.; Armour, R. W., Polarizability anisotropy from crystal refractive indices. I. Lorentz internal field approximation with application to amino acid data. *The Journal of Physical Chemistry* **1967,** 71, (9), 2846-2853.

(81) Sun, X. Y.; Garetz, B., Factors controlling polymorph formation in nonphotochemical laser-induced nucleation (NPLIN) of aqueous glycine solutions. *Abstr. Pap. Am. Chem. Soc.* **2006,** 231.

(82) Sun, X. Y.; Garetz, B. A.; Myerson, A. S., Polarization switching of crystal structure in the nonphotochemical laser-induced nucleation of supersaturated aqueous L-histidine. *Crystal Growth and Design* **2008,** 8, (5), 1720-1722.

(83) Knott, B. C.; Doherty, M. F.; Peters, B., A simulation test of the optical Kerr mechanism for laser-induced nucleation. *J. Chem. Phys.* **2011,** 134, (15).

(84) Nakamura, K.; Hosokawa, Y.; Masuhara, H., Anthracene crystallization induced by single-shot femtosecond laser irradiation: Experimental evidence for the important role of bubbles. *Crystal Growth and Design* **2007,** 7, (5), 885-889.

(85) Knott, B. C.; Larue, J. L.; Wodtke, A. M.; Doherty, M. F.; Peters, B., Communication: Bubbles, crystals, and laser-induced nucleation. *J. Chem. Phys.* **2011,** 134, (17).

(86) Ward, M. R.; Jamieson, W. J.; Leckey, C. A.; Alexander, A. J., Laser-induced nucleation of carbon dioxide bubbles. *J. Chem. Phys.* **2015,** 142, (14).

(87) Ward, M. R.; Mackenzie, A. M.; Alexander, A. J., Role of Impurity Nanoparticles in Laser-Induced Nucleation of Ammonium Chloride. *Crystal Growth and Design* **2016,** 16, (12), 6790-6796.

(88) Ward, M. R.; Copeland, G. W.; Alexander, A. J., Chiral hide-and-seek: Retention of enantiomorphism in laser-induced nucleation of molten sodium chlorate. *J. Chem. Phys.* **2011,** 135, (11).

(89) Ward, M. R.; McHugh, S.; Alexander, A. J., Non-photochemical laser-induced nucleation of supercooled glacial acetic acid. *Phys. Chem. Chem. Phys.* **2012,** 14, (1), 90-93.

(90) Javid, N.; Kendall, T.; Burns, I. S.; Sefcik, J., Filtration Suppresses Laser-Induced Nucleation of Glycine in Aqueous Solutions. *Crystal Growth and Design* **2016,** 16, (8), 4196-4202.

(91) Liu, Y.; van den Berg, M. H.; Alexander, A. J., Supersaturation dependence of glycine polymorphism using laser-induced nucleation, sonocrystallization and nucleation by mechanical shock. *Physical Chemistry Chemical Physics* **2017,** 19, (29), 19386-19392.

(92) Yang, X.; Wang, X.; Ching, C. B., Solubility of Form α and Form γ of Glycine in Aqueous Solutions. *Journal of Chemical and Engineering Data* **2008,** 53, (5), 1133-1137.

(93) Lee, F.-M.; Lahti, L. E., Solubility of urea in water-alcohol mixtures. *Journal of Chemical and Engineering Data* **1972,** 17, (3), 304-306.

(94) Hahn, D. W., Light scattering theory. *Department of Mechanical and Aerospace Engineering, University of Florida* **2009**.

(95) Meurant, G., *Introduction to Dynamic Light Scattering by Macromolecules*. ed.; Elsevier Science: 2012.

(96) Soos, M.; Lattuada, M.; Sefcik, J., Interpretation of Light Scattering and Turbidity Measurements in Aggregated Systems: Effect of Intra-Cluster Multiple-Light Scattering. *J. Phys. Chem. B* **2009,** 113, (45), 14962-14970.

(97) Hassan, P. A.; Rana, S.; Verma, G., Making Sense of Brownian Motion: Colloid Characterization by Dynamic Light Scattering. *Langmuir* **2015,** 31, (1), 3-12.

(98) Finsy, R., Particle sizing by quasi-elastic light scattering. *Advances in Colloid and Interface Science* **1994,** 52, 79-143.

(99) Dowling, R.; Davey, R. J.; Curtis, R. A.; Han, G. J.; Poornachary, S. K.; Chow, P. S.; Tan, R. B. H., Acceleration of crystal growth rates: an unexpected effect of tailor-made additives. *Chem. Commun.* **2010,** 46, (32), 5924-5926.

(100) Clair, B.; Ikni, A.; Li, W. J.; Scouflaire, P.; Quemener, V.; Spasojevic-de Bire, A., A new experimental setup for high-throughput controlled non-photochemical laser-induced nucleation: application to glycine crystallization. *J. Appl. Crystallogr.* **2014,** 47, 1252-1260.